4-3-2017

Studies in Ultracold Ground State Atom-Rydberg Atom Interactions

Samuel C. Markson
University of Connecticut, samuel.markson@uconn.edu

Studies in Ultracold Ground State Atom-Rydberg Atom Interactions

Samuel Cyrus Markson, Ph.D.

University of Connecticut, 2017

Collisions involving Rydberg atoms reveal detailed information on the state of a background medium and can be used as diagnostic probes of temperature and density distributions in a neutral or ionized gas. Spectroscopy of Rydberg atoms in highly excited states reveals the interaction of the Rydberg electron with core electrons, including relativistic effects, and can be used for precise determination of fundamental constants. The advent of ultracold trapping and cooling methods in the last three decades has ushered in a new paradigm in Rydberg physics control and manipulation. The concept of the Rydberg blockade, for instance, allows for precise control of long-range dipolar interaction between atoms, creation of correlated many-body wave functions, and realization of macroscopic quantum entanglement and quantum logic operations. The formation of a new class of Rydberg molecules arising from ground and Rydberg atom collisions can be used to manipulate electron-atom scattering phase shifts, form and manipulate molecules with enormous permanent electric dipole moments, study Rydberg chemistry at the ultracold, and realize macroscopic quantum polaronic systems. In this thesis, I will investigate charge transfer from covalent ground-Rydberg collisions to form heavy ion pair states. In another related study, I explore the formation of spin-mixed ultralong range Rydberg molecules, by accounting for spin-dependent relativistic fine and hyperfine interaction. Such studies help to not only explain experimental observations, but also point to how molecular reactions can be controlled using small electric or magnetic fields.

Studies in Ultracold Ground State Atom-Rydberg Atom Interactions

Samuel Cyrus Markson

A Dissertation

Submitted in Partial Fulfillment of the

Requirements for the Degree of

Doctor of Philosophy

at the

University of Connecticut

2017

APPROVAL PAGE

Doctor of Philosophy Dissertation

Studies in Ultracold Ground State Atom-Rydberg Atom Interactions

Presented By

Samuel Cyrus Markson

Major Advisor _____

Susanne Yelin

Associate Advisor _____

Robin Cote

Associate Advisor _____

Phillip Gould

University of Connecticut

2017

Acknowledgements

I would like to express my gratitude for the support of Hossein Sadeghpour for his continued work both during the time we spent doing research together and during the writing of this dissertation. I am similarly grateful for the time spent by my collaborators—Seth Rittenhouse, Richard Schmidt, and James Shaffer—for the long hours of discussing and editing together. My education has been continuously enriched by my time at ITAMP, particularly as the young'n amongst so many talented postdocs and visiting scholars. I am severely indebted to Igor Pikovski, Richard Schmidt, Hannes Pichler, Johannes Knörzer, Chris Bostock, Swati Singh, Stefan Pabst, Chris Chang, Tony Lee, and now Rivka Bekenstein, as I am to Jim Babb and Christine Crowley for their stewardship over the ITAMP predoctoral fellow program. Less scientifically, I am deeply thankful to call Anton Mazurenko, Anton Goloborodko, Hamed Pakatchi, Tal Kachman, William Mallard, Nikolay Perunov, Oren Leaffer, and Amitai Bin-Nun my friends. I am deeply fortunate to have had the wisdom and guidance of my parents and brother, Jay Ben.

I was extremely fortunate and am grateful to have been funded these past few years by a graduate research fellowship from the NSF. I would like to thank the Physics departments at the University of Connecticut for their continued support during the course of my Ph.D. To Micki, to Dawn, to Prof. Yelin and the members of my committee, thank you.

Contents

Chapter 1

Introduction

Rydberg atoms are objects of intense and current interest for studies of long-range, strongly interacting systems [1, 2], and of coherent control of atomic and molecular reactions [3, 4, 5, 6, 7, 8, 9, 10]. This is due to the fact that the atoms possess many "extreme" properties, from large polarizabilities and transition dipoles to shrinking binding energies and spontaneous emission rates. A summary of the scaling of some of these properties with principal quantum number n is given in Table 1.1.

As a result, Rydberg atoms are highly tunable systems, and a slight modification to the principal affords a massive degree of system tunability. Conversely, this tunability can be used as a probe of the atom's surroundings, both in terms of ambient electromagnetic fields or surround-

Table 1.1: A summary of the scaling of various Rydberg atom properties with principal quantum number n [11]

binding energy	n^{-2}
level spacing	n^{-3}
polarizability	n^{7}
transition dipoles between neighboring electronic states	n^{2}
van der Waals coefficient	n^{11}
atomic radius	n^{2}
radiative lifetime	n^{3}
dipole-dipole interaction	n^{4}

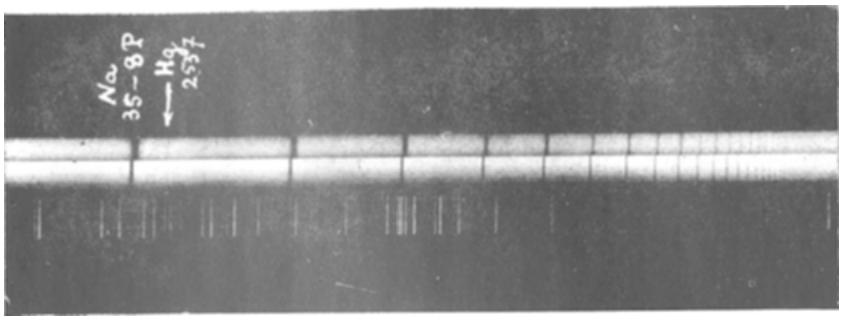

Figure 1.1: Line shifts with low (lower lines) and high (upper lines) background gas pressure, from original paper by Amaldi and Segrè [12]. Note that Rydberg electron-atom collision induce not only line shifts, but line broadening as well.

ing gases. The first work to study the effect of Rydberg atom-ground state atom interactions was done by Amaldi and Segrè [12], with accompanying theory by Enrico Fermi [13]. Collectively, they observe and explain pressure-sensitive shifts to the Rydberg line series, effectively measuring the electron-ground state atom scattering length.

With the advent of the tunable dye laser (thus enabling efficient and precise production of Rydberg atoms with specific principal and angular momentum), studies of Rydberg atom interactions saw a resurgence. Much of this work focused on the interaction of Rydberg atoms with radiation, both in an astrophysical [14], and laboratory context [15]. Other important studies used Rydberg atoms as useful benchmarks for fundamental physics, notably in experiments aimed at high-precision measurements of fundamental constants, e.g. the Rydberg constant [16, 17]. Seminal work on the interaction of Rydberg atoms with other atoms was done in the group of Haroche, who was the first to study dense Rydberg gases [18]. Haroche and others would go on to exploit the Rydberg atom in many studies of atom-photon interactions, both within cavity QED experiments [19], and as a probe of superradiance [20, 21],

Still more control was gained by the advent of ultracold atom trapping and control techniques [22]. Full quantum coherence, coupled with the Rydberg atom's unique tunability, has had significant implications for quantum information, where the nature of Rydberg-Rydberg or Rydberg-photon interactions may be exploited to produce quantum gates [23, 24, 25]. The strong, long-range interaction of Rydberg atoms—scaling as $\frac{1}{R^3}$ for internuclear distances R

on the order of twice the Rydberg atomic radius, and $\frac{1}{R^6}$ for longer distances—leads to the "Rydberg blockade," where within a blockade radius, only one atom may be excited to a Rydberg state. Details of these gates, and the Rydberg blockade which makes them possible, are given in Appendix A. The blockade has allowed for the creation of macroscopic entanglement between two Rydberg atoms [26, 27], as well as explorations into the production of exotic matter, including ultracold neutral plasmas [28].

Rydberg atoms also make for an interesting testbed in many-body physics, where a Rydberg atom is capable of interacting strongly and at long range with many other atoms in a condensate. A scheme to simulate spin-lattice physics with arbitrary n-body interactions has been proposed which exploits the tunable long-range interactions between Rydberg atoms [29]. Much recent work has been devoted to understanding Rydberg polarons [30], and experimentalists have even been capable of producing strongly interacting photons through EIT-mediated Rydberg-photon interactions [31]. The latter work suggests the possibility for all-photon quantum computation in the future.

Rydberg physics also has applications within chemistry, where Rydberg atoms or molecules are central intermediate states in resonance ionization spectroscopy [32]. Additionally, a number of coherent control schemes depend on the high polarizability of Rydberg states to steer an excited wavepacket into a desired final state [33, 34].

The focus of this thesis is on Rydberg molecules, which, very broadly defined, are molecules with one or more highly excited electrons. They may form as a combination of a Rydberg atom and a ground state atom [35, 36, 37], or between two excited state atoms [38]. In the former case, the Rydberg atom-ground state atom interaction can be understood as a scattering of the Rydberg electron (generally approximated as a free electron) from a ground state atom. Within this picture, many bizarre and interesting molecules have been predicted and detected, including the "trilobite" [36, 39], and "butterfly states" [37].

This thesis focuses on molecules formed via Rydberg atom-ground state atom scattering. In chapter 2, we review in greater detail the history of Rydberg physics, its astrophysical

relevance, and the basic formalism of quantum defect theory. In chapter 3, we review scattering theory and explain its relevance to Rydberg molecular physics. We also review the Born-oppenheimer approximation and the Landau-Zener formula—both key components to our calculations. In chapter 4, we describe how one may increase the efficiency of ion pair production via resonant charge-transfer from covalent Rydberg states [40]. In chapter 5, we describe how spin-dependent effects arising from the Rydberg electron spin-orbit interaction and the ground state atom valence electron hyperfine interaction have a significant impact on the formation of Cs Rydberg molecules [41]. Jointly, these discoveries illustrate the continuing flexibility of Rydberg systems, and suggest several new possibilities for further Rydberg research.

Chapter 2

The Rydberg Atom

2.1 A Brief History of Rydberg Spectroscopy

2.1.1 First Experimental Findings

The history of spectroscopy began in 1885 with the work of Swiss mathematician and schoolteacher J. J. Balmer. In his 1885 publication, *Notiz über die Spectrallinien des Wasserstoffs* [42], Balmer takes the experimental data of several groups (including both laboratory and astrophysical observations) on the lines of hydrogen to glean the following formula

$$\lambda \propto \frac{m^2}{m^2 - n^2} \tag{2.1}$$

where $n = 2$, and m is an integer greater than 2, encompasses the primary lines in the visible range. This result is all the more remarkable given the sparsity of data to which Balmer fit (see Fig 2.1).

In 1906, Theodore Lyman would discover the Lyman series (corresponding to $n = 1$ in the ultraviolet range) [43], and in 1908 Friedrich Paschen would discover the Paschen series (corresponding to $n = 3$ in the infrared range) [44]. These various lines could be collectively

Tabelle der Wellenlänge für die Wasserstofflinien in 10^{-7} mm.

Fraunhofer's Bezeichnung:	$H\alpha = {}^{9}/_{5}\,h$ C	$H\beta = {}^{4}/_{3}\,h$ F	$H\gamma = {}^{25}/_{21}\,h$ vor G	$H\delta = {}^{9}/_{8}\,h$ h	$H\varepsilon = {}^{19}/_{15}\,h$ nahe vor H_I	Ultraviolett $H_\zeta = {}^{16}/_{15}\,h$	$H\eta = {}^{81}/_{77}\,h$	$H\vartheta = {}^{25}/_{24}\,h$	$H_\iota = {}^{121}/_{117}\,h$	Mittelwerthe der Grundzahl h
Beobachter:										
Van d. Willigen [1]	6565,6	4863,94	4342,80	4103,8	(H_I=3971,3)	—	—	—	—	h = 3647,821
Ångström . . .	6562,10	4860,74	4340,10	4101,2	(H_I=3968,1)	—	—	—	—	h = 3645,589
Mendenhall . .	6561,62	4860,16	—	—	—	—	—	—	—	h = 3645,232
Mascart	6560,7	4859,8	—	—	(H_I=3967,2)	—	—	—	—	h = 3644,842
Ditscheiner . .	6559,5	4859,74	4338,60	4100,0	(H_I=3966,8)	—	—	—	—	h = 3644,460
Huggins	—	für die ultravioletten H-Linien weisser Sterne				3887,5	3834	3795	3767,5	h = 3643,846
Vogel	—	—	—	—	3969	3887	3834	3795	6769	h = 3644,379
Formel: $H = \frac{m^2}{m^2-2^2}h$	$m=3$	$m=4$	$m=5$	$m=6$	$m=7$	$m=8$	$m=9$	$m=10$	$m=11$	
h = 3645,6	6562,08	4860,8	4340	4101,3	3969,65	3888,64	3834,98	3797,5	3770,2	
h = 3645	6561	4860	4339,283	4100,625	3969	3888	3834,35	3796,875	3769,615	

1) Wenn man diesen, durchschnittlich um $^1/_{1500}$ höher stehenden Werthen nur $^1/_3$ soviel Gewicht beilegt, wie den übrigen Beobachtungen, so erhält man als genauen Mittelwerth für h: 3645.

Figure 2.1: Data from which Balmer hypothesized his original formula

described by the Rydberg formula

$$\frac{1}{\lambda} \propto \left(\frac{1}{m^2} - \frac{1}{n^2}\right) \tag{2.2}$$

which was introduced in 1890 (see Rydberg's handwritten notes in Fig. 2.1.1) [45, 46].

By then there were sufficient data to demonstrate the validity of Eq. 2.2 for elements in groups I, II, and III, but Rydberg wrote that "there is, however, no reason to doubt that the laws I have found can be applied in the same way to all elements" [45]. For a infinitely massive nucleus, the proportionality constant R_∞ in Eq. 2.2 is [47]

$$R_\infty = \frac{m_e e^4}{8\epsilon_0^2 h^3 c} = 1.0973731568539(55) \times 10^7 m^{-1} \tag{2.3}$$

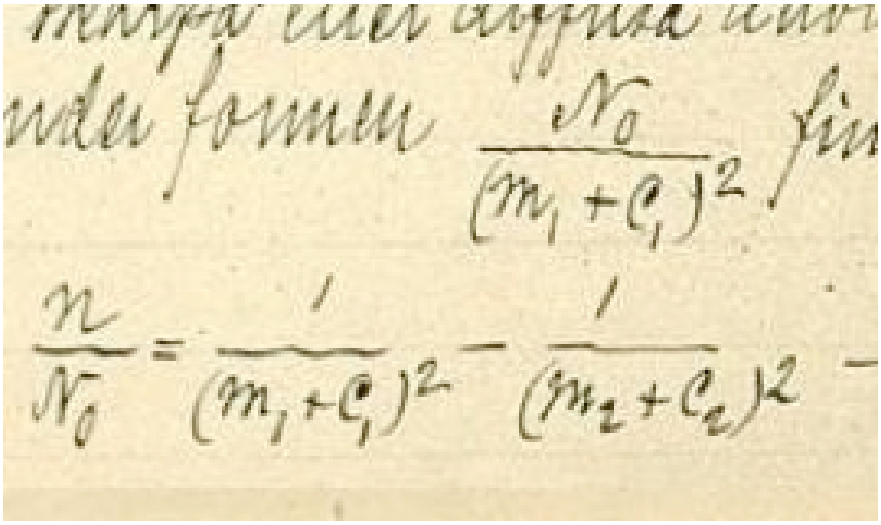

Figure 2.2: Rydberg's notes, in which he writes the original, eponymous formula [46]

2.1.2 Rutherford and the planetary model of the atom

While highly useful on its own for classification of spectra and identification of species from their observed spectra, the formula would not get any theoretical justification until the structure of the atom was better understood. The investigation of the atom began in earnest in the next century, however. In 1909, the Geiger-Marsden gold-foil experiment (sometimes referred to as the Rutherford gold-foil experiment, as it was performed at the behest of Ernest Rutherford) invalidated his former teacher J. J. Thomson's plum pudding model of the atom [48, 49] [1]. J. J. Thomson had previously posited that various "corpuscles" within the atom (today's protons and neutrons) were packed near-uniformly throughout the atomic volume (see Fig. 2.1.2). Somewhat on a whim, Rutherford instructed Geiger and his student Marsden to investigate the effect of α-particle collision on a thin film of matter. Rutherford relates the history of this experiment [50]:

> One day Geiger came to me and said, "Don't you think that young Marsden, whom I am training in radioactive methods, ought to begin a small research?" Now I had thought that too, so I said, "Why not let him see if any α-particles can be scattered

[1] The role that Rutherford played in demystifying the atomic structure is all the more remarkable when one considers that, just shortly before, Rutherford was awarded the Nobel prize in chemistry for his work on the disintegration of the nucleus and the nature of radioactivity

Number of corpuscles	60.	55.	50.	45.	40.	35.
Number in successive rings...	20 16 13 8 3	19 16 12 7 1	18 15 11 5 1	17 14 10 4	16 13 8 3	16 12 6 1
Number of corpuscles	**30.**	**25.**	**20.**	**15.**	**10.**	**5.**
Number in successive rings...	15 10 5	13 9 3	12 7 1	10 5	8 2	5

Figure 2.3: Structure of corpuscular rings calculated by J. J. Thomson, prior to Geiger/Marsden/Rutherford's discovery of the compacted nucleus

> through a large angle?" I may tell you in confidence that I did not believe that they would be, since we knew that the α-particle was a very fast massive particle, with a great deal of energy, and you could show that if the scattering was due to the accumulated effect of a number of small scatterings the chance of an α-particles's being scattered backwards was very small. Then I remember two or three days later Geiger coming to me in great excitement and saying, "We have been able to get some of the α-particles coming backwards..." It was quite the most incredible event that has ever happened to me in my life. It was almost as incredible as if you fired a 15-inch shell at a piece of tissue paper and it came back and hit you.

Perhaps if Marsden had been more busy, we'd be studying the interaction of Rydberg atoms with atomic corpuscles.

It is Rutherford who first uses Geiger/Marsden's data to test the possibility of an atom consisting of a oppositely charged nucleus and electrically charged cloud [51]. Rutherford was however not the first to consider such a structure for the atom; Rutherford himself mentions work by Nagaoka six years earlier that hypothesizes a "Saturnian" model for the atom, and

Nagoka in turn references previous work done by Maxwell [52]. Nagaoka writes:

> The system, which I am going to discuss, consists of a large number of particles of equal mass arranged in a circle at equal angular intervals and repelling each other with forces inversely proportional to the square of distance; at the centre of the circle, place a particle of large mass attracting the other particles according to the same law of force. If these repelling particles be revolving with nearly the same velocity about the attracting centre, the system will generally remain stable, for small disturbances, provided the attracting force. The system differs from the Saturnian system considered by Maxwell in having repelling particles instead of attracting satellites. The present case will evidently be *approximately* realized if we replace these satellites by negatives electrons and the attracting center by a positively charged particle.

Therefore, while the "planetary" model for the atom had been proposed before Rutherford's seminal paper, it was certainly not put on such an experimentally rigorous footing before Rutherford.

2.1.3 The Bohr Model

All is well until one begins to calculate. The trouble remained that, if the atom were indeed a negatively charged particles accelerating classically about a positively charged nucleus, Maxwell's equations would demand that the system radiate away its energy immediately. Some explanation for the nonzero minimum energy of the atom was due, and it came from Niels Bohr. In 1913, Bohr, inspired by Planck's quantized model for radiation [53, 54], reasoned that the action associated with a given electronic orbit could only take multiples of a particular quantum. He postulated:

- Hydrogen has only a single electron
- Different quantized atomic states correspond to different circular orbits about the nucleus

With these basic assumptions, Bohr is able to reproduce Eq. 2.2. It may well be considered the first fundamental, theoretical foray into spectroscopy, and, despite its shortcomings, is successful at reproducing the $\frac{1}{n^2}$ scaling with principal quantum number n associated with the quantized Coulomb potential.

Bohr's model has some significant shortcomings, and fails to explain the spectra of larger atoms, field-induced effects, and fine and hyperfine structure. These were addressed independently by Pauli's matrix-based approach to the quantum theory, and Schrödinger's wave-based approach. Both Pauli and Schrödinger independently arrived at solutions to the hydrogen atom that reproduce the Rydberg lines [55, 56]. The Schrödinger solution ψ_{nlm}, takes the form:

$$\psi_{nlm} = R_{nl}(r)Y_{lm}(\theta, \phi) \tag{2.4}$$

The Radial component $R_{nl}(r)$ takes the form

$$R_{nl} = \sqrt{(\frac{2Z}{na_\mu})^3 \frac{(n-l-1)!}{2n[(n+l)!]}} e^{\frac{-Zr}{na_\mu}} (\frac{2r}{na_\mu})^l L^{2l+1}_{n-l-1}(\frac{2Zr}{na_\mu}) \tag{2.5}$$

where L^{2l+1}_{n-l-1} are the generalized Laguerre polynomials, $a_\mu = \frac{\hbar}{\alpha\mu c}$, where μ is the reduced mass of the electron nucleus system, Z is the nuclear charge, α is the fine structure constant, and c is the speed of light.

The spherical harmonics have the form

$$Y_{lm}(\theta, \phi) = (-1)^m \sqrt{\frac{(2l+1)}{4\pi} \frac{(l-m)!}{(l+m)!}} P^m_l(\cos\theta) e^{im\phi} \tag{2.6}$$

where P^m_l are the associated Legendre polynomials.

2.2 Astrophysical Relevance

Rydberg atoms are more than just a laboratory curiosity; in fact, they are one of the more curious features of the interstellar medium. The interstellar medium is typically unfriendly to many molecules, due to constant bombardment by ionizing radiation, supersonic gas flows, shock waves, expanding H II regions, and remnants of supernova explosions. Despite that, interstellar space is, relative to our own environment, quite cold and dilute. For this reason, when Rydberg states do form, they are less liable to collision-induced decay then their Earth-bound counterparts might be. Astrophysical Rydberg atoms have been observed with principals as high as $n = 1009$ [57].

Moreover, the fact the Rydberg spectra can be known highly exactly, and the fact that they occur in the radio regime, makes them highly useful for characterization of elemental concentrations in various gaseous clusters.

Within the interstellar medium, Rydberg atoms typically form via radiative recombination—that is, an electron will collide with a cation and emit a photon

$$H^+ + e^- \rightarrow H(nl) + \hbar\omega \tag{2.7}$$

where, for hydrogen, $\hbar\omega = \epsilon_e + IP_n$ where ϵ_e is the kinetic energy of the electron and $IP_n = \frac{\hbar c R_\infty}{n^2}$ is the ionization potential for the n-th principal in hydrogen. Here, c is the speed of light and R_∞ is the Rydberg constant. This process can occur for either high or low n, resulting in radio or optical lines, respectively.

For radio lines, the velocity distribution of incident electrons is assumed to be thermal; thus, the velocity distribution is Maxwell-Boltzman

$$f(v) = \sqrt{(\frac{m}{2\pi k_B T})^3} 4\pi v^2 e^{-\frac{mv^2}{2k_B T}} \tag{2.8}$$

Taking this velocity distribution with the velocity dependent recombination cross-section $\sigma(nl|v)$

(as calculated in [58], [59]), we may compute the recombination rate coefficient

$$\alpha(nl;T) = \int f(v)v\sigma(nl|v)dv \tag{2.9}$$

Thus, the relative weights of different Rydberg states can be predicted by detailed balance. At low temperatures, α scales as $n^{-1}T^{-\frac{1}{2}}$, whereas at high temperatures, it scales as [60, 59, 61]

$$\alpha(n;T) \approx T^{-\frac{3}{2}} \ln(n^2 T) \tag{2.10}$$

In lower density plasmas, the process described by Eq. 2.7 is less significant. More significant is the process

$$H^+ + H(nl) \rightarrow H^+ + H(n'l') \tag{2.11}$$

as investigated in [62], where it was discovered that these collision regulate the populations of different l levels. The process

$$e^- + H(n) \rightarrow H^+ + e^- + e^- \tag{2.12}$$

was investigated in the same work [62], and found to regulate the population of different n levels. Rate coefficients for excitation, ionization, and three-body recombination (a chief source of thermalization in ultracold plasmas) were calculated for highly excited Rydberg atoms in [63, 64]. The earliest observations of astrophysical Rydberg atoms were in H II clouds (that is, clouds primarily consisting of ionized hydrogen atoms). These were predicted in [65], and reported in [66, 14].

Rydberg physics later found use in measurement of the relative abundance of helium to hydrogen in these clouds, as performed in [67, 68]. Rydberg atoms also occur in planetary nebulae—clouds of ionized gases more dense than the surrounding medium, formed from late-stage red giant stars. Measurements of radio recombination lines in NGC7027 were reported in [69]. Hydrogen is not the only element to exist in a Rydberg state in the interstellar medium.

Recombination lines in carbon were first reported in [70]. Even heavier elements (chiefly sulfur [71]) were seen in NGC2024 and W3, as reported in [72], and Orion A [73]. The physics of optical recombination lines has been studied in [74, 75, 76], with observations reported in the Orion Nebula and NGC7027 in [77].

In fact, the largest atoms ever observed were astrophysical; in 2007, the UTR- telescope near Kharkov found evidence of $\Delta n = 4$ transitions in carbon up to principals of $n = 1009$ in the Perseus arm at the front of the CasA supernova remnant [57].

2.3 Quantum Defect Theory

In the *ab initio* study of the Rydberg atom, it is sensible to split the problem into two separate ones—that of the core electrons and nucleus (i.e., the singly ionized core), and that of the excited Rydberg electron. This is reasonable due to the large discrepancy between the Rydberg and core electron wavelengths, due to their proximity (and lack thereof, respectively) to the ionization threshold. If we ignore effects stemming from polarization of the core induced by the Rydberg electron, we may assume that the Rydberg electron interacts with a completely frozen core, whose properties will be independent of energy of the Rydberg electron. Thus, the Rydberg electron calculation becomes that of a single electron problem in an energy-independent potential that takes the asymptotic form

$$V(r) = -\frac{e^2}{r},\ r \to \infty \tag{2.13}$$

due to the presence of the frozen, unpolarized core (e is the electron charge, r is the Rydberg electron's distance from the nucleus).

It is clear both that the Rydberg electron wavefunction will bear similarity to the solution for the Hydrogen-like atom (Eq. 2.5), and that WKB and classical approximations will become progressively more accurate with increasing Rydberg electron energy (due to progression towards the classical limit).

Of course, Eq. 2.13 cannot hold exactly, as the Rydberg core is neither frozen nor point-like. The more general form of the potential is

$$V(r) = -\frac{1}{r} + \frac{l(l+1)}{2r^2} + -\frac{1}{2}(\frac{\alpha_d}{r^4} - \frac{\alpha_q}{r^6}) + O(r^{-8}) \tag{2.14}$$

where we have used atomic units. Here $\frac{l(l+1)}{2r^2}$ is the effect from the centrifugal barrier for a Rydberg electron with angular momentum l, $\frac{\alpha_d}{r^4}$ is the contribution from the induced electric dipole in the adiabatic picture (where the Rydberg electron's position is regarded as a slow parameter), and $\frac{\alpha_q}{r^6}$ is the sum of the induced electric quadrupole, and several non-adiabatic effects from the reduced dipole. The derivation and form of these terms is given in [78]. Evaluating the energy shift within zeroth order perturbation theory, we have

$$\Delta E_n = \int_0^\infty dr r^2 R_{nl}(r) \left(-\frac{1}{2}(\frac{\alpha_d}{r^4} - \frac{\alpha_q}{r^6})\right) R_{nl}(r) = \frac{2R_\infty \mu_l}{n^3} \tag{2.15}$$

where R_∞ is the Rydberg constant, and

$$\mu_l = \frac{3\alpha_d}{4l^5} + \frac{35\alpha_q}{16l^9} \tag{2.16}$$

remembering that the unperturbed energy of the hydrogen atom is

$$E_n = -\frac{R_\infty}{n^2} \tag{2.17}$$

we have

$$E_{nl} = -\frac{R_\infty}{n^2} + \frac{2R_\infty \mu_l}{n^3} \tag{2.18}$$

which is in turn the Taylor expansion of

$$E_{nl} = -\frac{R_\infty}{(n-\mu_l)^2} \tag{2.19}$$

for small μ_l.

This suggests that the effect of polarization on the line positions retains the pattern described by Balmer, only with effective principal quantum numbers reduced by an amount μ_l, which decreases sharply with increasing angular momentum l. μ_l is the *quantum defect*, and will enable us to study Rydberg electrons in multi-electron atoms in an *ab initio* fashion to very high accuracy.

If we ignore the polarization terms α_d, α_q, we come to the equation

$$(-\frac{\hbar^2}{2m}\nabla^2 - \frac{1}{r} + \frac{l(l+1)}{r^2})\psi = E\psi \tag{2.20}$$

where the energy associated with angular momentum is contained in the angle-independent $\frac{1}{r^2}$ centrifugal energy term. The effect of the quantum defect is then introduced by letting E take the form given in Eq. 2.19.

$$-\frac{1}{2}\frac{d^2\psi(r)}{dr^2} - \frac{1}{r}\psi(r) + \frac{l(l+1)}{r^2}\psi(r) + \frac{1}{2(n-\mu)^2}\psi(r) = 0 \tag{2.21}$$

We make the transformations $l \mapsto l^* + \frac{1}{2}$, $r \mapsto \frac{(n-\mu_l)}{2}z$

$$\frac{d^2\psi(z)}{dz^2} + \frac{n-\mu_l}{z}\psi(z) + \frac{\frac{1}{4} - l^{*2}}{z^2}\psi(z) - \frac{1}{4}\psi(z) = 0 \tag{2.22}$$

which is simply the Whittaker equation. This will admit solutions

$$e^{(-\frac{z}{2})}z^{\mu+\frac{1}{2}}{}_1F_1(\mu - \kappa + \frac{1}{2}; 1+2\mu; z) \tag{2.23}$$

$$e^{(-\frac{z}{2})}z^{\mu+\frac{1}{2}}U(\mu - \kappa + \frac{1}{2}; 1+2\mu; z) \tag{2.24}$$

where ${}_1F_1$ and U are Kummer's and Tricomi's confluent hypergeometric function. Kummer's function will diverge as $r \to \infty$, and thus we may take only the second solution as the analytical

solution to the single-channel quantum defect theory.

More generally, the solution to the Schrödinger equation for a central potential can be represented in a basis of regular and irregular Coulomb wavefunctions (f and g respectively), such that

$$\psi = \frac{1}{r}(f(E,l,r)\cos\pi\mu_l + g(E,l,r)\sin\pi\mu_l) \tag{2.25}$$

This is the starting point for most descriptions of quantum defect theory, including Seaton's [79]. A simple rearrangement allows us to view μ_l as a scattering phase shift, and ψ as a scattering wavefunction

$$\psi = \frac{\cos\pi\mu_l}{r}(f(E,l,r) + \tan\pi\mu g(E,l,r)) \tag{2.26}$$

f and g have the forms

$$f(E,l,r) = (2r)^{(l+1)}e^{-\frac{r}{\kappa}}\frac{{}_1F_1(l+1-\kappa;2l+2;\frac{2r}{\kappa})}{(2l+1)!} \tag{2.27}$$

$$g(E,l,r) = \frac{\Gamma(l+1-\kappa)}{\pi\kappa^l}(W_{\kappa,l+\frac{1}{2}}(\frac{2r}{\kappa}) + (-1)^l S\frac{\Gamma(l+1+\kappa)}{2(2l+1)!}M_{\kappa,l+\frac{1}{2}}(\frac{2r}{\kappa})) \tag{2.28}$$

where $M_{k,\mu}(z)$, $W_{k,\mu}(z)$ are the Whittaker functions

$$M_{k,\mu}(z) = e^{-\frac{z}{2}}z^{\frac{1}{2}+\mu}{}_1F_1(\frac{1}{2}+\mu-k;1+2\mu;z) \tag{2.29}$$

$$W_{k,\mu}(z) = e^{-\frac{z}{2}}z^{\frac{1}{2}+\mu}U(\frac{1}{2}+\mu-k;1+2\mu;z) \tag{2.30}$$

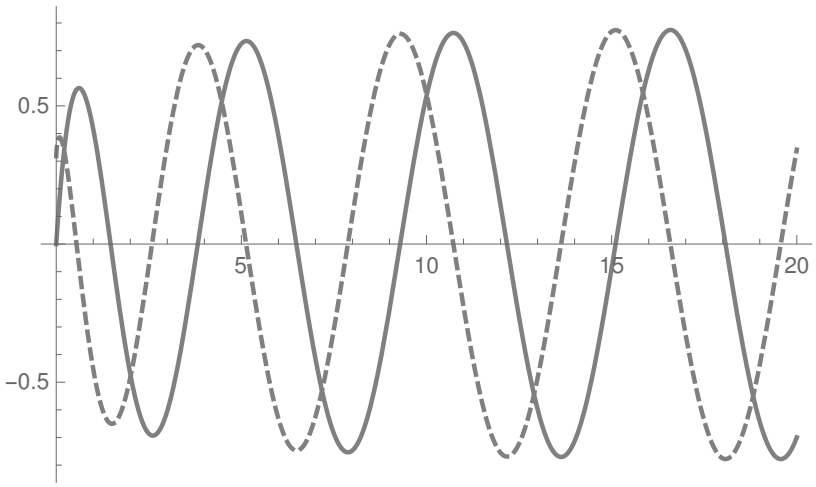

Figure 2.4: $f(-.26, 0, r)$ (solid) and $g(-.26, 0, r)$ (dashed); above threshold, solutions oscillate, asymptotically to a fixed phase separation as $r \to \infty$.

S and κ have the forms [80] [2]

$$S = \begin{cases} \cos\left(\pi |E|^{-\frac{1}{2}}\right), & \text{if } E < 0 \text{ and } r > 0 \\ 0, & \text{if } E < 0 \text{ and } r < 0 \\ e^{\pi e^{-\frac{1}{2}}}, & \text{if } E > 0 \text{ and } r > 0 \\ e^{-\pi e^{-\frac{1}{2}}}, & \text{if } E > 0 \text{ and } r < 0 \end{cases} \tag{2.31}$$

$$\kappa = \begin{cases} \frac{i}{\sqrt{E}}, & \text{if } E > 0 \\ \frac{-1}{\sqrt{-E}}, & \text{if } E > 0 \text{ and } r < 0 \\ \frac{1}{\sqrt{-E}}, & \text{if } E > 0 \text{ and } r > 0 \end{cases} \tag{2.32}$$

It is of course the case that, at large r (i.e., at large distance of the Rydberg electron from the nucleus and core electrons), the angular momentum of the Rydberg core and the Rydberg electron are separately conserved. Therefore, we may conceive of a basis ψ_i consisting of a product the asymptotic electronic eigenvectors and the $(N-1)$-electron wavefunction de-

[2] Here we adhere to the notation used in [80] even though, of course, we only care about the case where $r > 0$

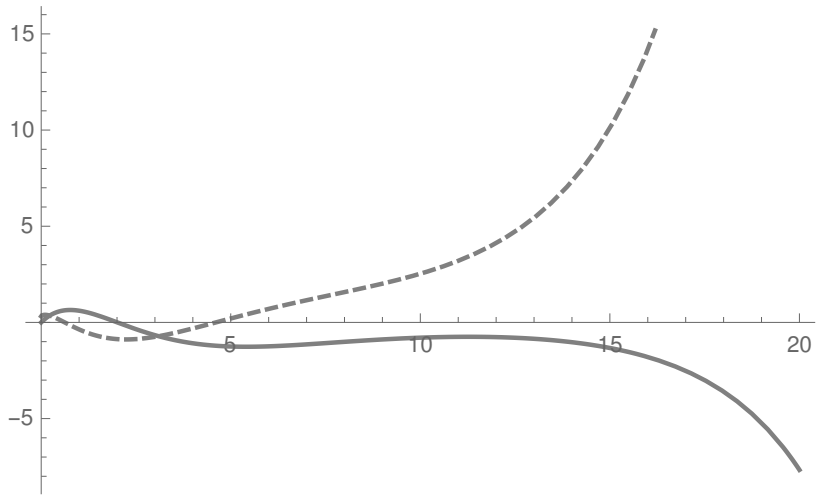

Figure 2.5: $f(-.26, 0, r)$ (solid) and $g(-.26, 0, r)$ (dashed); below threshold, solutions become exponential in the classically forbidden region.

scribing the Rydberg core (for an N-electron atom). At short range (up to a chosen radius r_c), however, the problem remains a full N-electron one. The eigenvectors resulting for this short-range problem will be denoted ϕ_α. ψ_i and ϕ_α both form, in principle, complete basis sets, and therefore the full wavefunction can be represented

$$\Psi = \sum_i A_i \psi_i = \sum_\alpha B_\alpha \phi_\alpha \tag{2.33}$$

At all ranges, ψ_i, ϕ_α can be written in a basis of Coulomb wavefunctions

$$\psi_i = \frac{1}{r} \left(\chi_i f(E_i, l, r) \cos \pi\nu_i - \chi_i g(E_i, l, r) \sin \pi\nu_i \right) \tag{2.34}$$

$$\phi_\alpha = \frac{1}{r} \left(\sum_j U_{j\alpha} \chi_j f(E_i, l, r) \cos \pi\mu_\alpha - \sum_j U_{j\alpha} \chi_j g(E_\alpha, l, r) \sin \pi\mu_\alpha \right) \tag{2.35}$$

Here χ_i is the combined core wavefunction (including spin and angular momentum) and angular momentum (including spin) Rydberg wavefunction, which fully separates from the Rydberg electron radial solution at long range (as in Eq. 2.34) but not at short range (as in Eq. 2.35).

The coefficients A_i and B_α are related by

$$A_i \cos \pi\nu_i = \sum_\alpha U_{i\alpha} B_\alpha \cos \pi\mu_\alpha \tag{2.36}$$

$$A_i \sin \pi\nu_i = -\sum_\alpha U_{i\alpha} B_\alpha \sin \pi\mu_\alpha \tag{2.37}$$

A small bit of manipulation then yields

$$A_i = \sum_\alpha U_{i\alpha} \cos \pi(\nu_i + \mu_\alpha) B_\alpha \tag{2.38}$$

$$0 = \sum_\alpha U_{i\alpha} \sin \pi(\nu_i + \mu_\alpha) B_\alpha \tag{2.39}$$

Eqs. 2.38, 2.39 will have a solution if and only if

$$\det |U_{i\alpha} \sin \pi(\nu_i + \mu_\alpha)| = 0 \tag{2.40}$$

Eq. 2.40 defines the quantum defect surface for the multichannel quantum defect problem.

Chapter 3

Scattering Theory and Rydberg Molecules

3.1 Scattering Formalism

The starting point for most of our inquires into quantum mechanics stem from the usual time-independent Schödinger equation

$$H\psi = E\psi \tag{3.1}$$

As is quite common, we find ourselves with a situation where the Hamiltonian in question, H, has the form

$$H = H_0 + V \tag{3.2}$$

where the eigenstates of H_0 are known, and maybe be denoted $|\phi\rangle$. We wish to study the effect of the perturbation V. This may in principle be done within Rayleigh-Schrödinger perturbation theory, but we can be a bit more precise by delaying our truncation; Instead, we maintain that the equation we wish to solve is

$$(H_0 + V)\,|\psi\rangle = E\,|\psi\rangle \tag{3.3}$$

which may be (nearly) re-expressed as

$$|\psi\rangle = \frac{1}{E - H_0} V |\psi\rangle + |\phi\rangle \tag{3.4}$$

$\frac{1}{E-H_0}$ may be denoted the *resolvent*. This is a more convenient form when considering scattering problems, since it allows us to consider perturbations from states with continuous spectra (which is at best awkward in Rayleigh-Schrödinger perturbation theory), and provides more points at which to truncate various series (and therefore more regimes in which to provide an closely approximate solution).

More properly, we should use the equation

$$|\psi^{(\pm)}\rangle = |\phi\rangle + \frac{1}{E - H_0 \pm i\epsilon} V |\psi^{(\pm)}\rangle \tag{3.5}$$

This is the **Lippmann-Schwinger** equation [81]; the imaginary term $i\epsilon$ added to the denominator in the resolvent makes contour integration of the equation well-defined, and the $\pm$ terms in $|\psi^{(\pm)}\rangle$ account for both incoming and outgoing waves.

We may consider the Lippmann-Schwinger equation in a position basis

$$\langle \vec{x}|\psi^{(\pm)}\rangle = \langle \vec{x}|\phi\rangle + \int d^3x' \, \langle \vec{x}| \, \frac{1}{E - H_0 \pm i\epsilon} \, |\vec{x}'\rangle \, \langle \vec{x}'| \, V \, |\psi^{(\pm)}\rangle \tag{3.6}$$

We make the assumption that the unperturbed states $|\phi\rangle$ are well-represented by plane waves. Therefore, in the position basis,

$$\langle \vec{x}|\phi\rangle = \frac{e^{ip\cdot x/\hbar}}{(2\pi\hbar)^{3/2})} \tag{3.7}$$

with normalization

$$\int d^3x \, \langle p'|\vec{x}\rangle \, \langle \vec{x}|p\rangle = \delta^{(3)}(p - p') \tag{3.8}$$

In the momentum basis, the Lippman-Schwinger equation would take the form

$$\langle p|\psi^{(\pm)}\rangle = \langle p|\phi\rangle + \frac{1}{E - (\frac{p^2}{2m}) \pm i\epsilon} \langle p| V |\psi^{(\pm)}\rangle \tag{3.9}$$

We evaluate the expectation of the resolvent in the position basis (the kernel of the resolvent, or the Green's function) by exploiting the completeness of the momentum basis

$$\langle \vec{x}| \frac{1}{E - H_0 \pm i\epsilon} |\vec{x}'\rangle = \int d^3p' \int d^3p'' \langle \vec{x}|p'\rangle \langle p'| \frac{1}{E - \frac{p'^2}{2m \pm i\epsilon}} |p''\rangle \tag{3.10}$$

$|p'\rangle$, $|p''\rangle$ are eigenstates of H_0, so

$$\langle p'| \frac{1}{E - \frac{p'^2}{2m} \pm i\epsilon} |p''\rangle = \frac{\delta^{(3)}(p' - p'')}{E - \frac{p'^2}{2m} \pm i\epsilon} \tag{3.11}$$

$$\langle \vec{x}|p'\rangle = \frac{e^{ip\cdot x/\hbar}}{(2\pi\hbar)^{3/2}} \tag{3.12}$$

$$\langle p''|\vec{x}\rangle = \frac{e^{-ip\cdot x/\hbar}}{(2\pi\hbar)^{3/2}} \tag{3.13}$$

Therefore the expectation of the resolvent becomes

$$\frac{1}{(2\pi\hbar)^3} \int d^3p' \frac{e^{ip\cdot(x-x')/\hbar}}{E - \frac{p'^2}{2m} \pm i\epsilon} \tag{3.14}$$

leaving us with a single 3-dimensional integral over momentum space. We let $p' \equiv \hbar k'$,

$$\frac{2m}{\hbar^2(2\pi)^3} \int_0^\infty k'^2 dk' \int_0^{2\pi} d\phi \int_{-1}^1 \frac{d(\cos\theta) e^{k'|\vec{x}-\vec{x}'|\cos\theta}}{k^2 - k'^2 \pm i\epsilon} \tag{3.15}$$

Initially evaluating the angular integrals, and extending the region of integration to negative

moment, we have the integral

$$\frac{-m}{4\hbar^2\pi^2}\frac{1}{i|\vec{x}-\vec{x}'|}\int_{-\infty}^{\infty}\frac{dk'k'(e^{ik'|\vec{x}-\vec{x}'|}-e^{-ik'|\vec{x}-\vec{x}'|})}{k'^2-k^2\mp i\epsilon}=$$
$$\frac{-m}{4\hbar^2\pi^2}\frac{1}{i|\vec{x}-\vec{x}'|}\int_{-\infty}^{\infty}\frac{dk'k'(e^{ik'|\vec{x}-\vec{x}'|})}{k'^2-k^2\mp i\epsilon}+\frac{-m}{4\hbar^2\pi^2}\frac{1}{i|\vec{x}-\vec{x}'|}\int_{-\infty}^{\infty}\frac{dk'k'(-e^{-ik'|\vec{x}-\vec{x}'|})}{k'^2-k^2\mp i\epsilon}= \quad (3.16)$$

This integral may be evaluated via contour integration (where finally the $\pm i\epsilon$ term in the denominator of the resolvent is justified).

Let us first shift the denominator of the original resolvent up by $i\epsilon$. There will then be poles at $k' \approx \pm k - i\epsilon$. The term

$$\frac{-m}{4\hbar^2\pi^2}\frac{1}{i|\vec{x}-\vec{x}'|}\int_{-\infty}^{\infty}\frac{dk'k'e^{ik'|\vec{x}-\vec{x}'|}}{k'^2-k^2-i\epsilon} \quad (3.17)$$

should therefore be evaluated by taking the integral with the contour encompassing the upper half plane (as $\lim_{k'\to i\infty} e^{ik'|\vec{x}-\vec{x}'|}=0$), as in Fig. 3.1

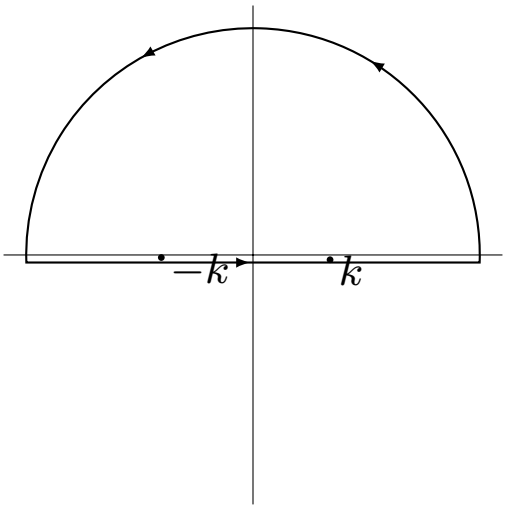

Figure 3.1: Contour in the upper half plane encloses poles

Two poles are encompassed by the contour, each with residue

$$-\frac{m}{4\hbar^2\pi^2}\frac{1}{i|\vec{x}-\vec{x}'|}\frac{e^{ik|\vec{x}-\vec{x}'|}}{2} \quad (3.18)$$

By contrast

$$\frac{m}{4\hbar^2\pi^2}\frac{1}{i|\vec{x}-\vec{x}'|}\int_{-\infty}^{\infty}\frac{dk'k'e^{-ik'|\vec{x}-\vec{x}'|}}{k'^2-k^2\mp i\epsilon} \tag{3.19}$$

should be evaluated by taking the integral with the contour encompassing the lower half plane (as $\lim_{k'\to -i\infty} e^{-ik'|\vec{x}-\vec{x}'|}=0$), This contour contains no poles. Thus, the integral has the overall

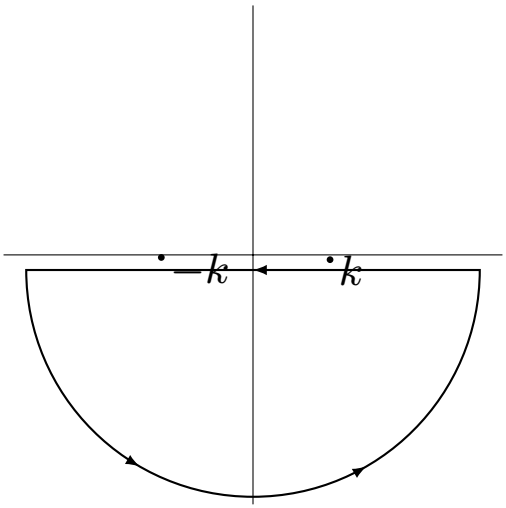

Figure 3.2: Lower contour contains no poles

value (multiplying the sum of the residues by $2\pi i$, according to Cauchy's theorem)

$$-\frac{m}{2\pi\hbar^2}\frac{e^{ik|\vec{x}-\vec{x}'|}}{|\vec{x}-\vec{x}'|} \tag{3.20}$$

Were we to shift the resolvent by $-i\epsilon$, it may be easily shown that the integral will have value

$$-\frac{m}{2\pi\hbar^2}\frac{e^{-ik|\vec{x}-\vec{x}'|}}{|\vec{x}-\vec{x}'|} \tag{3.21}$$

Therefore,

$$\langle\vec{x}|\,\frac{1}{E-H_0\pm i\epsilon}\,|\vec{x}'\rangle=-\frac{m}{2\pi\hbar^2}\frac{e^{\pm ik|\vec{x}-\vec{x}'|}}{|\vec{x}-\vec{x}'|} \tag{3.22}$$

This is quite handy, as it allows us to write the Lippmann-Schwinger equation with only the

perturbing potential operator from before:

$$\langle \vec{x}|\psi^{(\pm)}\rangle = \langle \vec{x}|\phi\rangle - \frac{2m}{\hbar^2}\int d^3x' \frac{e^{\pm ik|\vec{x}-\vec{x}'|}}{4\pi|\vec{x}-\vec{x}'|}\langle \vec{x}'|\, V\, |\psi^{(\pm)}\rangle \tag{3.23}$$

The potential is **local** if

$$\langle \mathbf{x}'|\, V\, |\mathbf{x}''\rangle = V(\vec{x}')\delta^{(3)}(\vec{x}'-\vec{x}'') \tag{3.24}$$

and therefore

$$\langle \vec{x}|\psi^{(\pm)}\rangle = \langle \vec{x}|\phi\rangle - \frac{2m}{\hbar^2}\int d^3x' \frac{e^{\pm ik|\vec{x}-\vec{x}'|}}{4\pi|\vec{x}-\vec{x}'|}V(\vec{x}')\langle \vec{x}'|\psi^{(\pm)}\rangle \tag{3.25}$$

Using the law of cosines, and assuming $|\vec{x}| \gg |\vec{x}'|$,

$$|\vec{x}-\vec{x}'|^2 = |\vec{x}|^2 + |\vec{x}'|^2 - 2|\vec{x}||\vec{x}'|\cos\theta \to |\vec{x}-\vec{x}'| \approx |\vec{x}| - |\vec{x}'|\cos\theta \tag{3.26}$$

θ being the angle between $\vec{x}$ and $\vec{x}'$.

Eq. 3.24 then becomes:

$$\langle \vec{x}|\psi^{(+)}\rangle = \langle \vec{x}|\vec{k}\rangle - \frac{1}{4\pi}\frac{2m}{\hbar^2}\frac{e^{ikr}}{r}\int d^3x' e^{-i\vec{k}'\cdot\vec{x}'}V(\vec{x}')\langle \vec{x}'|\psi^{(+)}\rangle \tag{3.27}$$

We let

$$\langle \vec{x}|\psi^{(+)}\rangle = \frac{1}{(2\pi)^{\frac{3}{2}}}\left[e^{i\vec{k}\cdot\vec{x}} + \frac{e^{ikr}}{r}f(\vec{k}',\vec{k})\right] \tag{3.28}$$

where $f(\vec{k}',\vec{k})$ is the **scattering amplitude**,

$$f(\vec{k}',\vec{k}) = \frac{1}{4\pi}(2\pi)^{\frac{3}{2}}\frac{2m}{\hbar^2}\int d^3x' e^{-i\vec{k}'\cdot\vec{x}'}V(\vec{x}')\langle \vec{x}'|\psi^{(+)}\rangle \tag{3.29}$$

3.2 Scattering Length Formalism

Let us assume that the perturbing potential is spherically symmetric. That is to say that the spherical tensor operator $\hat{T}$ associated with the perturber commutes with both $\vec{J}^2$ and $\hat{J}_z$, $\hat{J},\ \hat{J}_z$ being the total angular momentum operator and its projection along the z-axis, respectively. Therefore,

$$[J_z, T_q^{(k)}] = \hbar q T_q^{(k)} = 0 \tag{3.30}$$

$$[J_\pm, T_q^{(k)}] = \hbar\sqrt{(k \mp q)(k \pm q + 1)}T_{q\pm1}^{(k)} = 0 \tag{3.31}$$

This is to say that $q = 0$ (the commutation relations given above may be regarded as the definition of the spherical tensors $T_q^{(k)}$, as described in Sakurai [81]; requiring commutation of J_z, $T_q^{(k)}$ necessitates that either $q = 0$, or $T_q^{(k)} = 0$).

By the Wigner-Eckart theorem [81],

$$\langle jm|\, T_q^{(k)}\, |j'm'\rangle = \langle j'm'kq|jm\rangle\, \langle j||T^{(k)}||j'\rangle \tag{3.32}$$

Setting $q = 0$, we have

$$\langle jm|\, T_q^{(0)}\, |j'm'\rangle = \langle j'm'00|jm\rangle\, \langle j||T^{(k)}||j'\rangle = \langle j||T^{(k)}||j'\rangle\, \delta_{ll'}\delta_{mm'} \tag{3.33}$$

where, for the scattering Rydberg electron wavefunction, $j = l$, $m = l_z = m$.

This simple result is what allows us to express the Rydberg electron/atom scattering as a superposition of scattering contributions from different partial waves—s-wave, p-wave, etc. Thus,

$$f(\vec{k}', \vec{k}) = -\frac{1}{4\pi}\frac{2m}{\hbar^2}(2\pi)^3\, \langle k'|\, T\, |k\rangle = -\frac{1}{4\pi}\frac{2m}{\hbar^2}(2\pi)^3 \sum_l \sum_m T_l(E) Y_l^m(k') T_{l'}^{m'}(k) \tag{3.34}$$

By convention, $\vec{k}$ points along the z-axis. Furthermore, since

$$\langle l, m|\hat{z}\rangle = \sqrt{\frac{2l+1}{4\pi}}\delta_{m0} \tag{3.35}$$

we have

$$f(\vec{k}', \vec{k}) = \sum_{l=0}^{\infty}(2l+1)f_l(k)P_l(\cos\theta) \tag{3.36}$$

where $\frac{\vec{k}'\cdot\vec{k}}{|\vec{k}'||\vec{k}|} = \cos\theta$, again with the convention that $\vec{k}$ is along the z-axis, with $\vec{k}'$ at an angle θ from the z-axis (this definition of $\cos\theta$ is retained throughout this chapter).

The l-wave scattering amplitude $f_l(k)$ is related to $T_q^{(0)}$ by

$$f_l(k) = -\frac{\pi T_l(k)}{k} \tag{3.37}$$

where we have re-expressed the scalar operator $T_q^{(0)}$ as a scalar function of k. The scattering amplitude may be related to the *scattering length* A_l (or, for higher partial waves, the scattering volume, hypervolume, etc.) by

$$A_l = \lim_{k\to 0} -\frac{T_l(k)}{k(2l+1)} \tag{3.38}$$

We recall 3.28, and note that the expansion of $e^{i\vec{k}\cdot\vec{x}}$ in terms of spherical Bessel functions has the form (from [80], Eq. 10.60.7)

$$e^{i\vec{k}\cdot\vec{x}} = \sum_l (2l+1)i^l j_l(k)P_l(\cos\theta) \tag{3.39}$$

where $j_l(k)$ is the spherical Bessel function. From ([80], Eq. 10.52.3) we have the asymptotic form of $j_l(k)$

$$\lim_{r\to\infty} j_l(kr) = \frac{\sin\left(kr - \frac{1}{2}l\pi\right)}{kr} \tag{3.40}$$

Thus the asymptotic form of Eq. 3.28 becomes

$$\lim_{r\to\infty}\langle\vec{x}|\psi^{(+)}\rangle = \frac{1}{(2\pi)^{\frac{3}{2}}}\sum_l\left[(2l+1)i^l\frac{\sin(kr-\frac{1}{2}l\pi)}{kr}P_l(\cos\theta)+\frac{e^{ikr}}{r}(2l+1)f_l(k)P_l(\cos\theta)\right] \quad (3.41)$$

$$= \frac{1}{(2\pi)^{\frac{3}{2}}}\sum_l(2l+1)\frac{P_l(\cos\theta)}{2ik}\left[[1+2ikf_l(k)]\frac{e^{ikr}}{r}-\frac{e^{-i(kr-l\pi)}}{r}\right] \quad (3.42)$$

Thus, the Lippmann-Schwinger equation in the position basis yields the sum of an ingoing unmodified wave, and an outgoing wave with the prefactor

$$S_l(k) = 1+2ikf_l(k) \quad (3.43)$$

By probability conservation, the scattering matrix $S_l(k)$ must be unitary, and thus we may write

$$S_l = e^{2i\delta_l} \quad (3.44)$$

where δ_l is the *l-wave scattering phase shift*. Here the factor of 2 is purely a convention. Then

$$f_l(k) = \frac{e^{2i\delta_l}-1}{2ik} = -\frac{\tan\delta_l}{k} = \frac{\pi}{k}T_l(k) \quad (3.45)$$

where in the final step we have taken advantage of the unitarity of S_l, i.e. $|S_l(k)| = 1$. Clearly then,

$$T_l(k) = \frac{\tan\delta_l(k)}{\pi} \quad (3.46)$$

Thus, the zero-momentum scattering length (volume, etc.) is related to T by

$$a_l^{2l+1} = \lim_{k\to 0}\left[-\frac{\pi T_l(k)}{k^{(2l+1)}}\right] \quad (3.47)$$

Thus, we are able to express the scattering amplitude (and therefore Hamiltonian) as a sum of components specified by l-wave scattering components, each dependent on incident momentum k.

3.3 Phase Shift Calculation from Central Potential

Thus far, we have not described the calculation of the scattering phase shifts (i.e., scattering lengths) themselves. In collisions with multi-electron atoms and ions, this calculation can become quite complicated; however, if the particle is incident upon a known potential $V(r)$, the phase shift will have an analytical form.

The position space scattering solution Eq 3.42 can be written in a basis of spherical Hankel functions (in turn combinations of the spherical Bessel functions j_l and y_l) $h_l^{(1)} = j_l + iy_l$ and $h_l^{(2)} = j_l - iy_l$

$$\langle \vec{x} | \psi^{(+)} \rangle = \frac{1}{(2\pi)^{\frac{3}{2}}} \sum_l i^l (2l+1) A_l(r) P_l(\cos\theta) \tag{3.48}$$

$$A_l = c_{1,l} h_l^{(1)}(kr) + c_{2,l} h_l^{(2)}(kr) \tag{3.49}$$

We may solve for the coefficients $c_{1,l},\ c_{2,l}$ by fitting to the proper asymptotic behavior (per Eq. 3.42). From ([80], Eq. 10.52.4), in the limit $kr \to \infty$

$$h_l^{(1)}(kr) = i^{-l-1} \frac{e^{ikr}}{kr} \tag{3.50}$$

$$h_l^{(2)}(kr) = i^{l+1} \frac{e^{-ikr}}{kr} \tag{3.51}$$

Thus

$$c_{1,l} = \frac{1}{2} e^{2i\delta_l} \tag{3.52}$$

$$c_{2,l} = \frac{1}{2} \tag{3.53}$$

We may take the logarithmic derivative of $A_l(r)$, taking R to be some long-range value of r

$$\beta_l \equiv \left(\frac{r}{A_l}\frac{dA_l}{dr}\right)_{r=R} = kR \frac{e^{2i\delta_l} h_l^{(1)\prime}(kR) + h_l^{(2)\prime}(kR)}{e^{2i\delta_l} h_l^{(1)}(kR) + h_l^{(2)}(kR)} \tag{3.54}$$

Solving for δ_l yields

$$\delta_l = \frac{1}{2i} \ln \frac{kRh_l^{(1)'}(kR) - \beta_l h_l^{(1)}(kR)}{kRh_l^{(2)'}(kR) - \beta_l h_l^{(2)}(kR)} \tag{3.55}$$

Eq. 3.55 supplies us with an analytical form for δ_l; if we are able to construct a potential or pseudopotential for the system of interest, we are able to calculate the phase shift for arbitrary partial waves.

3.4 The Fermi Pseudopotential

Having established the basics of scattering theory, we now apply it directly to the problem of the interaction of an electron with a neutral alkali atom. We follow the derivation given in Omont [82], but it should be noted that this theory was originally applied by Fermi to the experimental results of Amaldi and Segré in explaining pressure-sensitive line shifts in the Rydberg series [13, 12]. For this reason, this technique is often referred to as the Fermi pseudopotential method.

Let the Hamiltonian of the electron be

$$H = T_e + V + V' = H_0 + V' \tag{3.56}$$

where T_e is the Rydberg electron kinetic energy, V is the potential energy resulting from the interaction of the Rydberg electron with the Rydberg atom core, and V' is a perturbing interacting stemming from the interaction of the Rydberg electron with a neutral atom. Let G be the resolvent of the full, perturber Hamiltonian H.

$$G = \frac{1}{E - H} \tag{3.57}$$

and G_0 the resolvent of the unperturbed Hamiltonian H_0

$$G_0 = \frac{1}{E - H_0} \tag{3.58}$$

G may additionally be represented by the expansion

$$G = G_0 + G_0 V' G_0 + G_0 V' G_0 V' G_0 + \cdots \tag{3.59}$$

We make an expansion in the T-matrix [83] [1]

$$T(E(R)) = V' + V' \langle G_0 \rangle (R) T(E(R)) \tag{3.60}$$

where

$$E(R) = E - V(R) \tag{3.61}$$

is the Rydberg electronic kinetic energy at an internuclear distance R. Note that T is related to the S-matrix by

$$S = 1 + 2iT \tag{3.62}$$

and to the scattering amplitude by

$$\frac{\langle \vec{k} | T | \vec{k'} \rangle}{k} = \delta(|\vec{k}| = |\vec{k'}| = k) f(\vec{k}, \vec{k'}) \tag{3.63}$$

$\langle G_0 \rangle (R)$ is the expectation of the unperturbed resolvent at internuclear distance R.

We note that

$$G = G_0 + G_0 T \left[G_0^{-1} \left(1 - (G_0 - \langle G_0(R) \rangle) T \right) \right] \tag{3.64}$$

[1] There is some ambiguity in the literature with regard to the use of either K, the reactance matrix, or T, which is usually called the T-matrix. Omont additionally uses the notation R, which we avoid due to our use of the variable R to represent the internuclear distance, and Weisskopf uses X. We adhere when possible to Taylor [83].

To show this, let

$$Y = G_0 + G_0 T \left[G_0^{-1} \left(1 - (G_0 - \langle G_0(R) \rangle) T \right) \right] \tag{3.65}$$

The T-matrix definition may be rearranged

$$1 + \langle G_0 \rangle (R) T = V'^{-1} T \tag{3.66}$$

then

$$Y = G_0 + G_0 T \left(G_0^{-1} V'^{-1} T - T \right)^{-1} \tag{3.67}$$

then

$${G_0}^{-1} = G^{-1} + V' \tag{3.68}$$

and finally

$$Y = G_0 + G_0 V' G = G \tag{3.69}$$

If $\langle G_0(R) \rangle$ is neglected , Eq. 3.64 becomes

$$G = G_0 + G_0 \bar{T} \sum_0^\infty (G_0 \bar{T})^n G_0 \tag{3.70}$$

Eq. 3.59 and Eq. 3.64 then together imply that

$$V'(R) = \bar{T}(E(R)) \tag{3.71}$$

Thus, the T-matrix can be used as a surrogate for the perturbing potential. Omont notes that this result is the same as one produced by Ivanov [84].

Having related the perturbing potential to the T-matrix, we can now express expectations of the perturbing potentials in terms of expectations of scattering amplitudes—i.e., we can express the Rydberg electron-neutral perturber scattering potential in terms of partial waves, using the formalism developed previously. Therefore, we may take the expectation $\bar{T}(E(R))$

between states $|i\rangle$ and $|j\rangle$ in a momentum basis

$$\langle \Psi_i | \bar{T}(E(R)) | \Psi_j \rangle = \frac{1}{(2\pi)^3} \int d\vec{p} d\vec{p'} d\vec{r} d\vec{r'} \langle \vec{p'} | \bar{T}(E(R)) | \vec{p} \rangle e^{i\vec{p'}\cdot(\vec{r'}-\vec{R}) - i\vec{p}\cdot(\vec{r}-\vec{R})} \langle \Psi_j(r') | \Psi_i(r) \rangle \tag{3.72}$$

If the matrix $\bar{T}(E(R))$ is assumed to be local, only values of r, r' close to R make a contribution. Then p and p' in the integral in Eq. 3.72 remain close to

$$k_R = \sqrt{\frac{2m}{\hbar}(E - V'(R))} \tag{3.73}$$

which is to say that the wavelength of the electron is constant over the region of interaction. Then

$$\langle \Psi_i | \bar{T}(E(R)) | \Psi_j \rangle = \langle \Psi_i | V'(R) | \Psi_j \rangle = 2\pi \sum_l (2l+1) T_l(R) P_l \left(\frac{\overleftarrow{\nabla} \cdot \overrightarrow{\nabla}}{k_R^2} \right) \Psi_j^*(R) \Psi_i(R) \tag{3.74}$$

where we have used Eqs. 3.36 and 3.37. $\overleftarrow{\nabla}$, $\overrightarrow{\nabla}$ are the gradient operating acting to the left (on the bra) and the right (on the ket) respectively.

The first two terms are

$$\langle \Psi_j | V_0(R) | \Psi_i \rangle = 2\pi T_0(R) \Psi_i^*(R) \Psi_j(R) = 2\pi a_0(k) \Psi_i^*(R) \Psi_j(R) \tag{3.75}$$

$$\langle j | V_1(R) | i \rangle = 6\pi \frac{T_1(R)}{k_R^2} \Psi_i^*(R) \Psi_j(R) = 6\pi a_1^3(k) \Psi_i^*(R) \overleftarrow{\nabla} \cdot \overrightarrow{\nabla} \Psi_j(R) \tag{3.76}$$

Thus, we have a series expansion for the scattering potential expressed as a sum of s-wave, p-wave, and higher terms.

Hinckelmann and Spruch give the following expressions for $T_0(R)$, $T_1(R)$ [85]

$$T_0(R) = a_0 + \frac{\pi}{3} \alpha k_R + \frac{4}{3} \alpha k_R^2 \ln(2k_R d) \tag{3.77}$$

$$T_l(R) = -\frac{\pi}{2}\frac{\alpha k_R}{(2l+3)(2l+1)(2l-1)},\ l \geq 1 \tag{3.78}$$

where α is the dipole polarizability, a_0 is the zero-momentum s-wave scattering length, and d is a scalar on the order of the dimension of the atom [82].

3.5 Born-Oppenheimer Approximation

The problem of the Rydberg diatomic molecule is, strictly speaking, a many-body one. Even if we freeze all the core electrons of the various atoms, we are still left with the valence electrons and nuclei. The full Hamiltonian may thus take the following form

$$H(\vec{r}_e, \vec{r}) = H_n(\vec{r}) + H_e(\vec{r}_e; \vec{r}) \tag{3.79}$$

where $\vec{r},\ \vec{r}_e$ are the positions of the nuclei and electrons respectively. $H_n(\vec{r}),\ H_e(\vec{r}_e; \vec{r})$ are Hamiltonian components corresponding to the nuclear and the electronic degrees of freedom (parametrized by the nuclear phase space coordinates), respectively. $H_n(\vec{r})$ may be divided between kinetic and potential components, such that

$$H_n(\vec{r}) = T_n(\vec{r}) + V_n(\vec{r}) \tag{3.80}$$

In the non-relativistic case, these take the form

$$T_n(\vec{r}) = -\frac{\hbar^2}{2M_i}\sum_i \overrightarrow{\nabla}^2 \tag{3.81}$$

$$V_n(\vec{r}) = \sum_I \sum_{J>I} \frac{Z_I Z_J}{R_{IJ}} \tag{3.82}$$

where summation indices indicate the nuclei, Z_I is the nuclear charge of the Ith nucleus, M_I is the mass of the Ith nucleus, and R_{IJ} is the internuclear distance between the Ith and Jth nucleus.

Similarly, $H_e(\vec{r}_e;\vec{r})$ has the exact, non-relativistic form

$$-H_e(\vec{r}_e;\vec{r}) = \frac{-\hbar^2}{2}\sum_i \frac{\overrightarrow{\nabla}^2}{m_e} - \sum_i\sum_I \frac{Z_I}{r_{iI}} + \sum_i\sum_{j>i}\frac{1}{r_{ij}} \tag{3.83}$$

where capital indices indicate nuclei, lowercase indicate electrons, m_e is the electron mass, r_{iI} is the distance between the ith electron and Ith nucleus, and r_{ij} is the distance between the ith and jth electrons.

We may define an operator $H_{\text{adiabatic}}$

$$H_{\text{adiabatic}}(\vec{r}_e;\vec{r}) = H_e(\vec{r}_e;\vec{r}) + V_n(\vec{r}) \tag{3.84}$$

which in turn will admit eigenfunctions which may be parametrized by the nuclear positions $\vec{r}$.

$$H_{\text{adiabatic}}(\vec{r}_e;\vec{r})\,|\zeta(\vec{r}_e;\vec{r})\rangle_i = E_{i,\text{electronic}}\,|\zeta(\vec{r}_e;\vec{r})\rangle_i \tag{3.85}$$

The total Hamiltonian $H = T_n(\vec{r}) + H_{\text{adiabatic}}(\vec{r}_e;\vec{r})$ will have solutions $|\Psi(\vec{r}_e,\vec{r})\rangle$ that can be expressed as an expansion of adiabatic wavefunctions $|\zeta(\vec{r}_e;\vec{r})\rangle_i$ (the so-called *Born-Oppenheimer expansion*) [86]

$$|\Psi(\vec{r}_e,\vec{r})\rangle = \sum_i |\zeta(\vec{r}_e;\vec{r})\rangle_i\,|\psi_i(\vec{r})\rangle \tag{3.86}$$

We may apply the full Hamiltonian to this solution and integrate away the electronic degrees of freedom (here $\langle\zeta_k|$ is an arbitrary electronic wavefunction)

$$\langle\zeta_k|\,H\,|\Psi(\vec{r}_e,\vec{r})\rangle = \sum_i \langle\zeta_k|\,T_n\,|\psi_i(\vec{r})\rangle\,|\zeta_i\rangle + E_{i,\text{electronic}}\,|\psi_k(\vec{r})\rangle = E\,|\psi_k(\vec{r})\rangle \tag{3.87}$$

The nuclear kinetic energy operator T_n will act on both the electronic and nuclear wave-

functions, since the electronic wavefunctions are parametrized by the nuclear positions.

Taking this convention, we have

$$\sum_i \langle\zeta_k|\, T_n\, |\psi_i(\vec{r})\rangle\, |\zeta_i\rangle = \sum_j \left[-\frac{\hbar^2}{2m_j} \overrightarrow{\nabla}_j^2\, |\psi_k\rangle - \frac{\hbar^2}{2m_j} \sum_i \left(2\, \langle\zeta_k|\, \overrightarrow{\nabla}_j\, |\zeta_i\rangle \cdot \overrightarrow{\nabla}_j + \langle\zeta_k|\, \overrightarrow{\nabla}_j^2\, |\zeta_i\rangle \right) |\psi_i\rangle \right] \tag{3.88}$$

Here the index j denotes the j-th nuclear degree of freedom (thereby indicating its spatial derivatives and masses).

Here we define the non-adiabatic coupling matrix elements for the j-th vibrational degree of freedom $\tau_{ki,j}$, $\tau^{(2)}_{ki,j}$ to be

$$\tau_{ki,j} = \langle\zeta_k|\, \overrightarrow{\nabla}_j\, |\zeta_i\rangle \tag{3.89}$$

$$\tau^{(2)}_{ki,j} = \langle\zeta_k|\, \overrightarrow{\nabla}_j^2\, |\zeta_i\rangle \tag{3.90}$$

The full solution to the Schrödinger equation is then a coupled system made up of that defining the adiabatic electronic wavefunctions and

$$\frac{-\hbar^2}{2} \overrightarrow{\nabla}^2\, |\psi_i\rangle + E_i\, |\psi_i\rangle - \frac{\hbar^2}{2} \sum_k (2\tau_{ki} \cdot \overrightarrow{\nabla} + \tau^{(2)}_{ki})\, |\psi_k\rangle = E\, |\psi_k\rangle \tag{3.91}$$

Within the adiabatic approximation, $\tau_{ki} \to 0,\ \tau^{(2)}_{ki} \to 0$, yielding

$$\frac{-\hbar^2}{2} \overrightarrow{\nabla}^2\, |\psi_i\rangle + E_{i,\text{electronic}}\, |\psi_i\rangle = E\, |\psi_k\rangle \tag{3.92}$$

We may regard $E_{i,\text{electronic}}$ as a potential energy function (referred to either as a *potential energy curve*, in one dimension, or a *potential energy surface* in many), and in so doing the nuclear problem takes the form of the usual time-independent Schrödinger equation; we may use all usual techniques in solving this problem.

This adiabatic approximation may be justified heuristically within perturbation theory. To

first order

$$\nabla_j |\zeta_i\rangle = \frac{|\zeta_i\rangle' - |\zeta_i\rangle}{\epsilon} \tag{3.93}$$

with m_j being the nuclear mass, and where

$$|\zeta_i\rangle' = |\zeta_i\rangle + \sum_{k \neq i} \frac{\langle \zeta_k | \hat{V}'(\epsilon) | \zeta_i \rangle}{E_k - E_i} |\zeta_k\rangle \tag{3.94}$$

By the Virial theorem, when E_k is not close to E_i, the denominator $E_k - E_i$ will scale as $\frac{1}{m_e}$, the reciprocal of the mass of the electron. Thus, $\frac{1}{m_j}\tau_{ki,j} \cdot \overrightarrow{\nabla}_j$ should scale as $\frac{m_e}{m_j}$. The scaling of $\tau_{ki}^{(2)}$ will scale similarly, for similar reasons. Given that the nuclear mass is three or more orders of magnitude larger than the electronic mass, it is usually safe to neglect these terms.

3.6 Non-Adiabatic Effects and the Landau-Zener Formula

Trouble of course arises when E_k becomes close to E_i. To address this, we follow the derivation for the Landau-Zener formula given in [87].

We have two eigenfunctions, ψ_1 and ψ_2 which exchange characteristics at the crossing—i.e., we are in an adiabatic picture. However, due to the non-adiabatic behavior that occurs at the crossing,

$$\lim_{t \to \infty} \psi = A\psi_1 + B\psi_2 \tag{3.95}$$

To simplify the problem and arrive at an analytical form for the crossing probability, we assume that the nuclear motion is wholly classical. Furthermore, we assume that the transition region is sufficiently small that $E_1 - E_2$, in the diabatized picture, may be regarded as linear in time, i.e.

$$E_1 - E_2 = \alpha t \tag{3.96}$$

where α is real, and, for convenience, positive. Furthermore, the coupling in the diabatic picture, f, is regarded as being constant over the region where non-adiabatic effects are non-

negligible. We will assume that f is real and positive.

From the assumption that the nuclear dynamics are classic, we have

$$\psi = A\psi_1 e^{-i\int E_1 dt} + B\psi_2 e^{-i\int E_2 dt} \tag{3.97}$$

where we have assumed (as we will throughout) that $\hbar = 1$. Taking the time-independent Schrödinger equation

$$i\frac{\partial\psi}{\partial t} = H\psi \tag{3.98}$$

We have the pair of coupled equations

$$\frac{dA}{dt} = -ifBe^{i\int \alpha t dt} \tag{3.99}$$

$$\frac{dB}{dt} = -ifAe^{-i\int \alpha t dt} \tag{3.100}$$

which may be decoupled to discover

$$\frac{d^2A}{dt^2} - i\alpha t\frac{dA}{dt} + f^2A = 0 \tag{3.101}$$

$$\frac{d^2B}{dt^2} - i\alpha t\frac{dB}{dt} + f^2B = 0 \tag{3.102}$$

Letting $\tilde{A} = e^{\frac{i\pi}{4}\alpha t^2}A$, we find

$$\frac{d^2\tilde{A}}{dt^2} + (f^2 - \frac{i\alpha}{2} + \frac{\alpha^2}{4}t^2)\tilde{A} = 0 \tag{3.103}$$

which is the Weber equation (whose solutions are the parabolic cylinder functions. Upon the substitution

$$z = \sqrt{\alpha}e^{\frac{-i\pi}{4}}t \tag{3.104}$$

$$\gamma = \frac{f^2}{\alpha} \tag{3.105}$$

Eq. 3.103 takes the the more familiar form

$$\frac{d^2\tilde{A}}{dt^2} - (-i\gamma - \frac{1}{2} + \frac{1}{4}z^2)\tilde{A} = 0 \tag{3.106}$$

We take the solution [88]

$$A(z) = 2^{\frac{i\gamma}{2}-\frac{1}{4}}(iz)^{-\frac{1}{2}}{}_1F_1(-\frac{i\gamma}{2} - \frac{1}{4}, -\frac{1}{4}, -\frac{1}{2}z^2) \tag{3.107}$$

where ${}_1F_1(a;b;z)$ is Kummer's confluent hypergeometric function. We want to know the value of A as $z \to e^{\frac{-i\pi}{4}}\infty$ (i.e., when $t \to \infty$). To do this, we take note of the asymptotic form of Eq. 3.107

$$\lim_{t\to\infty} A(i\sqrt{\alpha}e^{\frac{-i\pi}{4}}t) = e^{\frac{-i\pi}{4}(i\gamma+1)i}e^{\frac{-i\alpha t^2}{4}}(\sqrt{\alpha}t)^{-i\gamma-1} + \frac{\sqrt{2\pi}}{\Gamma(i\gamma+1)}e^{\frac{-\pi\gamma}{4}}e^{\frac{i\alpha t^2}{4}}(\sqrt{\alpha}t)^{i\gamma} \tag{3.108}$$

From which we can find

$$A(\infty) = P_{\text{adiabatic}} = \frac{2\pi\gamma e^{-\pi\gamma}}{\Gamma(i\gamma+1)\Gamma(-i\Gamma+1)} \tag{3.109}$$

$$= 2e^{-\pi\gamma}\sinh\pi\gamma \tag{3.110}$$

$$= 1 - e^{-2\pi\gamma} \tag{3.111}$$

$A(-\infty) = 1$, and Eq 3.111 therefore yield the probability of adiabatic passage. Conversely, the probability of non-adiabatic (diabatic) crossing, the so-called Landau-Zener probability, is

$$P_{\text{diabatic}} = e^{-2\pi\gamma} \tag{3.112}$$

Chapter 4

Charge Transfer in Ultracold Rydberg/Ground-State Atomic Collisions: Ion-Pair Production

4.1 Motivation

The ion pair states form when covalent Rydberg states couple to the long-range ion-pair state—i.e., a Rydberg molecular state where the Rydberg atom has localized, metastably, at the center of a non-Rydberg perturber atom. That is, a *molecular* ion-pair state may be seen as analogous to a Rydberg *atom*, where the role of the Rydberg electron has been supplanted by an anion (see Fig. 4.1), and is therefore sometimes referred to in the literature as a *heavy Rydberg state* (HRS).

We are interested in these heavy Rydberg states for many of the same reasons that we study their lighter cousins; for example, the heavy Rydberg states will exhibit an infinite spectrum of vibrational levels which follow a Rydberg progression with a heavy electron mass, as well as large permanent electric dipole moments. They are also long-range states and thus have typically negligible Franck-Condon (FC) overlap with the usual short-range molecular lev-

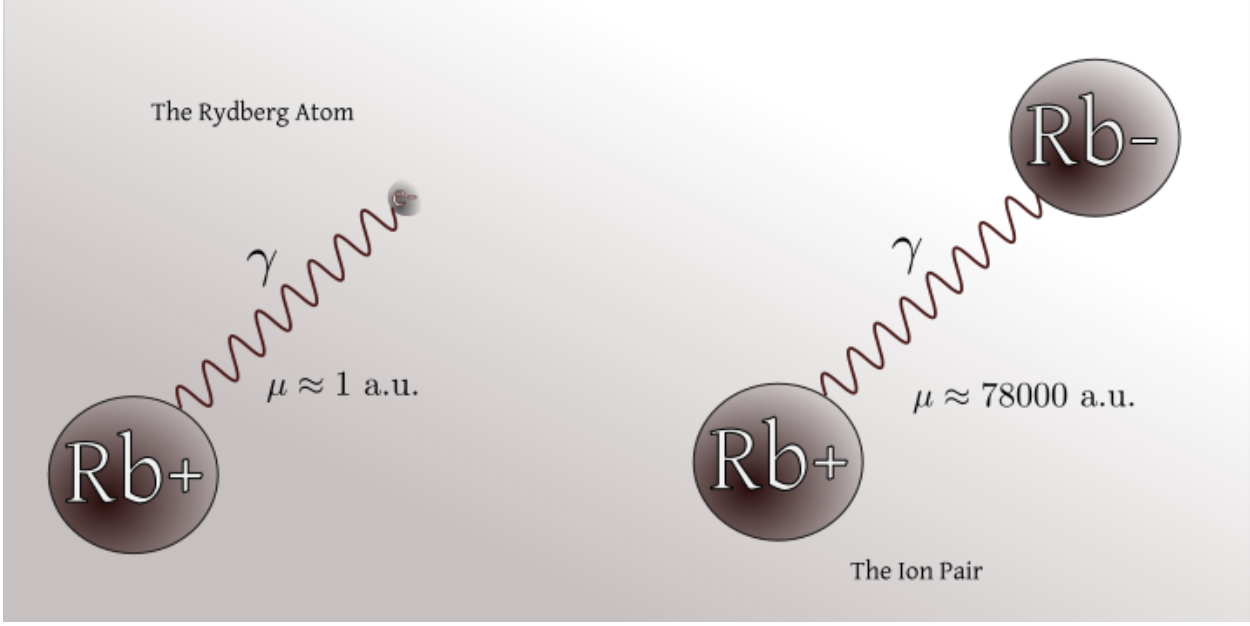

Figure 4.1: Rydberg atoms and the ion pair molecule are analogous

els. These HRS have been experimentally observed in several molecular species, relying on excitation from bound molecular levels [89, 90, 91, 92].

The prevailing issue with indirect excitation of bound molecules, such as in H_2 and Cl_2 [89, 90, 91, 92], is that it is not *a priori* possible to identify a set of long-lived intermediate heavy Rydberg states to which ion the pair states couple. In a recent work [8], it was proposed to directly pump long-lived HRS from ultracold Feshbach molecular resonances, just below the avoided crossings between the covalent potential energy curves and the ion-pair channel. The predominant excitation to HRS occurs near the avoided crossings, because the non-adiabatic mixing allows for favorable electronic transitions to the HRS. When the nuclear HRS wave function peaks at the classical turning point, the internuclear FC overlap increases.

In this work, we develop an analytical, but asymptotic model for one-electron transfer, merging single-center potentials for the Rb atom, and demonstrate efficient field control over the rate of ion-pair formation. Adiabatic potential energy curves are calculated along with the radial non-adiabatic coupling and dipole transition matrix elements. We compare our adiabatic potential energies with the Born-Oppenheimer (BO) potential energy curves from Ref. [93]. We

find that with modest off-resonant external fields, we can alter the avoided crossing beween the covalent HRS and ion-pair channels, and modify the behavior of the nuclear wave function at the classical turning points; hence, control the FC overlaps and rate of ion-pair formation.

This excitation occurs at larger internuclear separations, where the overlap and transition dipole moments between the ground and ion-pair states are significant. The method proposed in [8] requires adiabatic rapid passage or multiphoton transitions to enhance this excitation, while in the present work, only off-resonant fields are employed to increase the efficiency of ion-pair production.

4.2 Methodology and Results

The present charge transfer model relies on one active electron participating in the process of ion-pair excitation. For the charge transfer to occur, the Rb valence electron is ionized from one center, separated from the other neutral center by a distance R. The ionization process is calculated in the one-electron effective potential model of Ref. [94]. The interaction of the electron with the neutral Rb atom is modeled by the short-range scattering of the low-energy electron from the ground-state Rb atom. This is done with a symmetric inverse hyperbolic cosine (Eckart) potential.

The two-center Hamiltonian matrix elements are constructed by expanding in a basis of atomic Rb Rydberg orbitals and the single bound orbital in the Eckart potential. The resulting generalized eigenvalue equation is solved for the adiabatic potential energy curves, radial coupling and electronic dipole matrix elements. Our control scheme hinges on modifying the avoided crossing gap between the 5s+7p and ion-pair states by applying an off-resonant field, thereby tuning the Landau-Zener crossing probabilities between the ion-pair and covalent states.

We assume a single active electron, and therefore assume that the other, ground state electron remains frozen to its rubidium center, and may therefore be absorbed into the pseu-

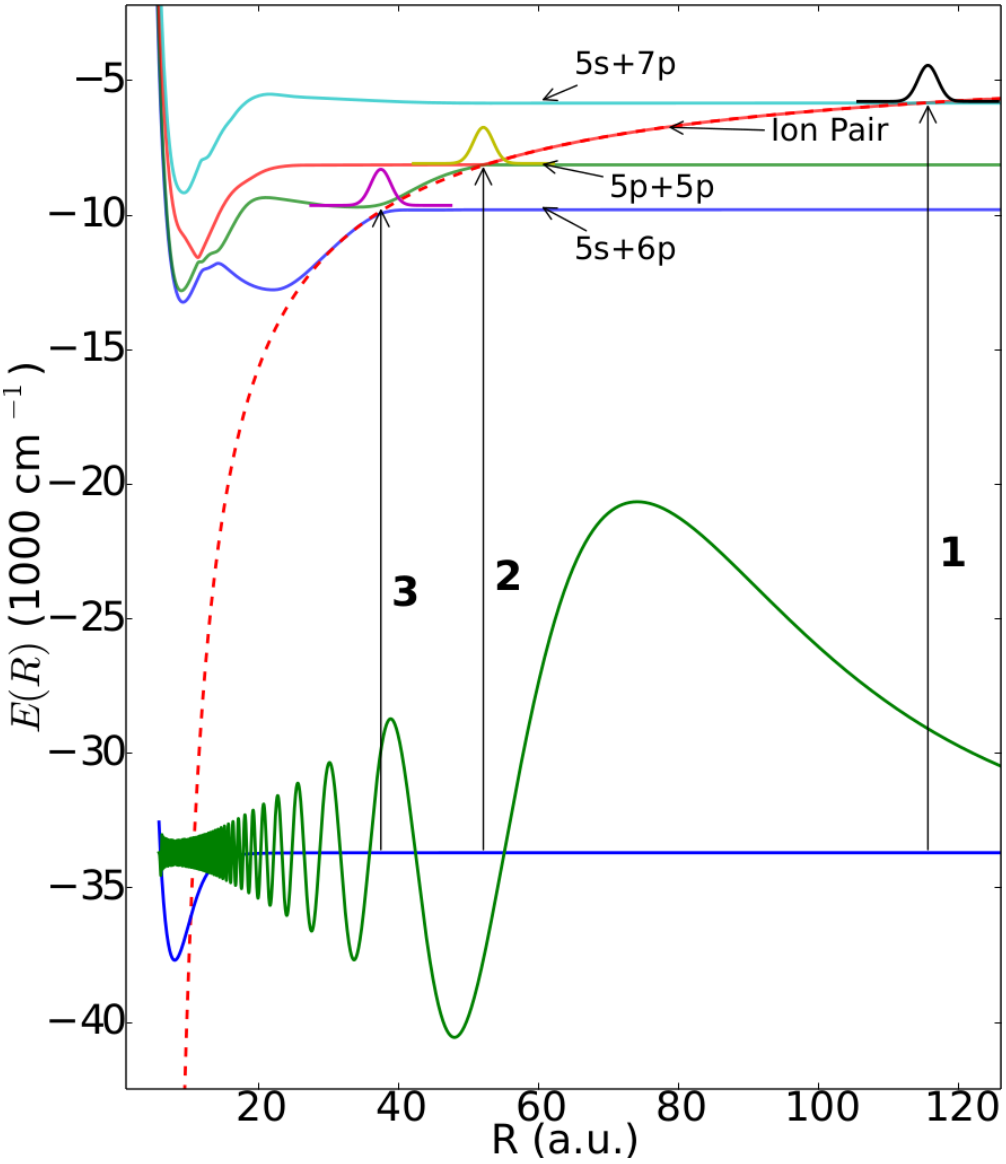

Figure 4.2: Scheme from [8] relied on excitation to the Rb(5s)+Rb(6p)/Rb^++Rb^- or Rb(5p)+Rb(5p)/ion-pair crossings (excitations 2 and 3). Here, we focus on the crossing between Rb(5s)+Rb(7p) and ion-pair channels (excitation 1). Both schemes from [8] require multiphoton excitation or chirped pulse rapid adiabatic passage. Excitation 1, directly to the Rb(5s)+Rb(7p)/ion-pair crossing, can more easily be controlled with dc electric fields. Additionally, the Franck-Condon factors for this excitation are favorable from the $\nu = 124$ Feshbach molecule vibrational wave function (green curve). The dashed curve is the ion-pair potential.

dopotential itself. The two-center potential for the Rb_2 Rydberg-excited molecule is the sum of two single-center potentials,

$$V_{\text{model}}(r_a, r_b; R) = V_1(r_a; R) + V_2(r_b; R) \tag{4.1}$$

where V_1 represents the potential felt by the valence electron due to the Rb core, and the pseudopotential V_2 binds the electron to the neutral rubidium atom; r_a and r_b represent the distances between the electron and the cation/neutral atom, respectively.

We require that the potential in Eq. 4.1 correctly reproduce the asymptotic dissociation energies for all the relevant Rydberg and ion-pair states [95]. We further enforce that the known energy-independent e^--Rb scattering length and the Rb electron affinity are reproduced, i.e. $a_{sc} = -16.1$ a.u. [96] and EA=-0.01786 a.u. [95].

The valence-electron potential, V_1 [94] correctly reproduces the observed atomic energies [95],

$$V_1(r_a) = -\frac{Z_l(r_a)}{r_a} - \frac{\alpha_c}{2r_a^4}(1 - e^{-(r_a/r_c)^6}) \tag{4.2}$$

where

$$Z_l(r_a) = 1 + (z-1)e^{-a_1 r_a} - r(a_3 + a_4 r_a)e^{-a_2 r_a}$$

with z being the nuclear charge; α_c, r_c, a_1, a_2, a_3, a_4 are fitting parameters taken from [94]. The terms of the potential account for screening of the nuclear charge due to core electrons and effect of core polarizability.

For the neutral rubidium electron affinity, we use the radial Eckart potential [97].

$$V_2(r_b) = -V_0 \cosh^{-2}(\frac{r_b}{r_0}) \tag{4.3}$$

where V_0 and r_0 are parameters related in a set of coupled equations to the electron affinity and e^--Rb scattering length; see appendix A. We assume an e^--Rb(5s) zero-energy scattering length. A different technique would use the energy-dependent scattering length. The

polarization term due to the Rydberg electron can be introduced via the regularized Fermi pseudopotential method [98].

The Hamiltonian matrix is constructed from a suitable basis for each center and may be conveniently represented in prolate spheroidal coordinates

$$r = \frac{R}{2}(\xi + \kappa\eta),\ \cos\theta = \frac{1+\kappa\xi\eta}{\xi+\kappa\eta}$$

where $\kappa = +1(-1)$ represents the radial coordinate of the left(right) centers, $\xi \in [1, \infty),\ \eta \in [-1, 1]$.

We solve the generalized eigenvalue problem:

$$\mathbf{H}\vec{\Psi} = E(R)\mathbf{S}\vec{\Psi} \tag{4.4}$$

where $\mathbf{H}$ and S are the Hamiltonian and overlap matrices in the truncated basis:

$$\mathbf{H}_{jj'} = \langle\phi_j^{(a)}|\, H_0^{(a)} + V_2\,|\phi_j^{(a)}\rangle \tag{4a}$$

$$\mathbf{H}_{kk'} = \langle\phi_k^{(b)}|\, H_0^{(b)} + V_1\,|\phi_k^{(b)}\rangle \tag{4b}$$

$$\mathbf{H}_{jk} = \langle\phi_j^{(a)}|\, H_0^{(b)} + V_1\,|\phi_k^{(b)}\rangle = \langle\phi_k^{(b)}|\, H_0^{(a)} + V_2\,|\phi_j^{(a)}\rangle \tag{4c}$$

$$\mathbf{S}_{jj'} = \langle\phi_j^{(a)}|\phi_j'^{(a)}\rangle = \delta_{jj'} \tag{4d}$$

$$\mathbf{S}_{kk'} = \langle\phi_k^{(b)}|\phi_k'^{(b)}\rangle = \delta_{kk'} \tag{4e}$$

$$\mathbf{S}_{jk} = \langle\phi_j^{(a)}|\phi_k^{(b)}\rangle \tag{4f}$$

The full wave function is comprised of $\{\phi_j^{(a)}(\frac{R}{2}(\xi+\eta))\}$ centered on V_1, and $\{\phi_k^{(b)}(\frac{R}{2}(\xi-\eta))\}$ centered on V_2, i. e. $\Psi_i = \sum_j^{n_a} c_{ij}\phi_j^{(a)} + \sum_k^{n_b} c_{ik}\phi_k^{(b)}$. The truncated basis set contains atomic orbitals, $\{\phi_j^{(a)}\} = \{(5\text{-}9)s, (5\text{-}11)p, (4\text{-}6)d\}$, and the short-range wave function

for scattering of electrons from V_2, $\{\phi_k^{(b)}\} = \{\cosh^{-2\lambda}(\frac{r_b}{r_0})\sqrt{z}\ {}_2F_1(0, -2\lambda+1, \frac{3}{2}, z)\}$, with $z = -\sinh^2(\frac{r_b}{r_0})$, and $\lambda = 1.35094$; see Appendix C.4. ${}_2F_1(a, b; c; z)$ is the hypergeometric function [99]. The above one-electron orbitals are single-center orbitals calculated in the potential V_1, Eq. (4.2), and include the full quantum defects of the Rb(nl) states. We note that because we are concerned with interaction at large internuclear separations, there is little charge overlap between wave functions. One major feature of this asymptotic approach is that the permanent and transition dipoles, and non-adiabatic radial coupling matrix elements can now be calculated from the eigenstates of Eq. 4.4. Full details are available in Appendix C.4. The adiabatic potential energy curves, $E(R)$, are shown in Fig. 4.3. By construction, these adiabatic potentials correlate to the asymptotic dissociation energies for the Rydberg and ion-pair states and have avoided crossings between covalent and ion-pair channels. The Rb_2 BO potential energies in the region of Rb(5s)+Rb(6p) dissociation energy are superposed on the adiabatic potentials for comparison. The non-adiabatic coupling matrix element between the ion-pair channel with the molecular Rydberg curve dissociating to Rb(5s)+Rb(7s) is shown in the inset of Fig. 4.3.

4.3 Field Control of Covalent/Ion Pair Channels

The avoided crossing in the interaction of ion-pair channel (Rb^++Rb^-) and Rydberg channel (Rb(5s)+Rb(7p)) is nearly diabatic, i. e. the covalently populated vibrational states will predominantly dissociate to neutral atoms with little possibility of forming HRS and ion-pair states. This is reflected in the narrowness of the avoided crossing and the strength of the radial non-adiabatic matrix element. The two channels have non-zero dipole transition moment, so in an external field, they will mix and modify the transition probability for populating ion-pair states.

Near the avoided crossing, the electronic wave function becomes hybridized in the field, as in the first order of perturbation theory, $|\psi\rangle = |\psi_0\rangle - \sum_{k\neq 0} \frac{\langle\psi_k|\mathbf{F}\cdot\mathbf{z}|\psi_0\rangle}{E_0 - E_k} |\psi_k\rangle$, where $|\psi_k\rangle$ are the dipole-allowed states which couple to the initial state, $|\psi_0\rangle$. This hybridization is demonstrated

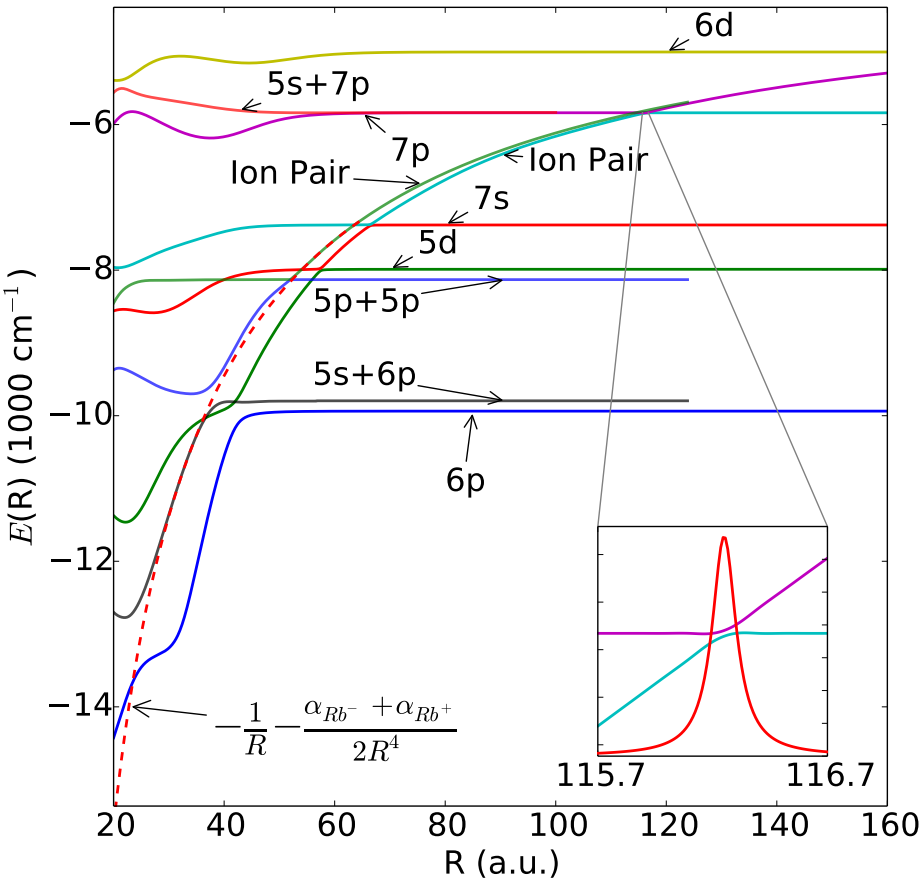

Figure 4.3: Molecular potential energy curves, overlaid with previous BO calculations [93, 100]. The inset shows avoided crossing at $R_c = 116.2$, along with non-adiabatic coupling matrix element between Rb(5s)+Rb(7p)/ion-pair channels. Potential curves correlating to Rb(5s)+Rb(6p), Rb(5p)+Rb(5p), and ion-pair states taken from [93], with potential curves correlating to Rb(5s)+Rb(7p) state taken from [100]. The ion-pair curve is fitted to $-\frac{1}{R}-\frac{\alpha_{\mathrm{Rb}^-}+\alpha_{\mathrm{Rb}^+}}{2R^4}$, where $\alpha_{\mathrm{Rb}^-} = 526.0$ a.u. [101], $\alpha_{\mathrm{Rb}^+} = 9.11$ a.u. [102] are the polarizabilities of the anion and cation respectively.

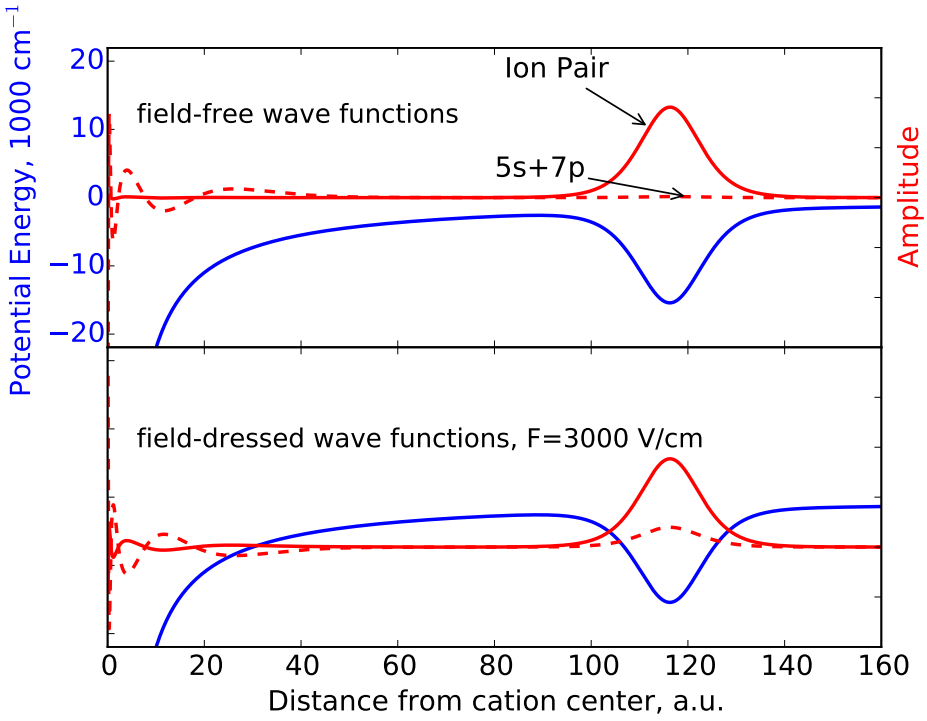

Figure 4.4: Hybridization of the wave functions at the avoided crossing by the field. The upper panel show the amplitude of the field-free electronic wave function along the internuclear axis as a function of distance from the cation center—the electronic states associated with the ion-pair and Rb(5s)+Rb(7p) channels have negligible overlap. The lower panel gives the dressed wave functions at $\mathbf{F} = 3000$ V/cm, showing significant overlap of the wave functions associated with the two channels. The blue line is the potential in Eq. 4.3 along the internuclear axis at $R = 116.2$ a.u.

in Fig. 4.4 for the two channels of interest. When the field is off, the wave function amplitude in the covalent Rydberg channel peaks near the avoided crossing. With the field on, the two amplitudes become comparable.

The probability that ion-pair states survive the single-pass traversal through the avoided crossing region in Fig. 4.3 is approximated by the Landau-Zener formula ([103], see also section 3.6):

$$P_{\text{adiabatic}} = 1 - \exp\left[-2\pi \frac{a^2}{\left|v \frac{\partial(E_2(R) - E_1(R))}{\partial R}\right|}\right] \tag{4.5}$$

where $v = \sqrt{\frac{2(E - V(R_c))}{m}}$ is the velocity of the wavepacket at crossing, $R = R_c$, a is the off-diagonal coupling between the two states at R_c, $\epsilon = E - V(R_c)$ is the collision energy, and

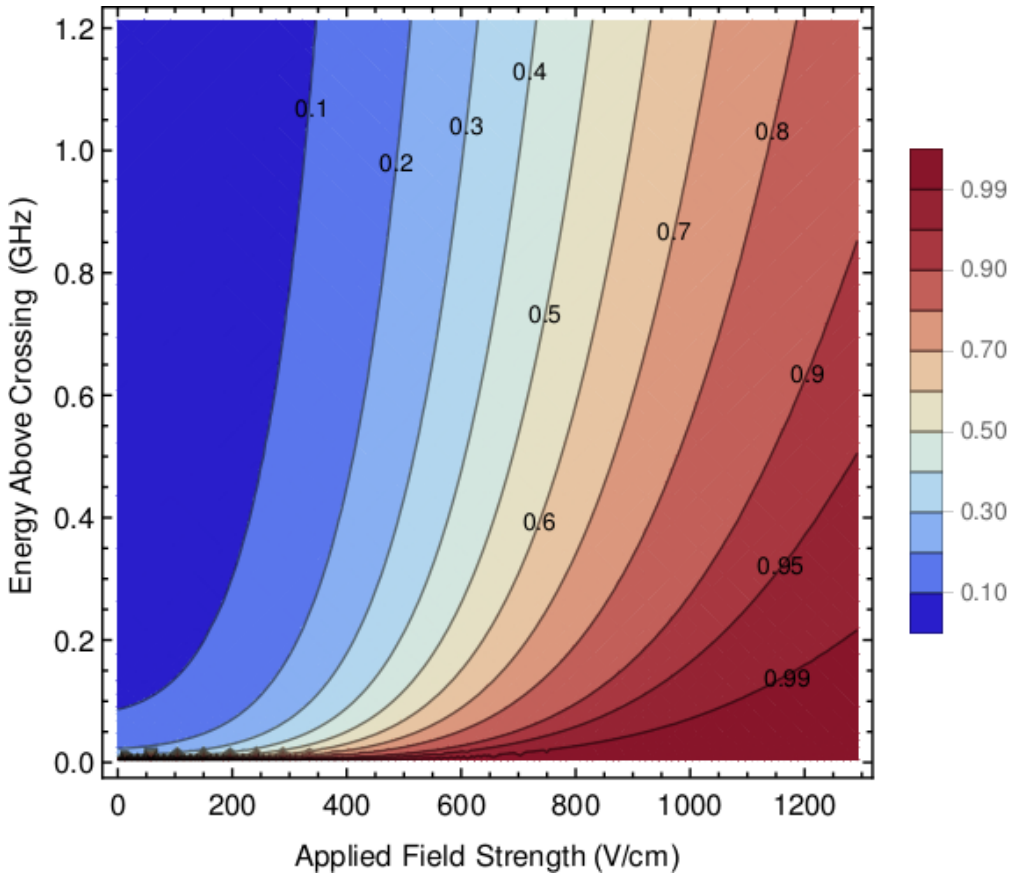

Figure 4.5: The control of ion-pair survival probability is demonstrated as a function of off-resonant electric field. The vertical axis is $\epsilon = E - R_c$. Classical ionization occurs for **F** > 2 MV/cm for states at E greater that of the 7p state. The vertical width of contour regions gives a measure of the survival probability of ion-pair states above a desired threshold for a laser-pulse-excited vibrational wavepacket. For example, at $\mathbf{F} \simeq 1500$V/cm., more than 2 σ_{std} (95%) of ion-pairs will survive at a laser linewidth of ~ 120 MHz.

$\frac{\partial(E_2(R)-E_1(R))}{\partial R}|_{R=R_c}$ is the relative slope of the intersecting curves at $R = R_c$.

Chapter 5

Fine and Hyperfine Corrections to Rydberg Molecular Calculations

5.1 Motivation

Fermi realized that the low-energy scattering of a Rydberg electron from a perturber gas atom can be effectively described by a short-range elastic scattering interaction; this model has had much subsequent success in determining low-energy electron-atom scattering lengths of many other species [104]. The form of zero-energy scattering of an s-wave electron from a perturber is then,

$$H_s(\vec{r},\vec{R}) = 2\pi a_s(0)\delta^{(3)}(\vec{r}-\vec{R}) \tag{5.1}$$

where $\vec{r}$ is the electronic coordinate, measured from the Rydberg core, $\vec{R}$ is the vector connecting the Rydberg nucleus to the perturber atom nucleus, and $a_s(0)$ is the zero-energy s-wave scattering length.

The delta-function contact interaction formalism can be extended to higher scattering angular momenta; an analytical form for p-wave scattering was derived by Omont [82], as

$$H_p(\vec{r},\vec{R}) = 6\pi a_p^3(k)\delta^{(3)}(\vec{r}-\vec{R})\overleftarrow{\nabla}\cdot\overrightarrow{\nabla} \tag{5.2}$$

where $a_p(k)$ is the k-dependent p-wave scattering volume

$$a_{\ell_{sc}}^{2\ell_{sc}+1}(k) = -\frac{\tan\delta_{\ell_{sc}}(k)}{k^{2\ell_{sc}+1}}. \tag{5.3}$$

Here ℓ_{sc} is the orbital angular momentum about the perturber atom and $\ell_{sc} = 0, 1$ denote s- and p-wave scattering of the electron from the perturber atom, respectively. $\delta_{\ell_{sc}}(k)$ is the (k-dependent) ℓ-th multipole component of the S-matrix (see Eq. 3.44).

The Born-Oppenheimer (BO) potential curves, as eigenstates of the Hamiltonian with H_s and H_p contributions, are highly oscillatory in internuclear distance R due to the admixture of Rydberg electron wave functions with high principal quantum numbers n. It was realized in [35, 105] that those multi-well BO potentials can support bound vibrational levels when $a_s(0) < 0$ as is the case for all alkali-metal atoms.

Such exotic molecular Rydberg states were realized in magnetic and dipole traps, first in an ultracold gas of Rb atoms [6], where such Rydberg molecules have $^3\Sigma$ $Rb_2(ns)$ spherical symmetry. It was confirmed that, even though such molecules were homonuclear, the mixing of Rb(ns) levels with Rb$(n-3, l>2)$ hydrogenic manifolds, produces appreciable permanent electric dipole moments in these molecular species [4]. The prediction for Rydberg molecules with kilo-Debye dipole moments (trilobite molecules) were realized with ultracold Cs atoms [106, 5] in which the Cs$(n-4, l>2)$ degenerate manifolds are energetically much closer to Cs(ns) levels, hence providing for much stronger mixing of opposite parity electronic states. More recently, butterfly molecules (Rydberg molecules stemming from the presence of p-wave resonances) were predicted [107, 105] and confirmed [108]. In increasingly dense gases, additional molecular lines stemming from the formation of trimers, tetramers, pentamers, etc. have been observed [109, 110, 30].

The above scattering formalism is spin-independent, i.e. while the scattering phase shifts depend separately on the total spin of electrons, the scattering amplitudes add up incoherently. For Rydberg excitation in a gas of alkali-metal atoms, the total spin channels are S $= |\mathbf{s}_r + \mathbf{s}_g| = 0, 1$ for singlet and triplet scattering, respectively, with $\mathbf{s}_r$ and $\mathbf{s}_g$ the Rydberg electron and the

perturber ground electron spins.

In this work we will account for all of the relevant and relativistic effects in Rydberg perturber atom scattering. We include all of the fine structure resolved s- and p-wave scattering Hamiltonians, the Rydberg electron spin-orbit, and the ground electron hyperfine interactions. From the resulting BO potentials we not only predict the spatial structure and energies of the Rydberg molecules but can also reproduce the spectral line profiles in the recent experiment [111] as shown in Fig. 5.1.

5.2 Hamiltonian

The total Hamiltonian with all spin degrees of freedom included is,

$$H = H_0 + H_{p,T} \cdot P_T + H_{p,S} \cdot P_S + H_{p,T} \cdot P_T + H_{p,S} \cdot P_S + H_{so} + H_{hf} \tag{5.4}$$

where H_0 is the Hamiltonian for the unperturbed Rydberg atom, and $H_{(s,p),T}$ and $H_{(s,p),S}$ are the (s-wave, p-wave) scattering Hamiltonians for triplet and singlet spin configurations, respectively. The operators $P_T = \mathbf{s}_r \cdot \mathbf{s}_g + 3/4$ and $P_S = 1 - P_T$ are the triplet and singlet projection operators for the total electronic spin.

It was first pointed out by Anderson *et al.* [112] that the ground state hyperfine interaction can mix singlet and triplet spin configurations. The hyperfine Hamiltonian is $H_{hf} = A_{hf}\mathbf{s}_g \cdot \mathbf{i}_g$, where $\mathbf{i}_g$ is the nuclear spin and A_{hf} is the hyperfine interaction; in Cs, the focus of this work, A_{hf} = 2298.1579425 MHz, and $i_g = 7/2$. Anderson *et al.* demonstrated this in Rb, where they observed bound vibrational levels due to mixing of singlet and triplet spins, even though the singlet zero energy scattering length for Rb is known to be small and positive. This is particularly important as, in magneto-optical and magnetic traps, spin alignment dictates that the interactions occur via the triplet scattering channel.

The spin-orbit interaction for the Rydberg electron, $H_{so} = A_{so}\mathbf{l}_r \cdot \mathbf{s}_r$, where $\mathbf{l}_r$ is the orbital momentum and A_{so} is the spin-orbit strength for $l_r \neq 0$ levels. Anderson *et al.* neglected this

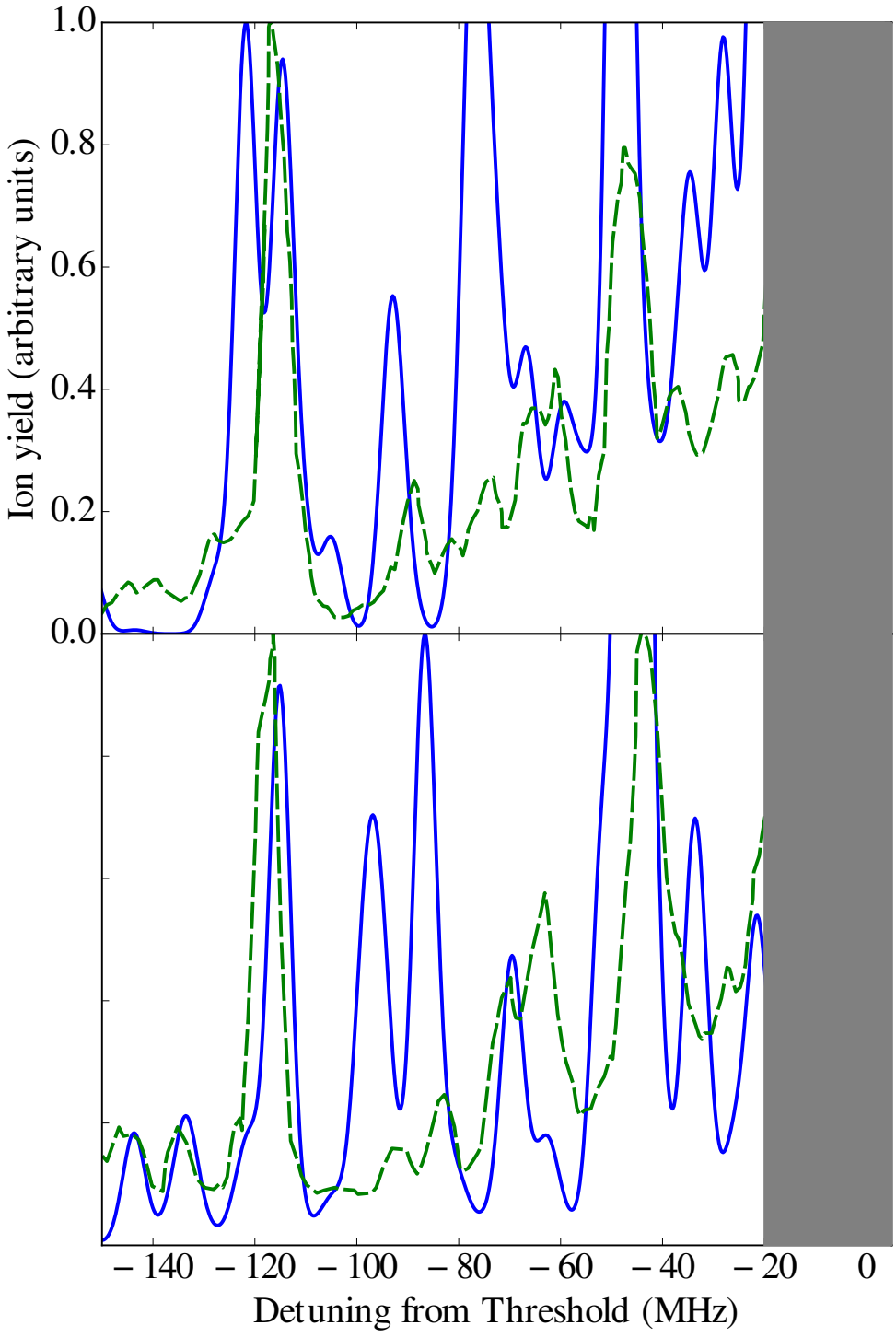

Figure 5.1: The spectral line profiles are calculated (solid lines) and compared with observed spectral line features (dashed lines) in the F=4 (a) and F=3 (b) manifolds. See text for a description of the calculated line profiles. The threshold zero energy is the atomic Rydberg level Cs($32p_{3/2}$). The experimental data are from Ref. [111].

term, because it scales as n^{-3}. For intermediate n, however, the spin-orbit splitting will be comparable to the hyperfine splitting. The details of the matrix elements of H_{so} and the terms for Cs(np) states will follow below.

Recent studies have explored the extent to which spin effects are necessary to properly predict, *ab initio*, the vibrational spectra of these molecules, largely concluding that fine, hyperfine, and p-wave effects can have significant effects on these spectra [112, 111]. To date, no study has incorporated all of the interaction terms (s-wave, p-wave, spin-orbit, and hyperfine) on the vibrational spectra of Cs Rydberg molecules. Due to the large hyperfine shift in ^{133}Cs, and the existence of several p-wave resonances at intermediate energies, these contributions can be significant in Cs. The current results are employed here to interpret the observations by Saßmannshausen *et al.* [111].

5.3 Hamiltonian Matrix Elements

The matrix elements of the unperturbed Rydberg Hamiltonian (H_0) are calculated from the solutions $\phi_{nl_rm_r}(\vec{r})$ to the equation $H_0\phi_{nl_rm_r}(\vec{r}) = -\frac{1}{2(n-\mu_{l_r})^2}\phi_{nl_rm_r}(\vec{r})$, where the quantum defects μ_{l_r} for Cs atom levels are used as follows:

l_r	μ_{l_r}
0	4.05739
1	3.57564
2	2.471396
3	0.0334998
4	0.00705658
≥ 5	0

We use the spherical coordinate system centered at the Rydberg core, as portrayed in Fig. 5.2. The Rydberg orbitals forming our truncated basis set are comprised of $\{ns, (n+1)s, np, (n-1)d, (n-3)l_r \geq 3, (n-4)l_r \geq 3\}$ Rydberg wave functions.

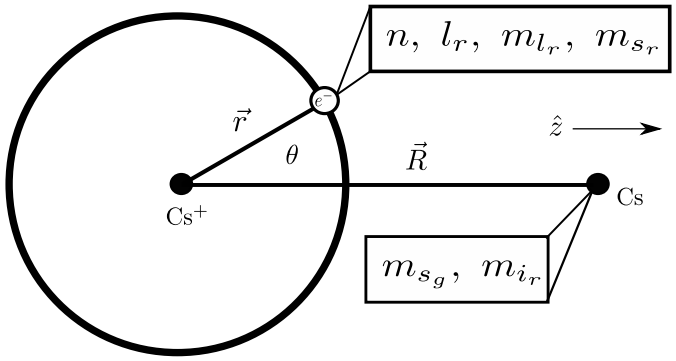

Figure 5.2: The coordinate system used throughout the text. Boxes show the six quantum numbers describing the basis set. The electron spins for the Rydberg and ground state atoms are: s_r, s_g, while the ground state atom nuclear spin i_g. Only the magnitude of the total angular momentum $\mathbf{K} = \mathbf{l}_r + \mathbf{s}_r + \mathbf{s}_g + \mathbf{i}_r$ and its projections are in general good quantum numbers.

The asymptotic form for the radial wave function is given by

$$F_{nl_r}(r) \propto r^{l_r} e^{-\frac{r}{n-\mu_{l_r}}} {}_1F_1\left(l_r - n + 1 + \mu_{l_r}, 2 + 2l_r, \frac{2r}{n-\mu_{l_r}}\right) \tag{5.5}$$

where ${}_1F_1$ is the confluent hypergeometric function. For $\mu_l = 0$, this reduces to the usual hydrogenic solution:

$$F_{nl_r}(r) = \sqrt{\left(\frac{2}{n}\right)^3 \frac{(n-l_r-1)!}{2n(n+l_r)!}} e^{-\frac{r}{n}} \left(\frac{2r}{n}\right)^{l_r} L_{n-l_r-1}^{(2l_r+1)}\left(\frac{2r}{n}\right) \tag{5.6}$$

where $L_n^{(\alpha)}$ is the generalized Laguerre polynomial. For non-integer quantum defects, the wave functions $F_{nl_r=1,2}$ diverge at origin. To remedy this problem, they are matched to numerically calculated wave functions at small-r [94].

Spin-dependent s-wave interaction.— The Hamiltonian matrix elements describing s-wave scattering between basis functions $|\phi_i\rangle$ and $\langle\phi_j|$ are,

$$\langle\phi_i|H_s|\phi_j\rangle = 2\pi \sum_S a_s^S(k) \langle\phi_i| \delta^{(3)}(\vec{R}-\vec{r}) |\phi_j\rangle \times \\ \langle s_{r_i}, m_{s_{r_i}}, s_{g_i}, m_{s_{g_i}}|S, m_{S_i}\rangle \langle S, m_{S_j}|s_{r_j}, m_{s_{r_j}}, s_{g_j}, m_{s_{g_j}}\rangle \quad (5.7)$$

where $|\phi_i\rangle$ is shorthand for the basis element $|n_i l_{r_i} m_{l_{r_i}} m_{s_{r_i}} m_{s_{g_i}} i_{s_{g_i}}\rangle$, and $m_{S_i} = m_{s_{r_i}} + m_{s_{g_i}}$ is the total spin projection along the internuclear axis. The s-wave scattering length $a_s^S(k)$ has been generalized to accommodate the ($S = 0, 1$) singlet and triplet scattering lengths.

Spin-dependent p-wave interaction.— Additional caution is necessary when dealing with the p-wave electron-atom scattering, which depends on the total electronic spin $\mathbf{S} = \mathbf{s}_r + \mathbf{s}_g$ and angular momentum $\mathbf{J} = \boldsymbol{\ell}_{sc} + \mathbf{S}$ centered on the perturber atom. The triplet ($S = 1$) p-wave scattering phase shift in Cs exhibits a relatively large splitting for J =0,1,2. This is in contrast to previous studies in Rb where the triplet p-wave scattering length is treated as a single resonance. The resulting Cs p-wave scattering interaction operator thus takes the form

$$\hat{H}_p = 6\pi \sum_{J,m_J;S,m_S} (a_p^{J,S}(k))^3 \delta^{(3)}(\vec{R}-\vec{r}) \overleftarrow{\nabla} \cdot \overrightarrow{\nabla} |Jm_J; Sm_S\rangle \langle Jm_J; m_S| \quad (5.8)$$

where $S = 0, 1$ and m_J is the projection of **J** along the internuclear axis. In the uncoupled basis $|nl_r m_{l_r}; Sm_S\rangle$, where $|nl_r m_r\rangle$ is a Rydberg orbital and $|Sm_S\rangle$ is the total spin state of the two electrons, matrix elements of this interaction take on the form

$$\langle\phi_i| \hat{H}_p |\phi_j\rangle = (\bar{a}_p^{m_{\ell_{sc}} m_S})^3(k) \delta_{m_{l_{r_i}} m_{l_{r_j}}} \delta_{m_{S_i} m_{S_j}} \cdot \langle\psi_i| \delta^{(3)}(\vec{R}-\vec{r}) \overleftarrow{\nabla} \cdot \overrightarrow{\nabla} |\psi_j\rangle \quad (5.9)$$

with the effective scattering volume as

$$(\bar{a}_p^{m_{\ell_{sc}} m_S})^3(k) = \sum_{J=0,1,2} \Big(\langle (\ell_{sc}=1) m_{\ell_{sc}}, (S=1) m_S | J m_J \rangle^2 \cdot (a_p^{J,S=1})^3(k) \Big) \cdot P_T + \Big(\langle (\ell_{sc}=1) m_{\ell_{sc}}, (S=0) m_S | (J=1) m_J \rangle^2 \cdot (a_p^{J=1,S=0})^3(k) \Big) \cdot P_S \quad (5.10)$$

where $\langle L m_{\ell_{sc}}, S m_S | J m_J \rangle$ is a Clebsch-Gordan coefficient coupling the orbital angular momentum of the Rydberg electron to the combined total spin of the ground state atom and Rydberg electron. Note that $m_{\ell_{sc}} = m_{l_r}$, since angular momentum projections are invariant under translation along the axis of projection. Because of the projection onto the p-wave relative angular momentum states, only Rydberg states with spatial angular momentum projection $m_l = 0$ or ± 1 contribute to the interaction.

The spatial integral in Eq. 5.9 can be evaluated as

$$\langle \phi_i | \, \delta^{(3)}(\vec{R} - \vec{r}) \overleftarrow{\nabla} \cdot \overrightarrow{\nabla} \, | \phi_j \rangle = \lim_{\vec{r} \to R\hat{z}} \Bigg\{ \frac{2l_i + 1}{4\pi} \delta_{m_{l_i} 0} \frac{\partial F^*_{n_i l_i}(r=R)}{\partial r} \frac{\partial F_{n_j l_j}(r=R)}{\partial r} + \delta_{|m_{l_i}| 1} F^*_{n_i l_i}(r=R) F_{n_j l_j}(r=R) \quad \cdot \int d(\cos\theta) d\phi \nabla Y^*_{l_i m_{l_i}}(\theta, \phi) \cdot \nabla Y_{l_j m_{l_j}}(\theta, \phi) \Bigg\} \delta_{m_{l_i} m_{l_j}}, \quad (5.11)$$

where $Y_{lm}(\theta, \phi)$ is a spherical harmonic, $F_{nl}(r)$ is the radial part of the Rydberg wave function, and we suppress the subindex r on (l, m) for notational convenience. It should be noted that the radial derivatives only act on wave functions with $m_l = 0$ while the angular derivatives $\nabla Y_{l_j m_{l_j}}$ are only non-zero for states with $m_l = \pm 1$.

S- and P-wave scattering phase shifts.— In order to fully characterize the electron-perturber interaction, the s- and p-wave scattering lengths must be determined. In the case of $a_p^{J=0,1,2,S=1}$ and $a_s^{S=1,0}$, these are derived by solving the scattering equation including the polarization potential $V_{e^-\text{-}Cs} = -\alpha/2r^4$ where $\alpha = 402.2$ a_0^3 is the polarizability of the ground state Cs atom.

We extract the phase shift by enforcing a hard wall boundary condition at short range ($r_0 \lesssim 3$ a.u.) on the polarization potential.

For $a_s^{(S=1,0)}$, we adjust the hard wall to reproduce experimentally known zero-energy scattering lengths. For $a_p^{J=0,1,2,S=1}$, the position of the hard wall by is chosen so as to enforce a resonance in the scattering phase shift, i.e. $\delta_E = \pi/2$, at a resonant energy E consistent with experimental measurements. While it is unlikely that this simple procedure captures all of the details of the p-wave electron-atom scattering process, the effects of the p-wave interaction on the molecular potentials are largely captured by the position and width of the ^3P_J scattering resonances. Specifically, we set the position of the $^3P_1$ to 8 meV, as observed [113]. The $^3P_0$ and $^3P_2$ resonance positions are set to respectively be 3.8 meV below and 7.2 meV above the $^3P_1$ resonance position in accordance with [114]. The energy-dependent phase shifts for S=0 and 1 spin scattering in s-wave and p-wave are shown in Fig 5.3.

Rydberg spin-orbit matrix elements.— The Rydberg electron spin-orbit Hamiltonian has the form $H_{so} = A_{so}(n, l_r)\mathbf{l}_r \cdot \mathbf{s}_r$, whose coefficients for Cs(np) states have been measured in [116]. The matrix elements are

$$\langle \phi_i | H_{so} | \phi_j \rangle = A_{so}(n, l_r)\mathbf{l}_r \cdot \mathbf{s}_r \tag{5.12}$$

where, for $l_r = 1, 2, 3$ [116]

$$A_{so}(n, l_r) = \left(l_r + \frac{1}{2}\right)^{-1} \left[A(l_r)(n - \epsilon(n, l_r))^{-3} + B(l_r)(n - \epsilon(n, l_r))^{-5} + C(l_r)(n - \epsilon(n, l_r))^{-7}\right] \tag{5.13}$$

where $\epsilon(n, l_r) = \epsilon^*(l_r) + a(l_r)(n - \epsilon)^{-2}$

The l_r-dependent parameters A, B, C, ϵ, a are

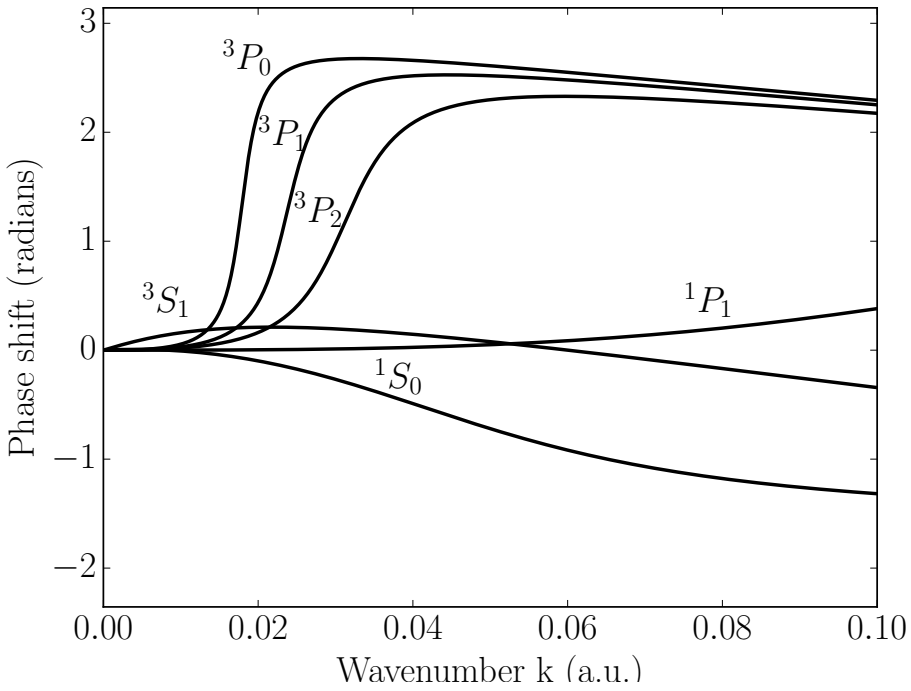

Figure 5.3: The $^{1,3}S_J$, $^{1,3}P_J$ electron- Cs($6s$) phase shifts as a function of the electron scattering momentum are reproduced here. The $^1P_1$ phase shift was obtained from a calculation by U. Thumm [115]. The $^{1,3}S_0$ and $^3P_{J=0,1,2}$ resonant phase shifts are obtained by matching a short distance boundary condition to experimental measurements of scattering resonances [113, 94].

	$l_r = 1$	$l_r = 2$	$l_r = 3$
$A(l_r)$ (MHz)	2.13925e8	6.02183e7	-9.796e5
$B(l_r)$ (MHz)	-5.6e7	-5.8e7	1.222e7
$C(l_r)$ (MHz)	3.9e8	0.0	-3.376e7
ϵ^*	3.57531	2.47079	0.03346
a	0.3727	0.0612	-0.191

while for $l_r \geq 4$, $A_{so}(n, l_r)$ takes on its hydrogenic values:

$$A_{so}(n, l_r) = \frac{\mu_0}{4\pi} g_l \mu_B^2 \frac{1}{n^3 l_r (l_r + \frac{1}{2})(l_r + 1)} \tag{5.14}$$

where g_l is the Landé g-factor, μ_0 is the vacuum permeability, and μ_B is the Bohr magneton.

In the uncoupled angular momentum basis, the operator $\mathbf{l}_r \cdot \mathbf{s}_r$ has the representation [81]

$$\mathbf{l}_r \cdot \mathbf{s}_r = l_{z_r} s_{z_r} + \frac{1}{2} l_{+_r} s_{-_r} + \frac{1}{2} l_{-_r} s_{+_r} \tag{5.15}$$

where $(l, s)_{r,\pm}$ are the ladder operators for the Rydberg electron orbital angular momentum and spin. This representation allows to determine the matrix elements between different combinations of angular harmonic $Y_{l_i,m_{l_i}}$ and spinors $\chi_{s_i,m_{s_i}}$

$$\langle Y_{l_i,m_{l_i}} \chi_{s_i,m_{s_i}} | \, \mathbf{l}_r \cdot \mathbf{s}_r \, | Y_{l_j,m_{l_j}} \chi_{s_j,m_{s_j}} \rangle \, . \tag{5.16}$$

They are

$$\langle \mathbf{l}_r \cdot \mathbf{s}_r \rangle = \begin{cases} m_{l_i} m_{s_i} & \text{if } l_i = l_j, s_i = s_j, \\ & \quad m_{l_i} = m_{l_j}, m_{s_i} = m_{s_j} \\ \frac{1}{2}\sqrt{l_i(l_i+1) - l_{z,i}(l_{z,i} \pm 1)} & \\ \cdot \sqrt{s_i(s_i+1) - s_{z,i}(s_{z,i} \mp 1)} & \text{if } l_i = l_j, s_i = s_j, \\ & \quad m_{l_i} = m_{l_j} - 1, \\ & \quad m_{s_i} = m_{s_j} + 1 \\ \frac{1}{2}\sqrt{l_i(l_i+1) - l_{z,i}(l_{z,i} \mp 1)} & \\ \cdot \sqrt{s_i(s_i+1) - s_{z,i}(s_{z,i} \pm 1)} & \text{if } l_i = l_j, s_i = s_j, \\ & \quad m_{l_i} = m_{l_j} + 1, \\ & \quad m_{s_i} = m_{s_j} - 1 \end{cases} \tag{5.17}$$

Through the ladder terms, the spin-orbit coupling will therefore couple Σ and Π- states, as well as singlet (S=0) and triplet (S=1) states.

Ground hyperfine matrix elements.— The ground electron hyperfine interaction Hamiltonian matrix elements are calculated as

$$\mathbf{s}_g \cdot \mathbf{i}_g = s_{z_g} i_{z_g} + \frac{1}{2} s_{+_g} i_{-_g} + \frac{1}{2} s_{-_g} i_{+_g} \tag{5.18}$$

where $(s, i)_{\pm,g}$ are the ladder operators for the perturber valence electronic and nuclear spins.

We chose to demonstrate the utility of our method toward calculation of the vibrational spectrum of Cs$(6s_{1/2})$-Cs$(32p_{3/2})$ Rydberg molecules [111]. For this particular Rydberg excitation, the fine-structure splitting $\Delta E_{32p_{1/2}-32p_{3/2}}$ is nearly degenerate with the ground state hyperfine splitting, $\Delta E_{hf} \approx 9.2$ GHz.

For ^{133}Cs with $i_g = 7/2$, therefore, our full basis, including angular momentum degrees of freedom, is

$$\begin{aligned}
\{32s, 33s, 32p, 31d, & n = 29, 3 \leq l_r \leq 28, \\
& n = 28, 3 \leq l_r \leq 27\} \\
& \times \{-l_r \leq m_{l_r} \leq l_r\} \\
& \times \left\{ m_{s_r} = \pm \frac{1}{2} \right\} \\
& \times \left\{ m_{s_g} = \pm \frac{1}{2} \right\} \\
& \times \left\{ m_{i_g} = \pm \frac{1}{2}, \pm \frac{3}{2}, \pm \frac{5}{2}, \pm \frac{7}{2} \right\}.
\end{aligned} \tag{5.19}$$

We truncate this basis such that no basis element has $|m_{l_r}| > 2$ The total number of basis states included in our calculation is 8480.

The projection of the total angular momentum, $\mathbf{K}$ onto $\mathbf{R}$, $m_K = m_{l_r} + m_{s_r} + m_{s_g} + m_{i_g}$ is a good quantum number, so that the basis set diagonalization need only be performed in blocks of 1060, 1008, 851, 638, 422, 209, and 52 elements, for $|m_K| = \frac{1}{2}, \frac{3}{2}, \frac{5}{2}, \frac{7}{2}, \frac{9}{2}, \frac{11}{2}, \frac{13}{2}$, respectively.

5.4 Results and Discussions

In Fig. 5.4, we show the full set of BO potential energy curves which result from the diagonalization of Eq. 5.4 with the basis functions defined in Sec. 5.3. This landscape of Rydberg potential energies reveals the influence of the three ${}^3P_J$ resonances. Due to the different widths of J-resonances, see Fig. 5.3, the avoided crossings of molecular potentials in R occur at different locations with the various unperturbed Rydberg manifolds. For example, near the 31d Rydberg level, the ${}^3P_1$ resonance crosses before the narrower ${}^3P_0$ resonance.

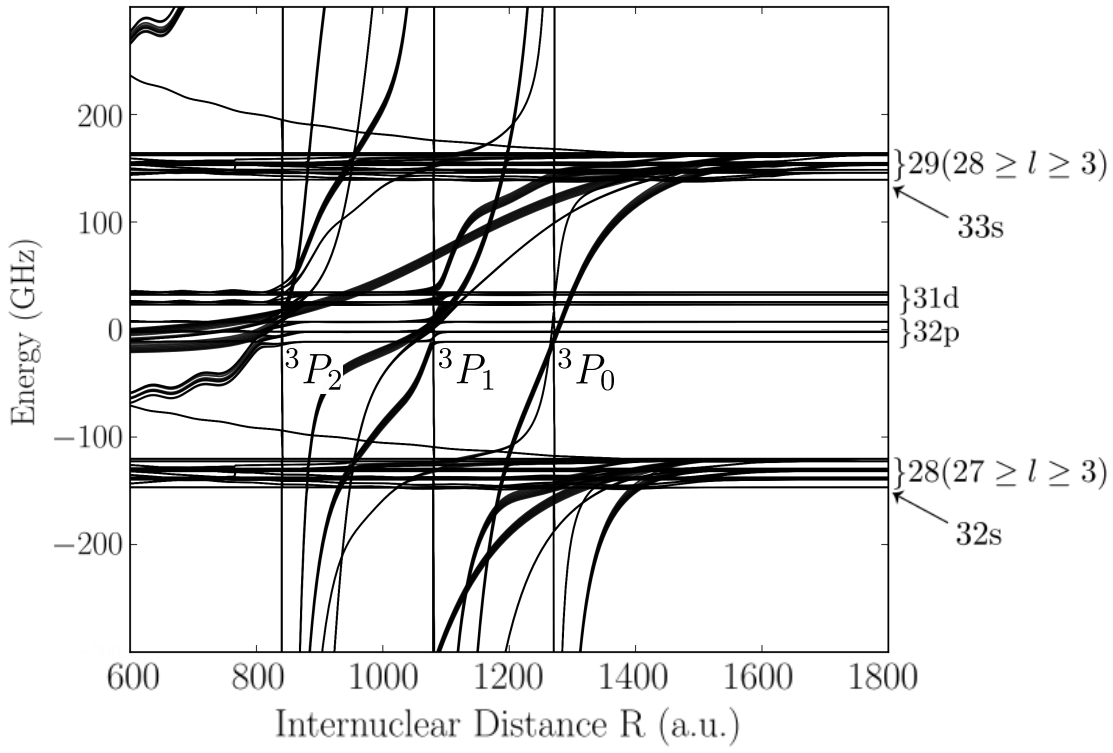

Figure 5.4: Born-Oppenheimer potential energy curves. The atomic Rydberg dissociation levels are indicated on the right side of the graph; two sets of degenerate hydrogenic manifolds are employed. Each Rydberg level is split due to SO and HF interactions in the Rydberg and ground states. On the scale shown, the Rydberg molecule energy landscape also highlights the dramatic influence of the ${}^3P_J$ resonances (labeled in the figure) which manifest themselves in the complicated set of avoided crossings.

While in Fig. 5.4 the potential energy curves are shown for all possible projections m_K,

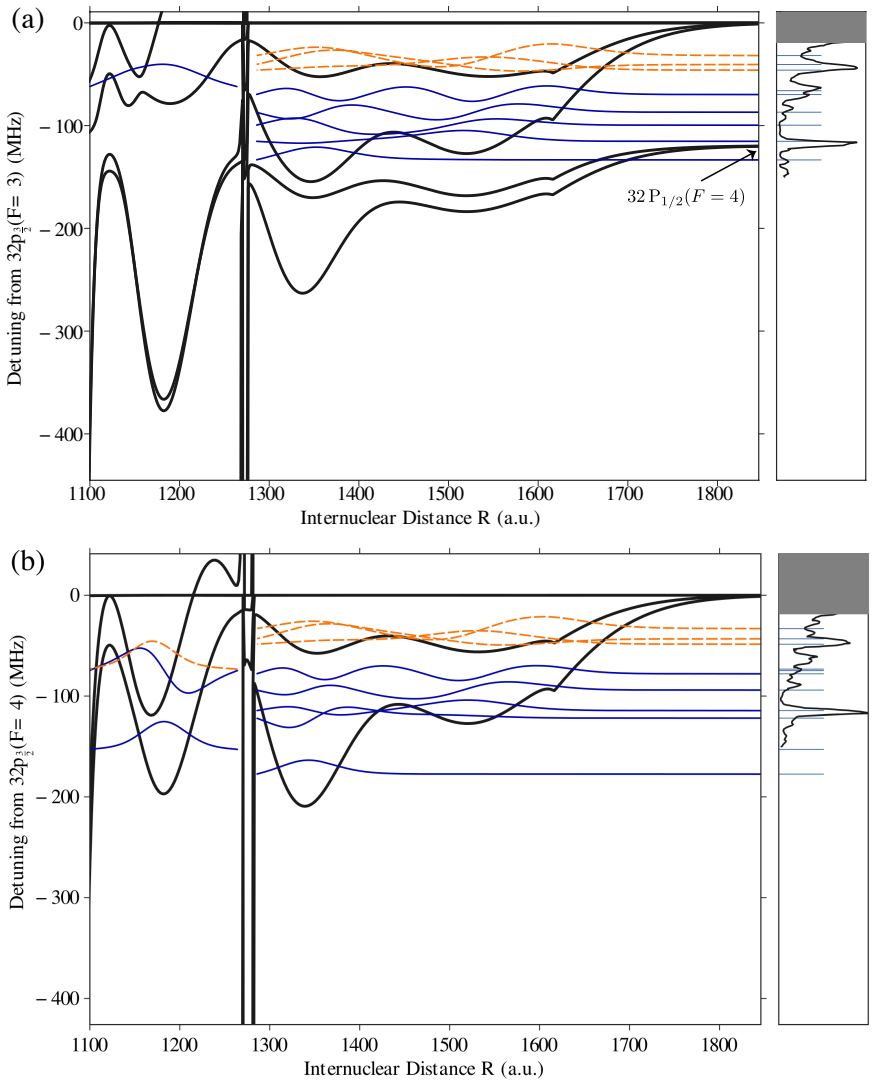

Figure 5.5: (a) The BO potential energy curves correlating to the Cs$(6s)$ - Cs$(32p_{3/2})$ F=3 asymptote, for the total projection quantum number $m_K = \frac{1}{2}$. There are two sets of potential curves (solid black): the lower two curves correlate to the Cs$(32p_{1/2})$ F=4 atomic threshold and are within ~ 100 MHz of the F=3 threshold because in Cs$(32p)$ excitation, the Rydberg spin-orbit and the ground hyperfine splittings are nearly degenerate. The lowest curve in each set corresponds to the predominantly triplet symmetry and the upper curve in each set becomes sufficiently attractive to support vibrational levels (dashed lines) due to the mixing of triplet and singlet channels. The vertical lines are due to the presence of a narrow $^3P_0$ scattering resonance which crosses several atomic Rydberg levels; another crossing due to the $^3P_1$ scattering resonance is near $R \sim 1100\ a_0$. In the F=3, $m_K = \frac{1}{2}$ manifold of states, the $\nu = 0$ vibrational states in the predominantly triplet and mixed electronic potentials have, respectively, permanent electric dipole moments of 9.8 and 3.7 D; (b) the potential energy curves correlating to the Cs$(6s)$ - Cs$(32p_{3/2})$ F=4 asymptote and the associated vibrational levels. The calculated vibrational energies are shown as blue sticks on the right side panes, which illustrate the experimental absorption sprectra.

in Fig. 5.5 we show in detail the BO potentials for $m_K = 1/2$. In the outer region, there are two distinct sets of curves; the lower set corresponds to the potential curves dissociating to the Cs$(6s_{1/2})$ - Cs$(32p_{1/2})$ $F = 4$ threshold, and the upper set of curves dissociate to the Cs$(6s_{1/2})$ - Cs$(32p_{3/2})$ $F = 3$ threshold. The $F = 3$ and $F = 4$ thresholds are within ~ 100 MHz of each other because in excitation of Cs$(32p)$, the Rydberg SO and the ground HF splittings are nearly degenerate. Within each set, the lowest curve refers to a predominantly triplet potential energy curve and the upper curve refers to the more mixed singlet/triplet potential. Generally, in the outer region, defined by internuclear distances R greater than all the p-wave resonance crossings, the predominantly triplet curve will have greater than 90% triplet character — the singlet mixing enters mainly through the $^1\Pi$ molecular symmetry — while the mixed curve will have between 60% and 70% triplet character. There will also be other non-binding potential energy curves (up to two more in a given m_K block) which largely have Π character. We stress that all of these molecular potentials are admixtures of Σ and Π symmetry states; Δ contributions are in principle also present, but not of significance here. On the scale of Fig. 5.5 the relativistic ^3P_J scattering resonances manifest themselves as sharp vertical lines.

We calculate the bound vibrational wave functions in the Born-Oppenheimer approximation using the previously calculated potential energy curves. The resulting Rydberg molecular binding energies are indicated by the thin blue lines in the rightmost pane of each figure, together with the absorption spectra measured in [111]. It is evident from the comparison that many of the spectral features in the experiment are reproduced in Fig. 5.5, which demonstrates that the experiment resolves different m_K vibrational lines.

The BO potential energy curves correlating to the Cs$(6s)$ - Cs$(32p_{3/2})$ F=3 and 4 asymptotes for $m_K = \frac{3}{2}$, $m_K = \frac{5}{2}$, $m_K = \frac{7}{2}$, and $m_K = \frac{9}{2}$, are shown in Figs. 5.6, 5.7, 5.8, 5.9. The corresponding molecular bound states lead to additional spectral features that can be identified by comparing the vibrational energies to the observed spectral features. For $m_K = \frac{9}{2}$, the $F = 4$ potential energy curves are not binding, and for the $F = 3$ potential energy curves, there is no contribution from the $^3P_0$ scattering resonance, and hence the absence of any

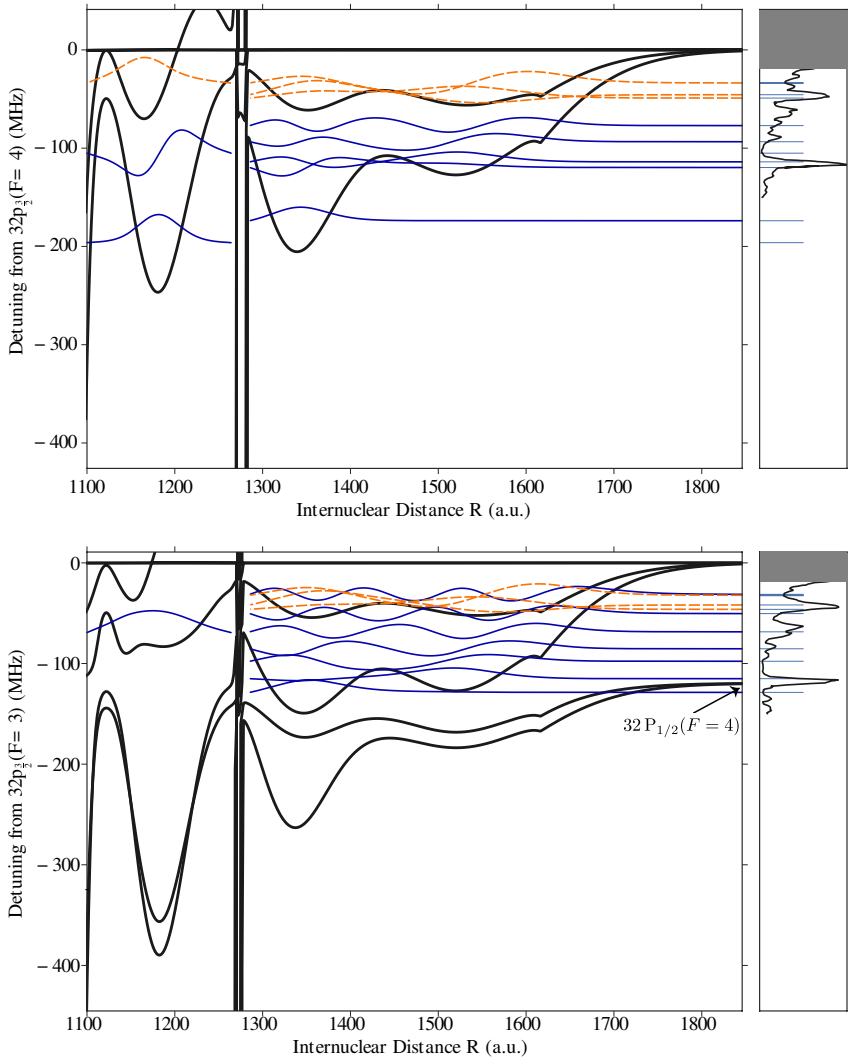

Figure 5.6: Potential energy curves for $|m_K| = \frac{3}{2}$, F=4 (upper), and F=3 (lower). For outermost wells, the curves are slightly less deep than for $|m_k| = \frac{1}{2}$.

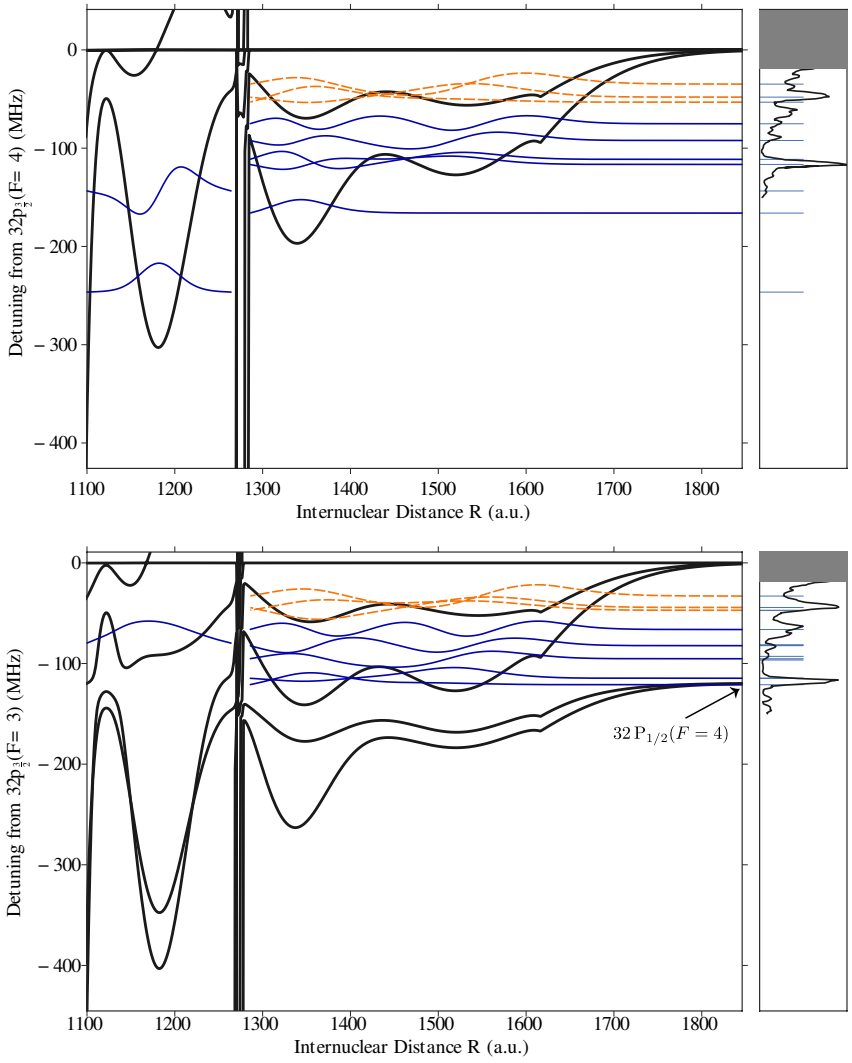

Figure 5.7: Potential energy curves for $|m_K| = \frac{5}{2}$, F=4 (upper), and F=3 (lower). For outermost wells, the curves are slightly less deep than for both $|m_k| = \frac{1}{2}$ and $|m_K| = \frac{3}{2}$.

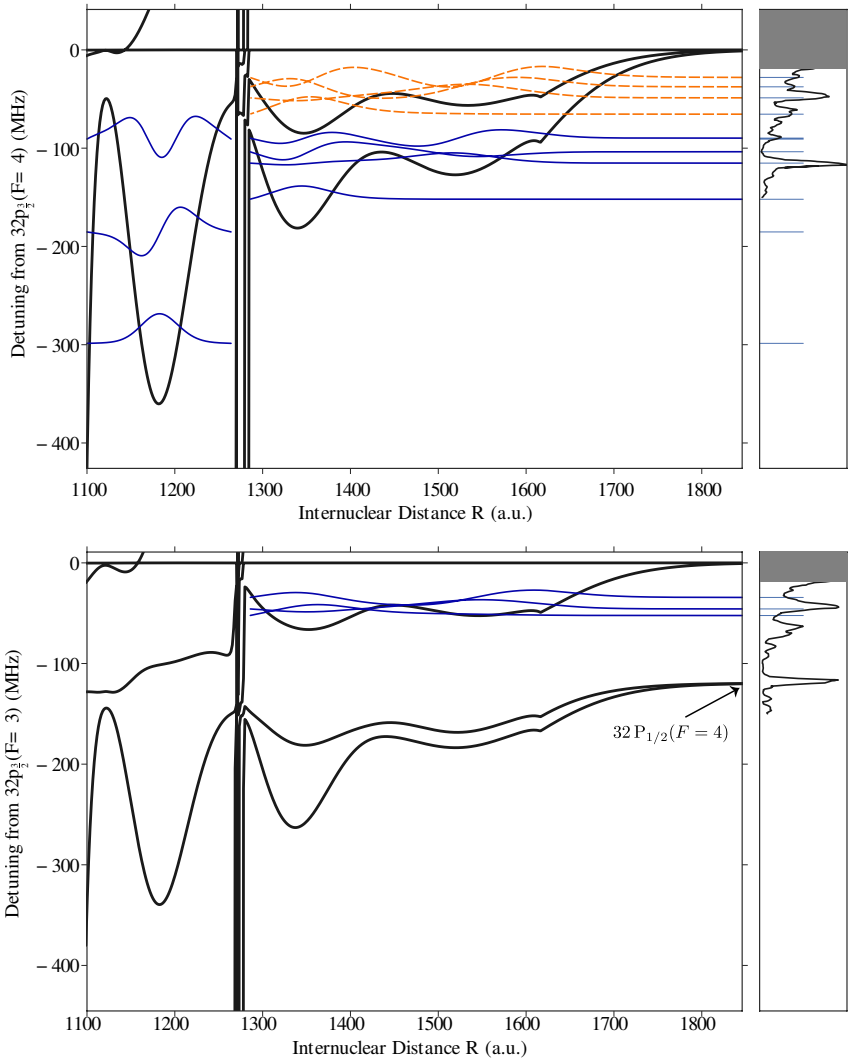

Figure 5.8: Potential energy curves for $|m_K| = \frac{7}{2}$, F=4 (upper), and F=3 (lower). For outermost wells, the curves are slightly less deep than for $|m_k| = \frac{1}{2}$, $|m_K| = \frac{3}{2}$, and $|m_K| = \frac{5}{2}$.

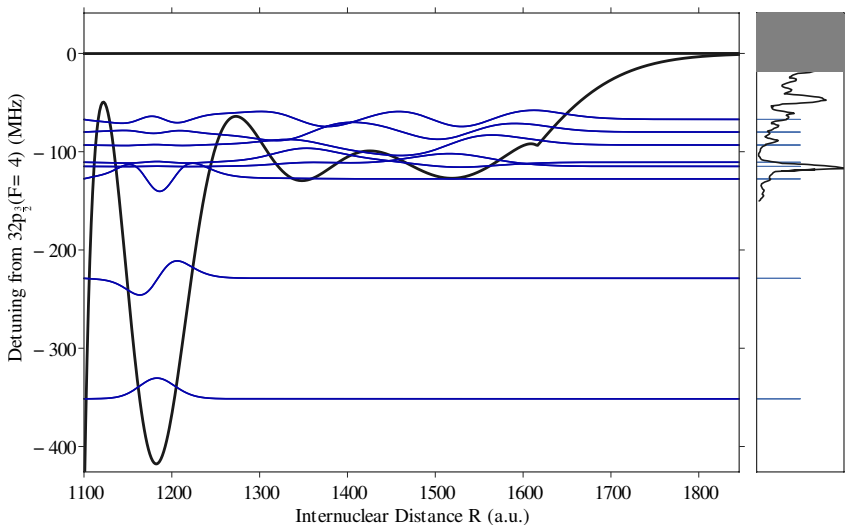

Figure 5.9: Potential energy curves for $|m_K| = \frac{9}{2}$. For Cs, this is the largest value of $|m_K|$ that will allow states of Σ molecular symmetry. Since J is forbidden from being 0, there is no $J = 0$ p-wave resonance.

sharp avoided crossings.

Spin weighting.— To accurately calculate the transition rates in photoassociation of trapped gas atoms into Rydberg molecules, we must take into account the electronic transition dipoles, as well as both the nuclear Franck-Condon and spin-overlap integrals. We assume that the atom pairs, which will bind into a Rydberg molecule, are initially in states $|6s(F_{r_0} = \bar{F}), 6s(F_{g_0} = \bar{F})\rangle$, i.e. the ground state atoms are in the same hyperfine state $\bar{F}$ when optically pumped [111], and $F_{r_0}(F_{g_0})$ refers to the hyperfine state of the ground state atom which will be Rydberg excited (will remain in the ground state). This initial state will be mixed uniformly and incoherently about $m_{F_r}, m_{F_g} \in \{-\bar{F}, \cdots, \bar{F}\}$. For a given initial m_{F_r}, m_{F_g}, the oscillator strength between two electronic states at internuclear distance R is proportional to

$$\langle 6s(F_{r_0}, m_{F_{r_0}}), 6s(F_{g_0}, m_{F_{g_0}})| \hat{d} |\psi\rangle \tag{5.20}$$

where $|\psi\rangle = \sum_i a_i |\phi_i\rangle$ are the calculated electronic eigenstates, and $\hat{d}$ is the electric dipole operator.

The overlap integral in Eq. 5.20 then becomes

$$O(R; m_{F_{r_0}}, m_{F_{g_0}}) = \langle 6s \cdots | \, \hat{d} \, | \psi(R) \rangle \, \langle F_{r_0} m_{F_{r_0}} | \psi(R) \rangle \, \langle F_{g_0} m_{F_{g_0}} | \psi(R) \rangle \, . \tag{5.21}$$

We neglect in $\langle 6s \cdots | \, \hat{d} \, | \psi \rangle$ the contributions to $|\psi\rangle$ other than the 32p state.

For experimentally realized temperatures, the wave function of the ground state atom pair is constant on the scale of the Rydberg molecule wave function. Therefore the vibrational Franck-Condon factors take the form,

$$FC_\nu(m_{F_{r_0}}, m_{F_{g_0}}) \propto \int dR R^2 \psi_\nu(R) O(R; m_{F_{r_0}}, m_{F_{g_0}}) \tag{5.22}$$

for a given vibrational state $\psi_\nu(R)$.

The overall Rydberg molecule formation rate is an incoherent sum over these Franck-Condon factors

$$\Gamma_\nu \sim \sum_{m_{F_{r_0}}} \sum_{m_{F_{g_0}}} |FC_\nu(m_{F_{r_0}}, m_{F_{g_0}})|^2 G_L, \tag{5.23}$$

where G_L accounts for the laser profile. The calculated absorption line profiles are compared with the observed spectra in Fig. 5.1, where a Gaussian laser line profile G_L of width 5 MHz was used [111]. The agreement with the measured spectra (dashed lines) is good. In this comparison the zero-energy triplet s-wave scattering length was adjusted by 5%, i.e. $a_s^T(0) = -20.71 \; a_0$.

Electric dipole moments.— Our approach also allows for the prediction of electric dipole moments of Rydberg molecules. For the electronic wave functions the transition and permanent electric dipole moments are

$$\langle \psi | \, \hat{d} \, | \psi \rangle = \sum_i \sum_j \langle \phi_i | \, \hat{d} \, | \phi_j \rangle \, a_i a_j. \tag{5.24}$$

Because of the mixing of the opposite parity $(n-1)d$ and $(n-3)l_r \geq 3$ states with np states in Cs, the Rydberg molecule obtains a permanent electric dipole moment (PEDM) [4, 5]. We note however that the dominant electronic transition is between the 32p and 31d atomic states whose dipole moment is $\langle 32p|\,\hat{d}\,|31d\rangle = 1583$ D; we neglect therefore all other contributions to the dipole moments. Thus, the spin-dependent dipole moments are

$$d^S(R) = \sum_i \sum_j \langle \phi_i|\,\hat{d}\,|\phi_j\rangle\, \delta_{m_{s_{r_i}},m_{s_{r_j}}} \delta_{m_{s_{g_i}},m_{s_{g_j}}} \delta_{m_{i_{g_i}},m_{i_{g_j}}} \tag{5.25}$$

and the vibrationally averaged PEDM are

$$d^S_\nu = \int dR \psi^*_\nu(R)\psi_\nu(R) d^S(R). \tag{5.26}$$

The PEDMs are calculated for the predominantly triplet (d^T_ν) and mixed (d^{S+T}_ν) $\nu = 0$ vibrational levels for each m_K value. For the $m_K = \frac{1}{2}$ potential dissociating to the J=3/2, F=3(F=4) threshold the dipole moments are d^T_0 = 9.8(8.5) D and d^{S+T}_0 = 3.7(3.7) D. For $m_K = \frac{3}{2}$, d^T_0= 9.1(8.6) D and d^{S+T}_0 = 1.7(3.2) D, while for $m_K = \frac{5}{2}$, d^T_0 = 7.8(8.2) D and d^{S+T}_0= 2.3(3.6) D, respectively.

Chapter 6

Summary and Outlook

6.1 Outlook

As laser systems and our understanding of atomic systems became more sophisticated, it is only natural that we would seek to go beyond the atom to molecular and many-body systems. Diatomic molecules—while the simplest testbed for what we could liberally consider "chemistry"—continue to excite and suprise us with their remarkable complexity and adaptability.

In our study of the ion pair, we show that a homonuclear bond need not be covalent. We make substantial improvements to the scheme presented in Ref. [8], suggesting a mechanism to sharply increased ion pair yields; additionally, we provide a generalizable but quite simple model for excited/ground state scattering with the possibility of localization of the excited electron. In the future, we expect future experiments working toward ion pair creation [117], including experiments using the recently observed butterfly state [108] as an intermediate state, since that state has conveniently large Franck-Condon overlap with the ion-pair state, and may have a favorable transition dipole moment as well (see Fig. 6.1).

We also explored the significance of spin-dependent effects in the calculation of Rydberg molecular vibrational levels; our finding is that, particularly for cesium, the effect is dramatic.

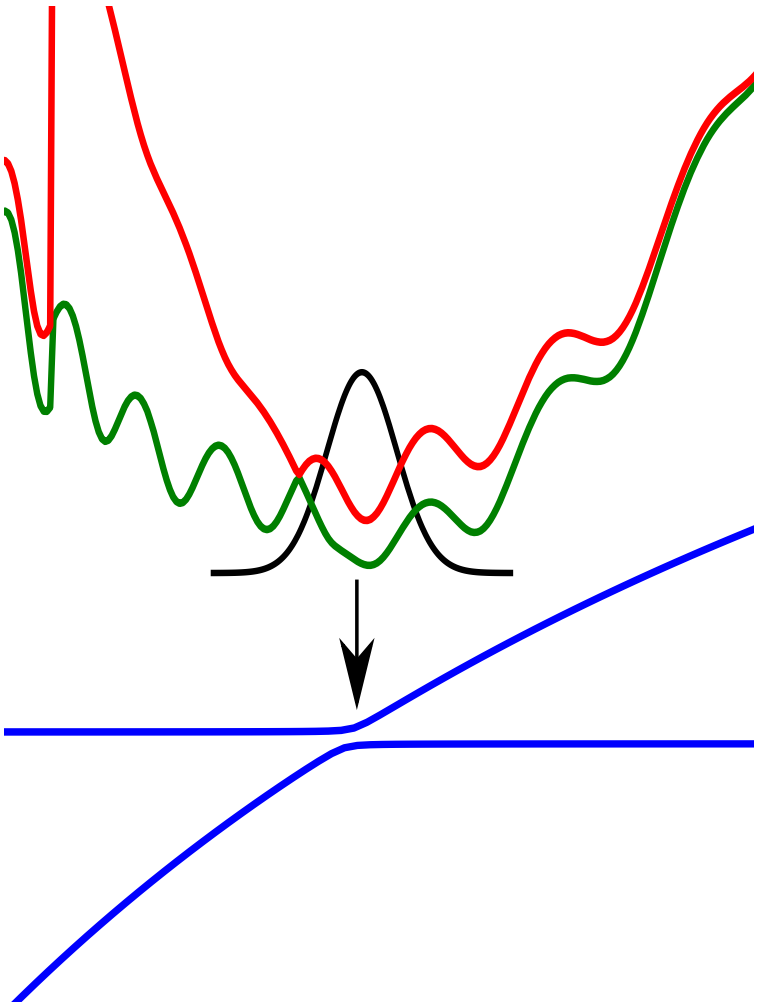

Figure 6.1: Butterfly states and the ion pair can exist with similar internuclear distances; therefore, we expect large Franck-Condon factors between them, and the butterfly state could serve as a useful precursor to the ion pair state. This would avoid the need for a DC Stark effect, as proposed in chapter 4.

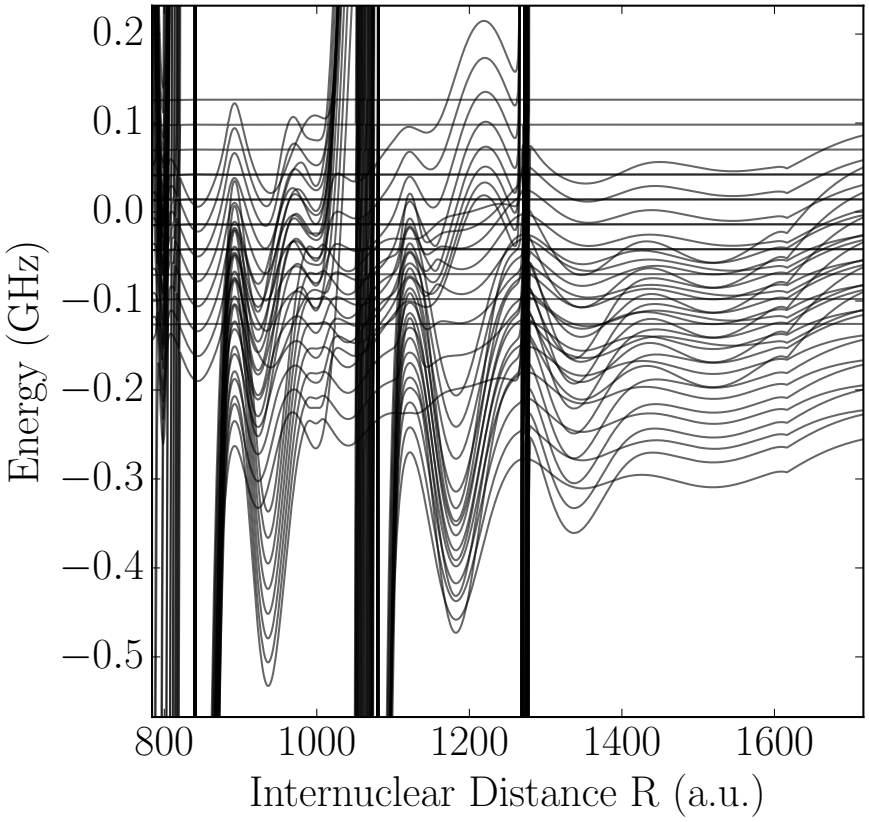

Figure 6.2: Cs Trilobite potential energy curves, as calculated in Chapter 5, but with a 10 G magnetic field applied in the z direction; shifted potential curves calculated by treating the magnetic field term within zeroth-order perturbation theory. It is clear that a modest magnetic field can enable spin-specific excitation.

The addition of the spin-orbit interaction will lead to mixing of Σ- and Π-states, while the addition of hyperfine effects will lead to mixing of the singlet and triplet interaction. We get substantially better agreement with experimental data than previous work [111]. Moreover, this work suggests many new avenues for control over individual spin configurations, or, conversely, for new forms of coherent control utilizing weak, static magnetic fields. Fig. 6.2 shows the dramatic effect that even a small field can have on these potential energy curves, when spin is explicitly considered. Additionally, spin-mixing due to the hyperfine interactions may have application in the production of the ion pair state, since, while the precursor in our scheme [40] is a triplet state covalent molecule, the final ion pair state has a singlet configuration.

We have endeavored to be explicit about the way in which results were calculated, including sections of code in some cases, such that any students who continue this work can do so with ease. Appendix C additionally explains how the knowledge of approximately good quantum numbers can lead to a substantial decrease in computational complexity when dealing with larger systems.

We consider the future of Rydberg molecular physics highly exciting. In particular, we look forward to new physics pertaining to the creation and manipulation of Rydberg molecules when considering spin effects and applied magnetic fields. While much work has been done regarding the effect of electric fields on Rydberg atoms and molecules, the effect of magnetic fields is relatively unstudied. Therefore, we expect many new advances in this frontier in the future.

Appendices

Appendix A

The Rydberg Blockade

A.1 Back-of-the-Envelope Blockade Explanation

The Rydberg blockade mechanism is simply considered by examining two neighboring atoms, and including the interaction between them within the dipole approximation. Let us consider a highly truncated two-particle Hamiltonian; we consider only the states $|\phi_1\rangle \otimes |\phi_2\rangle$ and $|\phi_1'\rangle \otimes |\phi_2'\rangle$. The 2×2 Hamiltonian, including dipole interaction, takes the form

$$\begin{bmatrix} 0 & \frac{\langle\phi_1|\hat{d}|\phi_1'\rangle \cdot \langle\phi_2|\hat{d}|\phi_2'\rangle}{R^3} \\ \frac{\langle\phi_1|\hat{d}|\phi_1'\rangle \cdot \langle\phi_2|\hat{d}|\phi_2'\rangle}{R^3} & \Delta_E \end{bmatrix} \tag{A.1}$$

where $\hat{d}$ is the dipole operator, R is the internuclear distance, and Δ_E is the separation of the energies of these two states when interactions are neglected. Diagonalization of this matrix yields the eigenvalues

$$\frac{\Delta_E}{2} \pm \sqrt{\frac{(\langle\phi_1|\,\hat{d}\,|\phi_1'\rangle \cdot \langle\phi_2|\,\hat{d}\,|\phi_2'\rangle)^2}{R^6} + \frac{\Delta_E^2}{4}} \tag{A.2}$$

This leads us to two significant regimes:

A.1.1 $\langle\phi_1|\,\hat{d}\,|\phi_1'\rangle \cdot \langle\phi_2|\,\hat{d}\,|\phi_2'\rangle \gg \Delta_E$

This is the strongly interacting regime; Eq. A.2 becomes approximately

$$\pm\frac{\langle\phi_1|\,\hat{d}\,|\phi_1'\rangle \cdot \langle\phi_2|\,\hat{d}\,|\phi_2'\rangle}{R^3} \tag{A.3}$$

This is the blockade, or dipole-dipole regime; if the perturbation from the neighboring Rydberg electron is sufficiently large to lead to a high degree of state mixing, there will be a significant shift, scaling as $\frac{1}{R^3}$ with internuclear distance R.

A.1.2 $\Delta_E \gg \langle\phi_1|\,\hat{d}\,|\phi_1'\rangle \cdot \langle\phi_2|\,\hat{d}\,|\phi_2'\rangle$

This is the weakly interacting regime; Eq. A.2 becomes approximately

$$\pm\Delta_E \pm \frac{\langle\phi_1|\,\hat{d}\,|\phi_1'\rangle \cdot \langle\phi_2|\,\hat{d}\,|\phi_2'\rangle}{\Delta_E R^6} \tag{A.4}$$

This is the van der Waals regime. Here the Rydberg-Rydberg interaction scales only as $\frac{1}{R^6}$ with internuclear distance R.

A.2 Logic Gates with Rydberg Atoms

The strong nonlinear behavior of the Rydberg blockade in the two-atom system open the possibility for quantum logic, as proposed by Jaksch et al. [23]. In their scheme, the two atoms have a ground state with two hyperfine levels, and a Rydberg state with is resonantly coupling the lower hyperfine state to a Rydberg state (that is, the coupling is in resonance before possible interactions between Rydberg atoms are considered). The atoms are separated such that they are in the strong coupling regime, and assumed to be individually addressable. The level scheme is portrayed in Fig. A.1 A π-pulse is applied to the first atom, followed by a 2π-pulse to the second atom, following by a π-pulse to the third atom. The full truth table describing

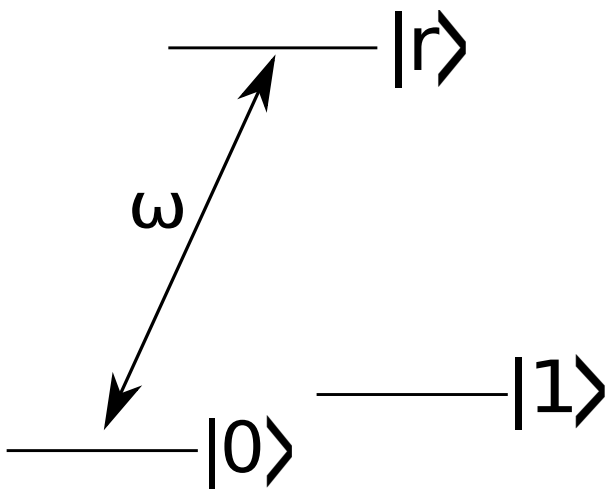

Figure A.1: Three-state scheme from Jaksch et al. [23] for a universal quantum gate.

possible results from this pulse sequence is then

$$\begin{array}{cccccccc} & \pi_1 & & 2\pi_2 & & \pi_1 & & \\ |0\rangle \otimes |0\rangle & \rightarrow & i\,|r\rangle \otimes |0\rangle & \rightarrow & i\,|r\rangle \otimes |0\rangle & \rightarrow & -|0\rangle \otimes |0\rangle \\ |0\rangle \otimes |1\rangle & \rightarrow & i\,|r\rangle \otimes |1\rangle & \rightarrow & i\,|r\rangle \otimes |1\rangle & \rightarrow & -|0\rangle \otimes |1\rangle \\ |1\rangle \otimes |0\rangle & \rightarrow & |1\rangle \otimes |0\rangle & \rightarrow & -|1\rangle \otimes |0\rangle & \rightarrow & -|1\rangle \otimes |0\rangle \\ |1\rangle \otimes |1\rangle & \rightarrow & |1\rangle \otimes |1\rangle & \rightarrow & |1\rangle \otimes |1\rangle & \rightarrow & |1\rangle \otimes |1\rangle \end{array} \tag{A.5}$$

which is equivalent to the NAND gate, and therefore universal.

Appendix B

The Adiabatic Picture of the Rydberg Atom

As in section 3.5, we are free to express the n-electron wavefunction for the Rydberg atom (i.e., with $n-1$ core electrons and a single Rydberg electron) as a product of Rydberg and core wavefunctions, where the latter are parametrized by the position of the Rydberg electron

$$\Psi(r_{\text{core}}, r_{\text{Rydberg}}) = \sum_i \psi_i(r_{\text{Rydberg}})\Phi_i(r_{\text{core}}; r_{\text{Rydberg}}) \tag{B.1}$$

Here r_{Rydberg} denotes the position of the Rydberg electron, and r_{core} denotes the positions of the core electrons.

Following the same procedure, as in section 3.5, the Schrödinger equation for the Rydberg electron wavefunctions $\psi_i(r_{\text{Rydberg}})$ becomes (using atomic units)

$$\left[-\frac{1}{2}(\overrightarrow{\nabla} + \tau)^2 - \frac{1}{r} + E_i\right]\psi_i = E\psi_i \tag{B.2}$$

where E_i is the energy of the state Φ_i. Here τ is a matrix whose elements take the form

$$\tau_{ij} = \langle\Phi_i| \frac{\partial}{\partial r_{\text{Rydberg}}} |\Phi_j\rangle \tag{B.3}$$

Thus far, the effect of interaction between the Rydberg and core electrons has not been accounted for. Since the kinetic energy of the Rydberg electron is quite small relative to the kinetic energies of the core electrons, it is often safe to neglect τ.

The effect of core polarization is most simply considered within perturbation theory, as in [118, 78]. There, the Rydberg-core electron interaction coupling states Ψ_i and Ψ_j is expanded into multipoles

$$V'_{ij}(r_{\text{Rydberg}}) = \sum_k \langle \Phi_i(r_{\text{core}}; r_{\text{Rydberg}})| \frac{(r_{\text{core}})^k}{(r_{\text{Rydberg}})^{k+1}} P_k(\cos\theta) \, |\Phi_j(r_{\text{core}}; r_{\text{Rydberg}})\rangle \tag{B.4}$$

where θ implies the angle between different core electron positions relative to the core-Rydberg electron axis. Considering $\tau \to 0$, and neglecting contributions higher than quadrupole, we have the energy shift for core configuration i

$$-\frac{\alpha_{d,i}}{2r^4_{\text{Rydberg}}} - \frac{\alpha_{q,i}}{2r^6_{\text{Rydberg}}} \tag{B.5}$$

where

$$\alpha_{d,i} = \sum_{j\neq i} \frac{2Q^{(1)}_{ij}Q^{(1)}_{ji}}{E_j - E_i} \tag{B.6}$$

is the dipole polarizability, and

$$\alpha_{q,i} = \sum_{j\neq i} \frac{2Q^{(2)}_{ij}Q^{(2)}_{ji}}{E_j - E_i} \tag{B.7}$$

is the quadrupole polarizability. The expectations of the core multipoles have been abbreviated as

$$Q^{(k)}_{ij} = \langle \Phi_i(r_{\text{core}}; r_{\text{Rydberg}})| \, (r_{\text{core}})^k P_k(\cos\theta) \, |\Phi_j(r_{\text{core}}; r_{\text{Rydberg}})\rangle \tag{B.8}$$

There will additionally be $\frac{1}{r^6_{\text{Rydberg}}}$ and smaller terms that stem from the non-adiabatic coupling τ; these are given in details in [78].

Appendix C

Relevant Techniques in Numerical Linear Algebra

The vast majority of problems in computational chemistry boil down to diagonalization of a Hamiltonian in a carefully chosen basis. The quality (and completeness) of that basis is the most important factor in the success of any calculation, but the fact that the best current algorithms for diagonalization of dense matrices achieve $\Omega(n^3)$ time complexity for $n \times n$ matrices makes the study of larger and larger systems progressively more difficult. In this section, we review the most significant algorithms for dense Hermitian matrix diagonalization, and explain how the $\Omega(n^3)$ scaling comes about. For additional detail on these our other algorithms, we point to the reader to the standard text by Burden and Faires [119].

C.1 Eigenvalues via Gaussian Elimination

For completeness, we describe how we solve for the eigenvalues of a matrix H via Gaussian elimination. The eigenvalue problem is concerned with finding λ, where

$$A\vec{v}_i = \lambda_i I \vec{v}_i \tag{C.1}$$

for identity matrix I and eigensystem $(\lambda_i, \vec{v}_i)$. Equivalently,

$$(A - \lambda_i I)\vec{v}_i = 0 \tag{C.2}$$

This equation will be satisfied if and only if the determinant of $(A - \lambda_i I)$ is zero. Thus, the problem is equivalent to the solution of n coupled linear equations. This will have greater than $\Omega(n^3)$ time

C.2 The Householder Transformation and its Use in Tridiagonalization

Most diagonalization schemes rely first on the transformation of the matrix in question into a tridiagonal form.

$$A = \begin{bmatrix} A_{11} & A_{12} & & & \\ A_{21} & A_{22} & A_{23} & & \\ & A_{31} & \ddots & \ddots & \\ & & \ddots & \ddots & A_{(n-1),n} \\ & & & A_{n,(n-1)} & A_{n,n} \end{bmatrix} \tag{C.3}$$

This may be achieved via successive application of the **Householder transformation**. This is simply a transformation corresponding to a reflection about a hyperplane passing through the origin. It has the form

$$\hat{P} = \hat{I} - 2\left|v\right\rangle\left\langle v\right| \tag{C.4}$$

for unit vector $|v\rangle$. Eq. C.4 may be viewed intuitively as the sum of the projection operator into the space complementary to the space spanned by $|v\rangle$ with the negation of the projection **onto** the space spanned by $|v\rangle$.

It may be shown that $\hat{P}$ is both Hermitian (trivially) and unitary, since

$$\hat{P}^\dagger\hat{P} = (\hat{I} - 2\left|v\right\rangle\left\langle v\right|)(\hat{I} - 2\left|v\right\rangle\left\langle v\right|) = \hat{I} - 4\left|v\right\rangle\left\langle v\right| + 4\left|v\right\rangle\left\langle v|v\right\rangle\left\langle v\right| = \hat{I} \tag{C.5}$$

Given a matrix A, we wish to determine a Householder transformation that will set all values beyond the second in the first column, and all values beyond the second in the first row of A,

to zero. That is

$$A^{(0)} = \hat{P}A\hat{P} = \begin{bmatrix} A_{11} & A_{12} & \cdots & 0 & 0 \\ A_{21} & A_{22} & A_{23} & & A_{2,n} \\ \vdots & A_{31} & \ddots & \ddots & \vdots \\ 0 & & \ddots & \ddots & A_{(n-1),n} \\ 0 & A_{n,2} & \cdots & A_{n,(n-1)} & A_{n,n} \end{bmatrix} \tag{C.6}$$

Let us denote $\vec{y}$ the leftmost column of $\hat{P}A$. We demand that $\vec{y}_{11} = A_{11}$, $\vec{y}_{21} = \alpha$, and $\vec{y}_{i1} = 0$, for $i \geq 3$

$$\vec{y} = \begin{bmatrix} A_{11} \\ \alpha \\ 0 \\ \vdots \\ 0 \end{bmatrix} \tag{C.7}$$

Then

$$y_1 = A_{11} - 2\sum_j v_1 v_j A_{j1} = A_{11} \tag{C.8}$$

$$y_2 = A_{21} - 2\sum_j v_2 v_j A_{j1} = \alpha \tag{C.9}$$

and

$$y_k = A_{k1} - 2\sum_j v_k v_j A_{j1} = 0 \tag{C.10}$$

for $k \geq 3$. Eq. C.8 may be ensured if $v_1 = 0$.

Let

$$r = \sum_{j=2} v_j A_{j1} \tag{C.11}$$

Then

$$2rv_2 = A_{21} - \alpha \tag{C.12}$$

and

$$2rv_j = A_{j1},\ j \geq 3 \tag{C.13}$$

We square both sides of these equations to obtain

$$4r^2 \sum_{j=2} v_j^2 = (A_{21} - \alpha)^2 + \sum_{j=3} {A_{j1}}^2 \tag{C.14}$$

$\vec{v}$ is normalized, so

$$4r^2 = -2\alpha A_{21}\alpha + \alpha^2 + \sum_{j=2} {A_{j1}}^2 \tag{C.15}$$

By the orthgonality of $\hat{P}$, we have that

$$\hat{P}\hat{P}\vec{y} = \hat{P} \begin{bmatrix} A_{11} \\ \alpha \\ 0 \\ \vdots \\ 0 \end{bmatrix} = \begin{bmatrix} A_{11} \\ A_{21} \\ \vdots \\ A_{n1} \end{bmatrix} \tag{C.16}$$

Thus

$$\langle y|^T \hat{P}\hat{P} |y\rangle = {A_{11}}^2 + \alpha^2 = \langle y|y\rangle = \sum_{j=1} {A_{j1}}^2 \tag{C.17}$$

and

$$\alpha^2 = \sum_{j=2} {A_{j1}}^2 \tag{C.18}$$

Thus

$$2r^2 = -\alpha A_{21}\alpha + \sum_{j=2} {A_{j1}}^2 \tag{C.19}$$

We take the convention

$$\alpha = -sgn(A_{21})\sqrt{\left(\sum_{j=2} {A_{j1}}^2\right)} \tag{C.20}$$

To ensure that $r = 0$ when $A_{21} = A_{31} = \cdots = A_{n1} = 0$. Then

$$2r^2 = \sum_{j=2} {A_{j1}}^2 + |A_{21}| \sqrt{\sum_{j=2} {A_{j1}}^2} \tag{C.21}$$

and

$$v_2 = \frac{A_{21} - \alpha}{2 \sum_{j=2} v_j A_{j1}} \tag{C.22}$$

$$v_j = \frac{A_{j1}}{2 \sum_{j=2} v_j A_{j1}},\ j \geq 3 \tag{C.23}$$

$$\hat{P}A = \begin{bmatrix} A_{11} & A_{12} & \cdots & & A_{1,n} \\ A_{21} & A_{22} & A_{23} & & A_{2,n} \\ \vdots & A_{31} & \ddots & \ddots & \vdots \\ 0 & & \ddots & \ddots & A_{(n-1),n} \\ 0 & A_{n,2} & \cdots & A_{n,(n-1)} & A_{n,n} \end{bmatrix} \tag{C.24}$$

$\hat{P}A$ is Hermitian, so clearly

$$A\hat{P} = \begin{bmatrix} A_{11} & A_{12} & 0 & \cdots & 0 \\ A_{21} & A_{22} & A_{23} & & A_{2,n} \\ \vdots & A_{31} & \ddots & \ddots & \vdots \\ A_{(n-1),1} & & \ddots & \ddots & A_{(n-1),n} \\ A_{n,1} & A_{n,2} & \cdots & A_{n,(n-1)} & A_{n,n} \end{bmatrix} \tag{C.25}$$

As explained before, $v_1 = 0$, so the leftmost column is unaffected by operation of $\hat{P}$ on the right (as the top row is unaffected by operation of $\hat{P}$ on the left); Eq. C.6 then clearly holds.

Treating $A^{(0)}$ in blocks,

$$\left[\begin{array}{c|cc} {A_{11}}^{(0)} & {A_{12}}^{(0)} & 0 \quad \cdots \\ \hline {A_{12}}^{(0)} & & \\ 0 & A^{(0)\prime} & \\ \vdots & & \end{array}\right] \tag{C.26}$$

let $A^{(0)\prime}$ be the lower right $(n-1)\times(n-1)$ block from $A^{(0)}$. We may in principle follow the same procedure as above to derive a $\hat{P}'$ for the lower right subspace. As before, $v_1 = 0$ (or, in the superspace, $v_1 = v_2 = 0$), so the two left columns and two upper rows of A will be unaffected by the application of this subsequent Householder transformation. We may therefore apply sucessive Householder transformations, one for each dimension of the matrix. Since matrix multiplication has computational complexity of $\Omega(n^3)$, and since we apply $2n$ such operations, we would expect the Householder tridiagonalization procedure to have complexity $\Omega(n^4)$. The procedure shown below circumvents the matrix multiplication step, however, and thus permits the entire tridiagonalization to be done in $\Omega(n^3)$ time.

```
def tridiagonalize(A):
  # A is an n-by-n symmetric matrix
  n=len(A)
  for k in range(1,n-1):
    alphasquared=sum([A[j-1,k-1]**2 for j in range(k+1,n+1)])
    if A[k,k-1]==0:
      alpha=-alphasquared**0.5
    else:
      alpha=-alphasquared**0.5*A[k,k-1]/abs(A[k,k-1])
    r=alphasquared-alpha*A[k,k-1]
    v=[0.0]*n
    v[k]=A[k,k-1]-alpha
    for j in range(k+2,n+1):
      v[j-1]=A[j-1,k-1]
```

```
    u=[0.0]*n
    for j in range(k,n+1):
      u[j-1]=(1.0/r)*sum([A[j-1,i-1]*v[i-1] for i in range(k+1,n+1)])
    vudot=0
    for i in range(k+1,n+1):
      vudot+=v[i-1]*u[i-1]
    z=[u[j-1]-vudot/2.0/r*v[j-1] if j>=k else 0.0 for j in range(1,n+1)]
    for l in range(k+1,n):
      for j in range(l+1,n+1):
        A[j-1,l-1]=A[j-1,l-1]-v[l-1]*z[j-1]-v[j-1]*z[l-1]
        A[l-1,j-1]=A[j-1,l-1]
      A[l-1,l-1]=A[l-1,l-1]-2*v[l-1]*z[l-1]
    A[n-1,n-1]=A[n-1,n-1]-2*v[n-1]*z[n-1]
    for j in range(k+2,n+1):
      A[k-1,j-1]=0
      A[j-1,k-1]=0
    A[k,k-1]=A[k,k-1]-v[k]*z[k-1]
    A[k-1,k]=A[k,k-1]
  return A
```

C.3 The Divide-and-Conquer Algorithm for Diagonalization of Tridiagonal Matrices

The most commonly used algorithm for the diagonalization of large matrices is the divide-and-conquer method, implemented in LAPACK as the sstevd (for already tridiagonal matrices) and ssyevd (for general dense matrices–i.e., this algorithm proceeds initially with tridiagonalization before beginning the divide-and-conquer scheme). In LAPACK, separate routines exist for different types.

To begin, we view the tridiagonal matrix H as the sum of two block diagonal groups H_1 and H_2 and a rank-1 perturbation $\lambda \left|p\right\rangle \left\langle p\right|$.

$$H = \left[\begin{array}{c|c} H_1 & \lambda \\ \hline \lambda & H_2 \end{array}\right] = \left[\begin{array}{c|c} H_1 & \\ \hline & H_2 \end{array}\right] + \left[\begin{array}{c|c} & \lambda \\ \hline \lambda & \end{array}\right] \tag{C.27}$$

Given the singular value decomposition of $H_1,\ H_2$, $H_1 = U_1 D_1 U_1^\dagger,\ H_2 = U_2 D_2 U_2^\dagger$, where $U_{1,2}$ are unitary and $D_{1,2}$ are diagonal, we have

$$H = \left[\begin{array}{cc} U_1 & \\ & U_2 \end{array}\right] \left(\left[\begin{array}{cc} D_1 & \\ & D_2 \end{array}\right] + \lambda \left|p\right\rangle \left\langle p\right| \right) \left[\begin{array}{cc} U_1^\dagger & \\ & U_2^\dagger \end{array}\right] \tag{C.28}$$

Let

$$D = \left[\begin{array}{cc} D_1 & \\ & D_2 \end{array}\right] \tag{C.29}$$

We then have the eigenvalue equation

$$(D + \lambda |p\rangle \langle p|) |\lambda\rangle = \lambda |\lambda\rangle \tag{C.30}$$

$$(D - \lambda I) |\lambda\rangle + \lambda |p\rangle \langle v|\lambda\rangle = 0 \tag{C.31}$$

$$\langle p|\lambda\rangle + \langle p| \lambda(D - \lambda I)^{-1} |p\rangle \langle v|\lambda\rangle = 0 \tag{C.32}$$

$$1 + \langle p| \lambda(D - \lambda I)^{-1} |p\rangle = 0 \tag{C.33}$$

$$\tag{C.34}$$

This is a system of n equations, the dimension of H (which is the dimension of $|p\rangle$. The roots of this system may be solved via Newton-Raphson; this method can solve for each root in $O(n)$ time, and as we must ultimately solve for n roots, thhe divide-and-conquer method ultimately produces eigenvalues in $O(n^2)$ time—a significant improvement in complexity over the QR factorization method.

C.4 A Technique for Diagonalization of Systems with Nearly-Good Quantum Numbers

As explained above, we are often fortunate when performing direct diagonalization to have a *conserved quantity* (alternately a *good quantum number*). This allows us to represent the full Hamiltonian in block diagonal form.

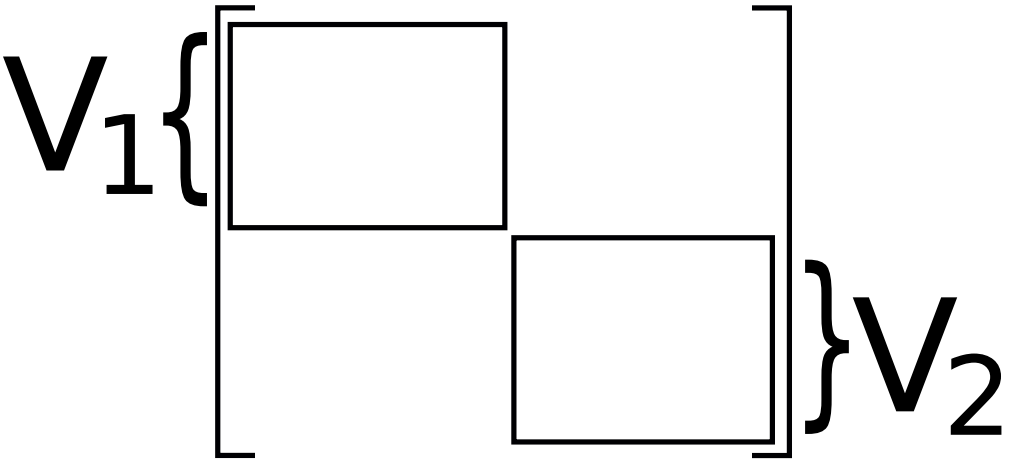

Figure C.1: When there is a known good quantum number, we may separate the Hamiltonian into blocks corresponding to elements with particular values of that quantum number

Since each block may be diagonalized separately (and since, in general, diagonalization takes $O(n^3)$ time for an $n \times n$ matrix), this represents a significant speedup.

In our work, the situation arises that we have a Hamiltonian H_0 with a particular conserved quantity, and a perturbation H_P that breaks that conservation. We are free to rearrange the order of the basis elements such that those elements which couple the two initially separate block are all indexed contiguously. The resultant Hamiltonian takes the form shown in Fig. C.2

Let n_1 denote the dimension of V_1, n_2 the dimension of V_2, m_P the dimension of V_p, m_1 the dimension of $V_1 \cup V_P$, m_2 is the dimension of $V_2 \cup V_p$, $m_P = m_1 + m_2$ is the dimension of V_P, $n = n_1 + n_2$ is the dimension of V, the full Hilbert space of the Hamiltonian.

Were we to naively diagonalize H, it would take $O(n^3)$ time. This is of course a major barrier to any expansion of our basis set (or of additional perturbatory corrections to the

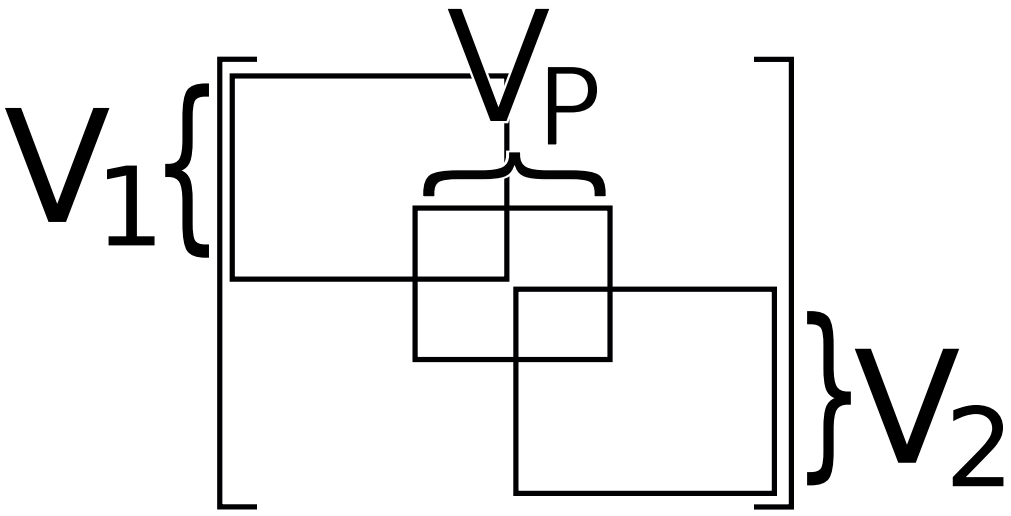

Figure C.2: V_p is a subspace of the full Hilbert space which overlaps with both V_1 and V_2

Hamiltonian that warrant such expansions). We can, however, take advantage of the sparsity of H by first tridiagonalizing V_P (in approximately $O(n^2 m)$ time). We denote i the index corresponding to the first basis element in V_p (which is also in V_1). We wish to find the Householder transformation $\hat{P} = \hat{I} - |v\rangle \langle v|$ which results in

$$H^{(1)}_{i+j,i} = 0,\ j \neq 0,\ 1 \tag{C.35}$$

where $\hat{P}H = H^{(1)}$.

As with the Householder transformations we derived for the fully dense matrix, we now solve for the elements of $|v\rangle$. There will be potentially $n_1 + m_2$ nonzero elements in $|v\rangle$, since $H_{ji}0,\ j \geq i + m$ already. As before,

$$v_i = 0,\ v_{i+1} = \frac{H_{i+1,i} - \alpha}{2r},\ v_{i+j} = \frac{H_{i+j,j}}{2r},\ j = 2, ...(n_1 + m_2 - 1) \tag{C.36}$$

where

$$\alpha = -sgn(H_{i+1,i}) \sqrt{\sum_{j=i+1}^{n_1+m_2} H^2_{j+i,i}} \tag{C.37}$$

and

$$r = \sqrt{\frac{1}{2}\alpha^2 - \frac{1}{2}H_{i+1,i}\alpha} \tag{C.38}$$

The complexity associated with the application of this Householder transformation is $O((n_1 + m_2)^2)$. To fully tridiagonalize the space V_P, we must apply m_1 such transformations, and then m_2 transformations with complexity $O((n_2 + m_1)^2)$. In total, the complexity of the full tridiagonalization of V_P is then $O(m_1(n_1 + m_2)^2) + O(m_2(n_2 + m_1)^2) \approx O(mn^2)$.

Having tridiagonalized rows i through $i + m - 1$, Householder transformations may be applied to the portions of H in $V_1,\ V_2$ disjoint from V_P as if they were entirely uncoupled. To show this, we remember that that for the $(i + m)$th row of V (the first row which is not coupled by H_P), the applied Householder transformation has the form $\hat{I} - |v\rangle \langle v|$, where $v_{i+m} = 0$. Therefore, the elements $H_{i+m,i+m-1}$ and $H_{i+m-1,i+m}$ will be unaffected by application of Householder transformations which will tridiagonalize the part of H spanned by V_2.

This is a substantial speedup, assuming $m \ll n$.

If our full Hamiltonian is composed of several such perturbations, each breaking a different conserved quantity, this scheme may be applied successively to significantly reduce the computational complexity of diagonalization (to $O(n^2)$, effectively). For example, let

$$H = H_0 + H_{FS} + H_{HF} + H_{\text{Magnetic Field}} \tag{C.39}$$

where

- H_0 is our unperturbed Hamiltonian (perhaps incorporating S- and P-wave scattering in our work), with good quantum numbers $\vec{L}$, $\vec{S}$ the orbital electronic, and electronic spin angular momenta, respectively.
- H_{FS} is the fine structure contribution, with good quantum number $\vec{J} = \vec{L} + \vec{S}$
- H_{HF} is the hyperfine structure contribution, with good quantum number $\vec{K} = \vec{J} + \vec{S_{\text{nuclear}}}$, $\vec{S_{\text{nuclear}}}$ being the nuclear spin.

- $H_{\text{Magnetic Field}}$ is a magnetic field, which retains no good quantum number.

The subspace which couples blocks of different K_z may be tridiagonalized first; then, within those nearly decoupled blocks, we may tridiagonalize the region which couples blocks of different J_z, then those of different $L_z,\ S_z$. Finally, essentially dense blocks of particular (K_z, J_z, L_z, S_z) may be tridiagonalized. Once the entire $n \times n$ matrix has been tridiagonalized, it may be diagonalized via the divide-and-conquer method described above.

Appendix D

The Eckart Potential

D.1 Bound states

The following is taken largely from Gol'dman, Krivchenkov [120]. Taking the Schrödinger equation with $V(r)$ from (4.3), we make the substitutions [120]

$$\psi = (\cosh \frac{r}{r_0})^{-2\lambda} u, \text{ where } \lambda = \frac{1}{4}(\sqrt{\frac{8\mu V_0 {r_0}^2}{\hbar^2} + 1} - 1)$$

The Schrödinger equation then becomes

$$\frac{d^2u}{dr^2} - \frac{4\lambda}{r_0} \tanh(\frac{r}{r_0})\frac{du}{dr} + \frac{4}{{r_0}^2}(\lambda^2 - \chi^2)u = 0 \tag{D.1}$$

with

$$\chi = \sqrt{-\frac{\mu E {r_0}^2}{2\hbar^2}}$$

Letting $z = -\sinh^2(\frac{r}{r_0})$ leads us to the hypergeometric equation

$$z(1-z)\frac{d^2u}{dz^2} + (\gamma - (\alpha + \beta + 1)z)\frac{du}{dz} - \alpha\beta u = 0 \tag{D.2}$$

where $\gamma = \frac{1}{2},\ \alpha = \chi - \lambda,\ \beta = -\chi - \lambda$. In spherical coordinates, only odd hypergeometric

solutions are valid:

$$u = \sqrt{z}\, F(-\lambda + \chi + \frac{1}{2}, -\lambda - \chi + \frac{1}{2}; \frac{3}{2}; z) \tag{D.3}$$

By enforcing asymptotic boundary conditions for the bound states ($u \to 0$ as $r \to \infty$),

$$\lambda - \chi = n + \frac{1}{2},\ n = 0, 1, 2, \cdots$$

giving the set of bound states

$$\psi_n = (\cosh \frac{r}{r_0})^{-2\lambda} u_n \tag{D.4}$$

where

$$u_n = N \sinh(\frac{r}{r_0}) F(-n, -2\lambda + n + 1; \frac{3}{2}; -\sinh^2(\frac{r}{r_0}))$$

(N is a normalizing constant), with corresponding energies

$$E_n = -\frac{2\hbar^2}{\mu {r_0}^2}(\frac{1}{4}\sqrt{\frac{8\mu V_0 {r_0}^2}{\hbar^2} + 1} - n - \frac{3}{4})^2 \tag{D.5}$$

D.2 Scattering States

With $E = \frac{\hbar^2 k^2}{2\mu}$, $\chi^2 = -\frac{\mu E {r_0}^2}{2\hbar^2} \to ikr_0 = 2\chi$ (μ is the effective mass) [120], and

$$u(r) = N \sinh(\frac{r}{r_0}) F(-\lambda + \frac{ikr_0}{2} + \frac{1}{2}, -\lambda - \frac{ikr_0}{2} + \frac{1}{2}, \frac{3}{2}, -\sinh^2 \frac{r}{r_0})$$

fulfilling the boundary conditions

$$\lim_{r\to 0} u(r) = 0,\ \lim_{r\to\infty} u(r) \simeq \sin(kr + \delta_0)$$

where δ_0 is the usual phase shift.

We note that $F(\alpha, \beta; \gamma; 0) = 1,\ \forall \alpha, \beta, \gamma$, and that

$$\lim_{r\to\infty} \sinh^2(\frac{r}{r_0}) \approx \frac{1}{2} e^{\frac{2r}{r_0}}$$

Using the asymptotic behavior of the Gaussian hypergeometric functions (see [99], p. 108, section 2.10, equation 2).

$$u(r) = Ae^{ikr} + Be^{-ikr}$$

where

$$A = 2^{-ikr_0} \frac{\Gamma(ikr_0)}{\Gamma(\frac{1-2\lambda+ikr_0}{2})\Gamma(1+\frac{2\lambda+ikr_0}{2})},\ B = A^\dagger$$

where we neglect a real factor common to A and B which will not affect the scattering phase shift. The phase shift itself has the form:

$$\delta_0 = \frac{1}{2i} \ln(-\frac{A}{A^\dagger}) \tag{D.6}$$

In the limit $ka \ll 1$, the Gamma functions may be expanded in a Taylor series about $ika = 0$,

$$\Gamma(ikr_0) = \frac{1}{ikr_0}\Gamma(1+ikr_0) \simeq \frac{1+ikr_0\psi^{(0)}(1)}{ikr_0}\Gamma(1)$$

$$\Gamma(\frac{1-2\lambda}{2} + \frac{ikr_0}{2}) \simeq \Gamma(\frac{1-2\lambda}{2})(1 + \frac{ikr_0}{2}\psi^{(0)}(\frac{1-\lambda}{2}))$$

$$\Gamma(1+\lambda+\frac{ikr_0}{2}) \simeq \Gamma(1+\lambda)(1+\frac{ikr_0}{2}\psi^{(0)}(1+\lambda))$$

where $\psi^{(0)}$ is the m^{th}-order polygamma function, i.e. $\psi^{(0)}(x) = \frac{d}{dx}\ln\Gamma(x)$. The final expression for δ_0 now becomes:

$$\delta_0 = kr_0[-\ln(2) + \psi^{(0)}(1) - \frac{1}{2}\psi^{(0)}(\frac{1-2\lambda}{2}) - \frac{1}{2}\psi^{(0)}(1+\lambda)] \tag{D.7}$$

which is related to the s-wave scattering length by the usual formula,

$$\lim_{k\to 0} k\cot\delta_0 = -\frac{1}{a_{sc}}$$

The parameters for the pseudopotential $V_2(r)$ (4.3) are hence found by solving the system of equations:

$$a_{sc} = r_0(-\ln(2) + \psi^{(0)}(1) - \frac{1}{2}\psi^{(0)}(\frac{1-2\lambda}{2}) - \frac{1}{2}\psi^{(0)}(1+\lambda)) \tag{D.8}$$

and

$$EA = -\frac{\hbar^2}{2\mu {r_0}^2}(\frac{1}{2}\sqrt{\frac{8\mu V_0 {r_0}^2}{\hbar^2}+1} - \frac{3}{2})^2 \tag{D.9}$$

There are multiple solutions to Eqs. (D.8 - D.9). However, since it is known that Rb^- has only one bound state, we impose the additional restriction:

$$N_{\text{bound}} = \lfloor \frac{1}{4}\sqrt{\frac{8\mu V_0 r_0^2}{\hbar^2}+1} + \frac{1}{4} \rfloor = 1$$

The solutions to Eqs. (D.8 - D.9) yield $r_0 = 9.004786$ a.u. and $V_0 = 0.061675$ a.u.

Appendix E

The Numerov Algorithm for the Time-Independent Schrödinger Equation

Differential equations of the form

$$\psi''(x) = g(x)\psi(x) \tag{E.1}$$

may be numerically solved to high accuracy (with propagation error $O(\Delta x^4)$ for step size Δx) via the Numerov-Cooley algorithm [1]

This may be shown for the Schrödinger equation

$$\psi''(x) = -\frac{2m}{\hbar^2}(E - V(x))\psi(x) \tag{E.2}$$

[1] In the case of the Schrödinger equation, where $g(x) = -\frac{2m}{\hbar^2}(E - V(x)$, E is not assumed to be know; if the only assumed boundary conditions are that the solution is normalized, taken with the Dirichlet boundary conditions at $x \lim 0,\ \infty$, general algorithms (i.e., those valid for differential equations of arbitrary form) will have $O(\Delta x)$ propagation error.

by first Taylor expanding $\psi(x)$

$$\psi(x+\Delta x) = \psi(x) + (\Delta x)\psi'(x) + \frac{(\Delta x)^2}{2!}\psi''(x) + \frac{(\Delta x)^3}{3!}\psi'''(x) + \frac{(\Delta x)^4}{4!}\psi''''(x) + \frac{(\Delta x)^5}{5!}\psi'''''(x) + O(\Delta x^6) \quad \text{(E.3)}$$

The sum of $\psi(x+\Delta x)$ and $\psi(x-\Delta x)$ will therefore contain no terms odd in Δx:

$$\psi(x+\Delta x) + \psi(x-\Delta x) = 2\psi(x) + (\Delta x)^2\psi''(x) + \frac{\Delta x^4}{12}\psi''''(x) + O(\Delta x^6) \quad \text{(E.4)}$$

We may rewrite this as

$$(\Delta x)^2\psi''(x) = \psi(x+\Delta x) + \psi(x-\Delta x) - 2\psi(x) - \frac{\Delta x^4}{12}\psi''''(x) + O(\Delta x^6) \quad \text{(E.5)}$$

$$\rightarrow \psi''(x) = \frac{\psi(x+\Delta x) + \psi(x-\Delta x) - 2\psi(x)}{\Delta x^2} - \frac{\Delta x^2}{12}\psi''''(x) + O(\Delta x^6) \quad \text{(E.6)}$$

Ultimately, we wish to solve for $\psi(x+\Delta x)$. The cleverness of the Numerov-Cooley algorithm rests upon using the differential equation as given to produce high-accuracy approximations for $\psi''(x)$ and $\psi''''(x)$. From the Schrödinger equation directly, we have

$$\psi''(x) = -\frac{2m}{\hbar^2}(E - V(x))\psi(x) \quad \text{(E.7)}$$

The fourth derivative may be approximated by taking the Taylor expansion (as above) for $\psi''(x)$, this time to fourth order:

$$\psi''(x+\Delta x) + \psi''(x-\Delta x) = 2\psi''(x) + \Delta x^2\psi''''(x) + O(\Delta x^4) \quad \text{(E.8)}$$

$$\psi''''(x) = \frac{\psi''(x+\Delta x) + \psi''(x-\Delta x) - 2\psi''(x)}{\Delta x^2} + O(\Delta x^2) \quad \text{(E.9)}$$

Substituting in the form for the second derivative taken from Eq. E.6, we have

$$\psi''''(x-\Delta x) = \frac{\frac{2m}{\hbar^2}(E-V(x+\Delta x))\psi(x+\Delta x) - \frac{2m}{\hbar^2}(E-V(x-\Delta x))\psi(x-\Delta x) + \frac{4m}{\hbar^2}(E-V(x))\psi(x)}{\Delta x^2} + O(\Delta x^2) \tag{E.10}$$

We thus have a complete expression for $\psi(x+\Delta x)$ to $O(\Delta x^4)$ which depends only on $\psi(x)$ and $\psi(x-\Delta x)$:

$$\begin{aligned}\psi(x+\Delta x) = 2\psi(x) - \psi(x-\Delta x) + \Delta x^2 \frac{2m}{\hbar^2}(E-V(x))\psi(x) \\ + \frac{\Delta x^2}{12}\left(\frac{2m}{\hbar^2}(E-V(x+\Delta x))\psi(x+\Delta x) - \frac{2m}{\hbar^2}(E-V(x-\Delta x))\psi(x-\Delta x)\right. \\ \left. + \frac{4m}{\hbar^2}(E-V(x))\right)\psi(x) + O(\Delta x^4)\end{aligned} \tag{E.11}$$

```
import numpy as np


def numerovprop(energy,potential,xind,y0,y1,dx,mass=1.0):
  h2=dx*dx
  f0=2.0*mass*(energy-potential[xind-1])
  f1=2.0*mass*(energy-potential[xind])
  f2=2.0*mass*(energy-potential[xind+1])
  y2=2.0*(1.0-(5.0/12.0)*h2*f1)*y1-(1.0+(1.0/12.0)*h2*f0)*y0
  y2=y2/(1.0*(1.0/12.0)*h2*f2)
  return y2



def generate_eigenfunction(
    grid,potential,energy_guess,mass,
```

```
  initialcorrection=-0.001,tolerance=10.0*-9,corrstep=0.0001):
dx=grid[1]-grid[0]
dx2=dx*dx

ngrid=len(grid)
psi=[0.0]*ngrid
psil=[0.0]*ngrid
psir=[0.0]*ngrid
energy=energy_guess
energyold=0.0
loopcontinue=True

desirednodes=principal-1
corrarrow=1
nodecount=0
while (loopcontinue):
  nodecount=0
  psil[1]=0.0
  psil[2]=1.0e-11

  for j in range(2,ngrid):
    psil[j]=numerovprop(energy,potential,j-1,psil[j-2],psil[j-1],dx,mass=mass)
    if sign(psil[j])!=sign(psil[j-1]) and sign(psil[j])!=0:
      nodecount=nodecount+1
  if nodecount>desirednodes:
    energy=energy-corrstep
    if corrarrow==-1:
      corrarrow=1
      corrstep=0.5*corrstep
```

```
elif nodecount<desirednodes:
  energy=energy+corrstep
  if corrarrow==1:
    corrarrow=-1
    corrstep=0.5*corrstep
else:


  psir[ngrid-1]=0.0
  psir[ngrid-2]=1.0e-11
  for j in range(ngrid-2,0,-1):
    psir[j]=numerovprop(energy,potential,j+1,psir[j+2],psir[j+1],-dx,mass=mass)
  k=np.argmax(psir)
  psir=map(lambda x: x/psir[k],psir)
  psil=map(lambda x: x/psil[k],psil)
  psi=[psil[j] if j<=k else psir[j] for j in range(0,ngrid)]


  corrcheck=1
  g=2.0*mass*(energy-potential[k])
  enerror=(psi[k-1]+psi[k+1]-(2.0-dx2*g)*psi[k])/dx
  if enerror>0:
    energy=energy-corrstep
    if corrarrow==-1:
      corrarrow=1
      corrstep=0.5*corrstep
  elif enerror<0:
    energy=energy+corrstep
    if corrarrow==1:
      corrarrow=-1
      corrstep=0.5*corrstep
```

```
    if corrstep<tolerance:
      loopcontinue=0


norm=np.sqrt((grid[2]-grid[1])*npdot(psi,psi))
psi=map(lambda x: x/norm,psi)
psiwithoutrweighting=[psi[j]/grid[j] for j in range(0,ngrid)]
return psiwithoutrweighting
```

Appendix F

A Classical Picture of the Quantum Defect

To gain a bit more intuition for this quantum defect, let us consider the Rydberg orbital as a classical, Keplerian one—i.e., the trajectory of a classical particle in a $\frac{1}{r}$ potential. The addition of polarization will cause the potential felt by the Rydberg electron to lose its radial symmetry, and therefore the Keplerian orbit taken by the electron will no longer be completely elliptical, but will include precession (see Fig. F.1). We have previously derived the defect-perturbed thresholds in Eq. 2.16. By the correspondence principle [121, 122], the difference in energy between two angular momentum states can be associated with the precessional frequency induced by the quantum defect onto this Keplerian orbit. Therefore, treating angular momentum as continuous, and taking the value of μ_l given in Eq. 2.16 while ignoring the quadrupole polarization, we have

$$\omega_{\text{precession}} = \frac{15 R_\infty \mu_l \alpha_d}{4 n^3 l^6} \tag{F.1}$$

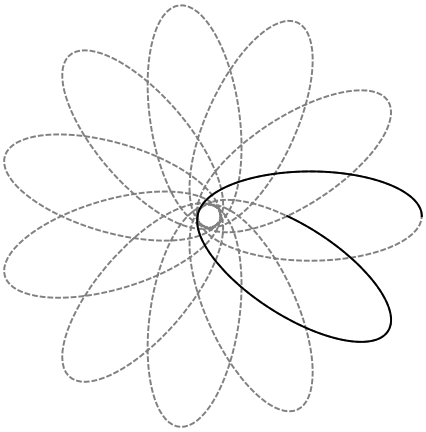

Figure F.1: Keplerian orbit with precession

Bibliography

[1] T. F. Gallagher. *Rydberg Atoms*. Cambridge University Press (2005).

[2] M. Saffman, T. G. Walker, and K. Mølmer. Reviews of Modern Physics **82** 2313 (2010).

[3] A. Krupp, A. Gaj, J. Balewski, P. Ilzhöfer, S. Hofferberth, R. Löw, T. Pfau, M. Kurz, and P. Schmelcher. Physical Review Letters **112** 143008 (2014).

[4] W. Li, T. Pohl, J. M. Rost, S. T. Rittenhouse, H. R. Sadeghpour, J. Nipper, B. Butscher, J. B. Balewski, V. Bendkowsky, R. Low, and T. Pfau. Science **334** 1110 (2011).

[5] D. Booth, S. T. Rittenhouse, J. Yang, H. R. Sadeghpour, and J. P. Shaffer. Science **348** 99 (2015).

[6] V. Bendkowsky, B. Butscher, J. Nipper, J. P. Shaffer, R. Löw, and T. Pfau. Nature **458** 1005 (2009).

[7] S. Osnaghi, P. Bertet, A. Auffeves, P. Maioli, M. Brune, J. M. Raimond, and S. Haroche. Physical Review Letters **87** 037902 (2001).

[8] A. Kirrander, S. Rittenhouse, M. Ascoli, E. E. Eyler, P. L. Gould, and H. R. Sadeghpour. Physical Review A **87** 031402 (2013).

[9] K. Ohmori. Annual Review of Physical Chemistry **60** 487 (2009).

[10] M. D. Lukin. Reviews of Modern Physics **75** 457 (2003).

[11] R. Löw, H. Weimer, J. Nipper, J. B. Balewski, B. Butscher, H. P. Büchler, and T. Pfau. Journal of Physics B: Atomic, Molecular and Optical Physics **45** 113001 (2012).

[12] E. Amaldi and E. Segrè. Il Nuovo Cimento **11** 145 (1934).

[13] E. Fermi. Il Nuovo Cimento **11** 157 (1934).

[14] B. Höglund and P. G. Mezger. Science **150** 339 (1965).

[15] T. F. Gallagher and W. E. Cooke. Physical Review Letters **42** 835 (1979).

[16] T. W. Hänsch, M. H. Nayfeh, S. A. Lee, S. M. Curry, and I. S. Shahin. Physical Review Letters **32** 1336 (1974).

[17] E. E. Eyler and F. M. Pipkin. Physical Review A **27** 2462 (1983).

[18] J. M. Raimond, G. Vitrant, and S. Haroche. Journal of Physics B: Atomic and Molecular Physics **14** L655 (1981).

[19] S. Haroche. pages 45–66 (1999). URL http://aip.scitation.org/doi/abs/10.1063/1.58235.

[20] M. Gross, P. Goy, C. Fabre, S. Haroche, and J. M. Raimond. Physical Review Letters **43** 343 (1979).

[21] T. Wang, S. F. Yelin, R. Côté, E. E. Eyler, S. M. Farooqi, P. L. Gould, M. Koštrun, D. Tong, and D. Vrinceanu. Physical Review A **75** 033802 (2007).

[22] S. Chu. Nature **416** 206 (2002).

[23] M. D. Lukin, M. Fleischhauer, R. Côté, L. M. Duan, D. Jaksch, J. I. Cirac, and P. Zoller. Physical Review Letters **87** 037901 (2001).

[24] D. Jaksch, J. I. Cirac, P. Zoller, S. L. Rolston, R. Côté, and M. D. Lukin. Physical Review Letters **85** 2208 (2000).

[25] A. V. Gorshkov, J. Otterbach, M. Fleischhauer, T. Pohl, and M. D. Lukin. Physical Review Letters **107** (2011).

[26] E. Urban, T. A. Johnson, T. Henage, L. Isenhower, D. D. Yavuz, T. G. Walker, and M. Saffman. Nature Physics **5** 110 (2009).

[27] T. Wilk, A. Gaëtan, C. Evellin, J. Wolters, Y. Miroshnychenko, P. Grangier, and A. Browaeys. Physical Review Letters **104** 010502 (2010).

[28] T. C. Killian, T. Pattard, T. Pohl, and J. M. Rost. Physics Reports **449** 77 (2007).

[29] H. Weimer, M. Müller, I. Lesanovsky, P. Zoller, and H. P. Büchler. Nature Physics **6** 382 (2010).

[30] R. Schmidt, H. Sadeghpour, and E. Demler. Physical Review Letters **116** 105302 (2016).

[31] O. Firstenberg, C. S. Adams, and S. Hofferberth. Journal of Physics B: Atomic, Molecular and Optical Physics **49** 152003 (2016).

[32] J. P. Young, G. S. Hurst, S. D. Kramer, and M. G. Payne. Anal. Chem.; (United States) **51** (1979).

[33] M. Y. Ivanov and A. Stolow. Chemical Physics Letters **265** 231 (1997).

[34] D. Townsend, B. J. Sussman, and A. Stolow. The Journal of Physical Chemistry A **115** 357 (2011).

[35] C. H. Greene, A. S. Dickinson, and H. R. Sadeghpour. Physical Review Letters **85** 2458 (2000).

[36] S. T. Rittenhouse and H. R. Sadeghpour. Physical Review Letters **104** 243002 (2010).

[37] T. Niederprüm, O. Thomas, T. Manthey, T. M. Weber, and H. Ott. Physical Review Letters **115** 013003 (2015).

[38] K. Singer, J. Stanojevic, M. Weidemüller, and R. Côté. Journal of Physics B: Atomic, Molecular and Optical Physics **38** S295 (2005).

[39] M. A. Bellos, R. Carollo, J. Banerjee, E. E. Eyler, P. L. Gould, and W. C. Stwalley. Physical Review Letters **111** 053001 (2013).

[40] S. Markson and H. R. Sadeghpour. Journal of Physics B: Atomic, Molecular and Optical Physics **49** 114006 (2016).

[41] S. Markson, S. T. Rittenhouse, R. Schmidt, J. P. Shaffer, and H. R. Sadeghpour. ChemPhysChem **17** 3683 (2016).

[42] J. J. Balmer. Annalen der Physik **261** 80 (1885).

[43] T. Lyman. The Astrophysical Journal **23** 181 (1906).

[44] F. Paschen. Annalen der Physik **332** 537 (1908).

[45] J. R. Rydberg. Philosophical Magazine Series 5 **29** 331 (1890).

[46] J. R. Rydberg. Z. Phys. Chem **5** 227 (1890).

[47] P. J. Mohr, D. B. Newell, and B. N. Taylor. Journal of Physical and Chemical Reference Data **45** 043102 (2016).

[48] H. Geiger and E. Marsden. Proceedings of the Royal Society of London. Series A, Containing Papers of a Mathematical and Physical Character **82** 495 (1909).

[49] H. Geiger. Proceedings of the Royal Society of London. Series A, Containing Papers of a Mathematical and Physical Character **83** 492 (1910).

[50] J. Needham. *Background to modern science: ten lectures at Cambridge arranged by the History of science committee, 1936*. Cambridge library of modern science. The Macmillan company; The University press, New York : Cambridge, Eng. (1938).

[51] E. Rutherford. Philosophical Magazine Series 6 **21** 669 (1911).

[52] H. Nagaoka. Philosophical Magazine Series 6 **7** 445 (1904).

[53] M. Planck. Verhandl. Dtsc. Phys. Ges. **2** 237 (1900).

[54] M. Planck. Annalen der Physik **4** 1 (1901).

[55] W. Pauli. Zeitschrift für Physik **36** 336 (1926).

[56] E. Schrödinger. *Collected Papers on Wave Mechanics: Third Edition*. American Mathematical Soc. (2003).

[57] S. V. Stepkin, A. A. Konovalenko, N. G. Kantharia, and N. Udaya Shankar. Monthly Notices of the Royal Astronomical Society **374** 852 (2007).

[58] W. J. Karzas and R. Latter. Astrophysical Journal **6** (1961).

[59] A. Burgess and M. J. Seaton. Monthly Notices of the Royal Astronomical Society **127** 355 (1964).

[60] M. J. Seaton. Monthly Notices of the Royal Astronomical Society **119** 81 (1959).

[61] D. R. Flower and M. J. Seaton. Computer Physics Communications **1** 31 (1969).

[62] D. Vrinceanu, R. Onofrio, and H. R. Sadeghpour. The Astrophysical Journal **747** 56 (2012).

[63] T. Pohl, D. Vrinceanu, and H. R. Sadeghpour. Physical Review Letters **100** 223201 (2008).

[64] D. Vrinceanu, R. Onofrio, and H. R. Sadeghpour. The Astrophysical Journal **780** 2 (2014).

[65] N. S. Kardashev. Astronomicheskii Zhurnal **36** 838 (1959).

[66] A. F. Dravskikh, Z. V. Dravskikh, V. A. Kolbasov, G. S. Misezhnikov, D. E. Nikulin, and V. B. Shteinshleiger. In *AKADEMIIA NAUK SSSR, DOKLADY*, volume 163, pages 332–334 (1965).

[67] E. Churchwell, P. G. Mezger, and W. Huchtmeier. Astronomy and Astrophysics **32** 283 (1974).

[68] E. Churchwell, L. F. Smith, J. Mathis, P. G. Mezger, and W. Huchtmeier. Astronomy and Astrophysics **70** 719 (1978).

[69] E. J. Chaisson and M. A. Malkan. Astrophys. J. **210** (1976).

[70] P. Palmer, B. Zuckerman, H. Penfield, A. E. Lilley, and P. G. Mezger. Nature **215** 40 (1967).

[71] R. F. Stebbings. *Rydberg States of Atoms and Molecules*. Cambridge University Press (1983).

[72] E. J. Chaisson, J. H. Black, A. K. Dupree, and D. A. Cesarsky. The Astrophysical Journal Letters **173** L131 (1972).

[73] R. A. Chevalier. Annual Review of Astronomy and Astrophysics **15** 175 (1977).

[74] R. M. Pengelly and M. J. Seaton. Monthly Notices of the Royal Astronomical Society **127** 145 (1964).

[75] M. Brocklehurst. Mon. Notic. Roy. Astron. Soc. 157: No. 2, 211-27. (1972).

[76] K. Giles. Monthly Notices of the Royal Astronomical Society **180** 57P (1977).

[77] R. I. Thompson and T. A. Boroson. The Astrophysical Journal Letters **216** L75 (1977).

[78] W. Clark and C. H. Greene. Reviews of Modern Physics **71** 821 (1999).

[79] M. J. Seaton. Monthly Notices of the Royal Astronomical Society **118** 504 (1958).

[80] F. W. J. Olver and National Institute of Standards and Technology (U.S.). *NIST handbook of mathematical functions*. Cambridge University Press : NIST, Cambridge; New York (2010).

[81] J. J. Sakurai and J. Napolitano. *Modern Quantum Mechanics*. Addison-Wesley (2011).

[82] A. Omont. Journal de Physique **38** 1343 (1977).

[83] J. R. Taylor. *Scattering theory: the quantum theory on nonrelativistic collisions*. Wiley, New York (1972).

[84] G. K. Ivanov. Optics and Spectroscopy **40** 554 (1976).

[85] O. Hinckelmann and L. Spruch. Phys. Rev., A 3: 642-8. (1971).

[86] M. Baer. *Beyond Born-Oppenheimer: Conical intersections and electronic non-adiabatic coupling terms*. Wiley, Hoboken, N.J. (2006).

[87] C. Zener. Proceedings of the Royal Society of London A: Mathematical, Physical and Engineering Sciences **137** 696 (1932).

[88] E. T. Whittaker and G. N. Watson. *A course of modern analysis*. Cambridge university press (1996).

[89] M. O. Vieitez, T. I. Ivanov, E. Reinhold, C. A. de Lange, and W. Ubachs. Physical Review Letters **101** 163001 (2008).

[90] M. O. Vieitez, T. I. Ivanov, E. Reinhold, C. A. de Lange, and W. Ubachs. The Journal of Physical Chemistry A **113** 13237 (2009).

[91] S. Mollet and F. Merkt. Physical Review A **82** 032510 (2010).

[92] R. C. Ekey and E. F. McCormack. Physical Review A **84** 020501 (2011).

[93] S. J. Park, S. W. Suh, Y. S. Lee, and G. H. Jeung. Journal of Molecular Spectroscopy **207** 129 (2001).

[94] M. Marinescu, H. R. Sadeghpour, and A. Dalgarno. Physical Review A **49** 982 (1994).

[95] A. Kramida. NIST atomic spectra database (version 5.2). http://physics.nist.gov/asd.

[96] C. Bahrim, U. Thumm, and I. I. Fabrikant. Journal of Physics B: Atomic, Molecular and Optical Physics **34** L195 (2001).

[97] C. Eckart. Physical Review **35** 1303 (1930).

[98] C. Fey, M. Kurz, P. Schmelcher, S. T. Rittenhouse, and H. R. Sadeghpour. New Journal of Physics **17** 055010 (2015).

[99] Bateman Manuscript Project, H. Bateman, A. Erdélyi, United States, and Office of Naval Research. *Tables of integral transforms. Based, in part, on notes left by Harry Bateman,*. McGraw-Hill, New York (1954).

[100] M. A. Bellos, R. Carollo, J. Banerjee, M. Ascoli, A.-R. Allouche, E. E. Eyler, P. L. Gould, and W. C. Stwalley. Physical Review A **87** 012508 (2013).

[101] I. I. Fabrikant. Journal of Physics B: Atomic, Molecular and Optical Physics **26** 2533 (1993).

[102] J. Mitroy, M. S. Safronova, and C. W. Clark. Journal of Physics B: Atomic, Molecular and Optical Physics **43** 202001 (2010).

[103] V. S. Lebedev and A. A. Narits. Journal of Experimental and Theoretical Physics **117** 593 (2013).

[104] D. C. Thompson, E. Kammermayer, B. P. Stoicheff, and E. Weinberger. Physical Review A **36** 2134 (1987).

[105] E. L. Hamilton, C. H. Greene, and H. R. Sadeghpour. Journal of Physics B: Atomic, Molecular and Optical Physics **35** L199 (2002).

[106] J. Tallant, S. T. Rittenhouse, D. Booth, H. R. Sadeghpour, and J. P. Shaffer. Physical Review Letters **109** 173202 (2012).

[107] A. A. Khuskivadze, M. I. Chibisov, and I. I. Fabrikant. Physical Review A **66** 042709 (2002).

[108] T. Niederprüm, O. Thomas, T. Eichert, C. Lippe, J. Pérez-Ríos, C. H. Greene, and H. Ott. Nature Communications **7** 12820 (2016).

[109] A. Gaj, A. T. Krupp, J. B. Balewski, R. Löw, S. Hofferberth, and T. Pfau. Nature Communications **5** (2014).

[110] M. Schlagmüller, T. C. Liebisch, F. Engel, K. S. Kleinbach, F. Böttcher, U. Hermann, K. M. Westphal, A. Gaj, R. Löw, S. Hofferberth, T. Pfau, J. Pérez-Ríos, and C. H. Greene. Physical Review X **6** (2016).

[111] H. Saßmannshausen, F. Merkt, and J. Deiglmayr. Physical Review Letters **114** 133201 (2015).

[112] D. A. Anderson, S. A. Miller, and G. Raithel. Physical Review A **90** 062518 (2014).

[113] M. Scheer, J. Thøgersen, R. C. Bilodeau, C. A. Brodie, H. K. Haugen, H. H. Andersen, P. Kristensen, and T. Andersen. Physical Review Letters **80** 684 (1998).

[114] U. Thumm and D. W. Norcross. Physical Review Letters **67** 3495 (1991).

[115] U. Thumm. private communication.

[116] P. Goy, J. M. Raimond, G. Vitrant, and S. Haroche. Physical Review A **26** 2733 (1982).

[117] P. Gould. private communication.

[118] S. Watanabe and C. H. Greene. Physical Review A **22** 158 (1980).

[119] R. L. Burden and J. D. Faires. *Numerical analysis*. PWS-Kent Pub. Co., Boston (1993).

[120] I. I. Gol'dman, V. D. Krivchenkov, B. T. Ge'likman, V. D. Lepa, and E. Marquit. *Problems in Quantum Mechanics*. Dover, Mineola, NY (2006).

[121] N. Bohr. Zeitschrift für Physik **2** 423 (1920).

[122] T. P. Hezel, C. E. Burkhardt, M. Ciocca, L.-W. He, and J. J. Leventhal. American Journal of Physics **60** 329 (1992).